# Mechanical Characterization of Thermoplastic Polyolefin (TPO) Foams

by

**Hsiao-Fung Steven Wong**

**A thesis submitted in conformity with the requirements**
**for the Degree of Master of Applied Science**
**Graduate Department of Mechanical & Industrial Engineering**
**University of Toronto**

*Your file Votre référence*
*ISBN: 978-0-494-40323-5*
*Our file Notre référence*
*ISBN: 978-0-494-40323-5*

# Mechanical Characterization of Thermoplastic Polyolefin (TPO) Foams

Hsiao-Fung Steven Wong 2007

Degree of Master of Applied Science
Department of Mechanical & Industrial Engineering
University of Toronto

# Abstract

This thesis investigated the effect of cellular morphologies on mechanical properties of Thermoplastic Polyolefin (TPO) cellular foams. Cellular closed-cell TPO foams were prepared using a two-stage batch method and injection molding process. The microstructure of these foamed samples was controlled by carefully altering the processing parameters of two different foaming processes. The foam morphologies were characterized in terms of the cell density, foam density and average cell size. Tensile properties, elastic recovery and impact resistance of various foamed TPO samples were correlated with different foam morphologies. This research is summarized in three major findings: 1) The weight reduced TPO can be achieved without sacrificing much of the mechanical strength by introducing cellular structure in the materials, 2) the elastic recovery of the TPO can be significantly improved by the cellular structure in the materials and (3) the impact resistance of the TPO foams is significantly reduced by the cellular structure in the materials.

# Acknowledgements

First, I would like to thank my mother, father and sister for their continuous financial and moral support. I would not have been able to come this far without them.

I would like to thank my supervisors, Professor Hani E. Naguib and Professor Chul B. Park, for their guidance and encouragement in this research. I would like to offer my sincere gratitude to my main supervisor Professor Naguib for providing support and encouragement throughout my study.

I would like to acknowledge the financial support of the Automobile of the 21st Century (AUTO21) Networks of Centres of Excellence of Canada, the Government of Ontario for supporting this research and the Department of Mechanical and Industrial Engineering for providing the University of Toronto Fellowship.

I would like to thank all my colleagues working in the Smart and Adaptive Polymer Laboratory and Microcellular Plastics Manufacturing Laboratory for their great help and friendship. They include Raymond Chu, Linus Leung, Steven Simkevitz, Esther Richards, Jo McRae, Ryan Kim, John Lee, Mohammed Serry, Mohammad Hasan and Chunmin Wang. For those of you who feel your names should be here, please accept my unwritten thanks.

# Table of Contents

# List of Tables

# List of Figures

# List of Symbols

$T$ = temperature, K

$D$ = diffusivity, $cm^2/s$

$h$ = thickness of the polymer sample, cm

$t$ = time, sec

$N$ = cell density, $cells/cm^3$

$A$ = area, $cm^2$

$\rho_p$ = density of the unfoamed polymer, $cells/cm^3$

$\rho_f$ = density of the foamed polymer, $cells/cm^3$

$\varphi$ = relative density of the foamed sample, $g/cm^3$

$w(air)$ = weight of the foamed sample in air, g

$w(H_2O)$ = weight of the foamed sample in water, g

$\rho(H_2O)$ = density of the water, $kg/m^3$ or $g/cm^3$

$E_f$ = tensile modulus of the foams,

$E_p$ = tensile modulus of the unfoamed polymer,

$\sigma_f$ = tensile strength of the foams,

$\sigma_p$ = tensile strength of the unfoamed polymer,

$\phi$ = fraction of sold in cell struts

$C_B$ = compression set

$t_o$ = original thickness of the sample

$t_i$ = instantaneous thickness of the sample

$t_n$ = thickness of the apparatus

# Chapter 1
# Introduction

## 1.1 Foam Materials

Polymeric foam is defined as the plastic material consisting of at least two phases: the solid polymer phase and the gaseous phase. In other words, this is the material which contains a large amount of very small gas bubbles in the polymer matrix. The gas bubbles in the foams are also referred to as cells or voids. Thus, the polymeric foam is also called the cellular polymer. Because of the cells present in the materials, the cellular polymer has less material per unit volume than the solid polymer. Therefore the weight and the material consumption of the plastic component can be reduced by using the cellular polymeric material.

In addition to the weight reduction of the component by using cellular plastic, the foam materials also exhibit superior vibration, acoustic and impact absorption capabilities, as well as high thermal and electrical insulation. These superior physical and mechanical properties allow the foams to be ideal for use in applications such as packaging, thermal/electrical insulation, sports equipment, and automotive and aircraft components.

Foam materials are divided into three categories: convectional foams, fine-celled

foams and microcellular foams. These categories are classified by the cell size and cell density of the foams. In general, the convectional foams have a cell size greater than 300μm and a cell density less than $10^6$cells/cm$^3$. The fine-celled foams have a cell size between 10μm and 300μm and a cell density between $10^6$cells/cm$^3$ and $10^9$cells/cm$^3$. The microcellular foams have a cell size less than 10μm and a cell density greater than $10^9$cells/cm$^3$. Furthermore, the foam materials are also classified by the cell structure: opened or closed cell foams. The opened cell foams have the microstructure that cells are interconnected to each other. On the other hand, the closed cell foams have cells which are insulated from each other in the material. Typically, the closed cell foams are used in the structure applications and the opened cell foams are mainly used in space filling and acoustic applications.

## 1.2 Microcellular Foams

Microcellular foams are defined as foams having average cell sizes in the range 1-10μm and cell densities from $10^9$ - $10^{15}$ cells/cm$^3$ [1-3]. The technology of creating a microcellular structure in the polymer matrix was invented by Suh et al. at Massachusetts Institute of Technology (MIT) in the early 1980s [4]. The concept of this technology is based on the idea of creating of a large amount of micro size gas bubbles in the polymer matrix by using high pressure, inorganic, physical or chemical blowing agents. This early foaming technology is called the batch foaming process. Other foaming technologies such as extrusion [5-10] and injection molding [11] were developed to increase the productivity and reduce the manufacturing cost. These commercially available foaming technologies are actually called the expansion foaming process. The expansion foaming

process in general consisted of these fundamental steps: (i) gas/polymer formation, (ii) the creation of gas bubbles in the polymer matrix (cell nucleation), (iii) the growth of these gas bubbles (cell growth) and (iv) the finalization of the cellular structure in the polymer (cell stabilization). In batch foaming process, physical blowing agent such as low boiling point liquid or non-reactive gas ($CO_2$ or $N_2$) is used to saturate the polymer samples at high pressure in the container to form the gas/polymer solution. After the polymer sample is fully saturated, the pressure is quickly released. This rapid drop in pressure and/or increase the temperature on the samples induces the cell nucleation and growth and results in foams with cell sizes in the order of micrometers [3, 12-16].

The unique structure of microcellular foams offers superior relative mechanical properties. For instance, microcellular foams have a large number of cells (bubbles) that have a size smaller than the critical flaws in the polymer. According to the Griffith crack hypothesis [17], the stress concentration around the bubbles decreases as the cell size decreases. Thus, there will not be a notable decrease in material strength as the cell size in the foamed material becomes very small. In addition, such small bubbles inhibit crack propagation by blunting the crack tip and thus increasing the amount of energy needed to propagate the crack in the microstructure [18, 19]. Therefore, the use of a microcellular foaming procedure can reduce the material weight and costs without major compromise to mechanical properties [20, 21].

These microcellular foams were created to reduce material and lower costs in certain polymer products in response to industrial needs [3]. Typically, microcellular foams are known to exhibit high impact strength (up to a five-fold increase over unfoamed plastics) [2, 3, 22], high toughness (up to a five-fold increase over unfoamed plastics) [12], high

stiffness-to-weight ratio (three to five times higher than unfoamed plastics) [2, 3], high fatigue life (up to a fourteen-fold increase over unfoamed plastics) [23], high thermal stability [24], low thermal conductivity [3], high thermal stability [3], low dielectric constant and reduced material weight and cost as compared to the unfoamed or conventional foam materials [25]. Therefore, microcellular foams have a great potential for applications in the automotive, aircraft, structural components and packaging industries.

## 1.3 Problem Statement and Objectives

The objective of this research is to investigate the correlations of the processing, structure and mechanical properties for cellular Thermoplastic Polyolefin (TPO) foams. Closed-cell TPO foams were processed using the aforementioned two-stage batch approach and specific mineral-filled TPO foams were prepared using the injection molding process. Nitrogen ($N_2$) was used as the physical blowing agent to process the cellular TPO foams. By carefully choosing the processing parameters, different cell morphologies of cellular foams could be successfully controlled. The effects of TPO composition on cell morphology and mechanical properties was studied for optimizing the design of TPO materials.

Tensile testing, elastic recovery and impact testing were conducted in order to investigate the relationships between the foaming parameters, foam morphologies and the mechanical properties. The cellular TPO foams were prepared with different processing parameters in order to examine their effects on the mechanical properties of the foam structure. Elastic modulus, tensile strength, elongation at break, elastic recovery and

impact resistance of the foamed TPO samples was characterized as a function of foaming parameters and cell morphologies.

The constitutional mechanical properties of solid foam structures were studied based on the characterization of the newly developed structure. A constitutive model was proposed to correlate the relationship between micro structure and macro properties of cellular TPO materials. Effect of foam density on mechanical properties was studied by comparing the low density fine-celled polyolefin foams and the high density microcellular foams.

Finally, the results of this research will allow designers to predict the microstructure and mechanical properties of microcellular TPO foams prepared from different sets of processing parameters for their specific engineering applications.

## 1.4 Organization of the Thesis

This thesis presents the effect of processing parameters on the cellular morphology and mechanical properties of cellular TPO foams. It was comprised in 7 chapters. A brief description on each chapter is listed as follows:

Chapter 1 introduces a general overview of microcellular foams, TPO composite materials, the objectives of this research and the structure of this thesis. Chapter 2 provides the literature survey, theoretical and technical background to the relevant research topics in detail. These topics include the review of batch foaming technology, cell morphology characterization and mechanical properties of polymeric materials. Chapter 3 presents the experimental results of processing, cell morphology characterization, and mechanical properties of microcellular TPO foams. A detailed

discussion on the effect of processing parameters on cell morphology and mechanical properties are provided. The constitutive models related to the structure and properties of various microcellular TPO foams are also presented in this chapter. Chapter 4 presents the investigation of the effect of cell morphology on elastic recovery of microcellular TPO foams. Chapter 5 presents the mechanical properties of injection molded TPO foams. Chapter 6 provides the summary and presents the conclusion in this research. Finally the recommendation of this thesis is presented in Chapter 7.

# Chapter 2
# Literature Survey and Theoretical Background

## 2.1 Introduction

In this chapter, a literature survey and background of the processing, characterization and mechanical properties of polymeric foams is provided. The subjects include a review of current batch foaming method, foam morphology characterization and the mechanical properties of foamed materials.

## 2.2 Thermoplastic Polyolefin (TPO) Composites

The automotive industry has been increasingly using TPO alloys in exterior and interior applications, such as bumper fascias, claddings and wire insulation, because of its excellent weatherability, low density and low cost [26-29]. However, TPO foams have not been utilized because the technologies for foaming TPO materials using two-stage batch or injection molding processes has not yet been developed. There is nonetheless a significant amount of interest in developing foamed TPO products since replacing solid TPO with a foamed counterpart could significantly reduce the material cost and fuel consumption.

The polypropylene (PP) is widely used in many engineering applications, as it has excellent physical and mechanical properties, as well as good recycling ability and is inexpensive. However, PP has relatively poor mechanical properties on impact and at low temperatures [26]. Therefore, a polymer blend was used to enhance these mechanical properties. For instance, the addition of polyethylene terephthalate (PET) in PP could enhance the stiffness at higher temperatures [30], the addition of ethylene methyl acrylate (EMA) would enhance the toughness [31] and the addition of rubbers/elastomers such as ethylene–propylene rubber (EPR) or engage will result in the improvement of impact resistance and scratch resistance of the PP material. This PP with rubber/elastomer toughened is called the thermoplastic polyolefin (TPO) [27, 32].

Blending elastomers with PP improves mechanical properties such as toughness, impact and compression properties. However, this sacrifices some mechanical properties such as the stiffness and hardness of the material. As a result, the inorganic filler such as talc and clay were added in the TPO formulation to improve the mechanical properties such as stiffness, hardness, impact strength and to further reduce the cost of the materials [33]. Furthermore, the addition of filler in the polymer may also enhance the nucleation process which could results in the increase of bubble in the final foam structure [34]. Two of the TPO materials used in this research, which is composed of specific mineral filler, are called the DTPO and TYC735X.

## 2.3 Review of Two-Stage Batch Foaming Process

Microcellular thermoplastic foams were first produced in a two-stage batch foaming process [19, 22, 35]. In the first stage, the polymer sample is placed in a high pressure

chamber, pressurized with a non-reactive gas such as $N_2$ or $CO_2$ at a desired saturation temperature. In the chamber under high gas pressure, the gas is dissolved in the polymer matrix until the polymer is fully saturated with gas and then becomes the polymer/gas solution. In this stage, it is critical to provide sufficient time to saturate the polymer with gas since the amount of gas dissolved in the polymer sample effects the final foam morphology. After the polymer is fully saturated with gas, the pressure in the chamber is released. The sudden pressure drop in the chamber results in the rapid decreases of the gas solubility in the polymer/gas solution. This thermodynamic instability induces cell nucleation in the polymer/gas solution. The foaming stage in the batch process is carried out by quickly heating the polymer sample to the desired foaming temperature at the desired foaming time. Since the cells nucleate after the rapid depressurization in the chamber, they cannot grow much due to the high stiffness and high viscosity of the polymer matrix. Thus, soften the material is required by heating the polymer sample to above its glass transition temperature. However, increases in the temperature of the polymer not only soften the material but also increases the diffusivity of the gas from polymer matrix. This results in the large amount of lost gas especially in the region close to the hot skin surface of the polymer sample. Due to this excessive gas loss, the cell size in the foam is limited. Therefore, the cell morphology of the final foam product which is produced by the batch foaming process has a cell size in micrometer and typically low volume expansion ratio.

The advantage of producing microcellular foam products by using the two-stage batch foaming process is that the cell nucleation stage and the foaming stage are independent of each other. The cell nucleation stage can be controlled by several factors:

the amount of adaptive in the polymer, the gas pressure and the pressure drop rate in the system. The foaming stage can be controlled by heating up the polymer sample after being taken out from the pressure chamber. Thus, the cell growth is controlled by the foaming temperature and the foaming time. By independently controlling the cell nucleation stage and foaming stage, the desired cell density, cell size and volume expansion ratio of the final foam products can be successfully obtained. In order to produce microcellular thermoplastic foam without notable decreases in material strength, a very high cell density and micro cell size in the foam are required. Typically, a high pressure drop rate and lower foaming temperature are used to induce a large amount of cell nucleation and limit the cell growth to avoid cell coalescence respectively.

However, the main disadvantage of producing microcellular foam products by using the two-stage batch process is that there is a very long time required to saturate the polymer with gas during the saturation stage. By providing sufficient time to let the gas completely diffuse into the polymer matrix under specific saturation pressure is critical in order to form a desired polymer-gas solution. The long saturation time is due to the very low gas diffusivity in the polymer. From the Equation 2.5 explained before, the time ($t_D$) required for the polymer to reach saturation could be approximated by using the equation shown as follows [36]:

$$t_D \simeq \frac{h^2}{4D} \tag{2.1}$$

**Equation 2.1** shows that the time required to saturate the polymer is dependent on the diffusivity (D) of the gas and the thickness (h) of the polymer sample. For instance, to saturate a PP sample which has a thickness of 3mm with $CO_2$ gas ($D=1.4\times10^{-11} m^2/s$) under the pressure of 101kPa at 25°C requires approximately 45 hours. The saturation

time can be reduced by increasing the system temperature during the saturation stage, since the diffusivity of gas increases with the temperature. Nevertheless, such long saturation time limits the productivity of producing polymeric foams using the batch foaming process in the plastic industry.

Many studies have been conducted to investigate the production of microcellular thermoplastic foams by utilizing the batch foaming process. Many polymers such as Polypropylene (PP) [37-39], Polystyrene (PS) [40-48], Poly(methyl methacrylate) (PMMA) [49-51], Poly(lactic-co-glycolic acid) (PLGA) [52,53], Polycarbonate (PC) [54], Polyethylene (PE) [55, 56], PE/PP composite [57, 58], Polyvinyl Chloride (PVC) [3] and Poly(ethylene terephthalate) (PET) [59-61] were successfully used to produce the microcellular structure by batch process method. These weight reduced microcellular foams with low cost and reasonable mechanical properties are able to replace the solid polymer in many engineering applications.

## 2.4 Mechanical Property of Polymeric Foams

Mechanical properties of materials describe the response or deformation of a material subjected to mechanical loads or forces. Materials used in load applications are called structural materials. For instance, a plastic bumper is a structural material since it is subjected to impact loading and compression loading during the collision. In such situations, it is necessary to know the behaviour of the material and to ensure the resulting deformation of the components will not be excessive and fracture will not occur.

The mechanical properties of materials include strength, modulus and elongation at break. The mechanical properties of materials could be varied depending on the testing

standards. Thus, standardized testing techniques are used to ensure the consistency of publishing material-property data. In North America, these standardized testing techniques are coordinated by American Society of Testing and Materials (ASTM). The ASTM defines standards for test specimens and test procedures for a variety of material property measurements. In this thesis, the mechanical testing of polymeric foams was conduced by following the ASTM standards.

The mechanical properties of materials are determined through destructive testing of material samples under controlled loading and environmental conditions that replicate the service conditions as closley as possible.. The loading conditions could be tensile, compressive, shear or impact at a constant or continuously fluctuated magnitude of loading. The environmental condition is another major factor to be considered for the structure materials which would be serviced under extreme whether conditions.

### 2.4.1 Tensile Tests of Polymeric Foams

The mechanical properties of polymeric foams have been extensively studied. As compared to the solid material, the mechanical properties of polymeric foams depend on the relative density and the cell morphology of the foams. Before replacing the solid polymeric materials, the mechanical properties of the polymeric foams with various cell morphologies is necessary to investigate before implement them into various engineering applications.

The tensile mechanical properties of cellular foams are rarely reported. Sun et al [63] studied the effect of cell morphology on mechanical properties of microcellular polysulfone, polyethersulfone and polyphenylsulfone foams prepared by two-stage batch

process. They found that the tensile modulus of these polysulfone foams increased with the square of their relative densities. The tensile strengths were proportional to foam densities. Fu et al [2] also found that the tensile modulus and tensile strength increased with the relative foams density. Their results confirm that foams with a finer cell structure have an advantage in mechanical properties against foams with a relatively coarse cell structure. Matuana et la [3, 20] investigated the effect of cell morphology on tensile properties of polyvinyl chloride (PVC). They found that although the tensile modulus and strength decreased with the relative density, the specific tensile modulus and the specific tensile strength were maintained independent of the relative foam density, as well as the specific elongation at break increased as relative density decreases.

More researches also proven that the relative foam density is by far the most influential parameter over mechanical properties of cellular liner low density polyethylene (LLDPE) [64], polyurethane [21], polycarbonate [1, 65, 66] glass-fiber reinforced polycarbonate [67], polystyrene [68], polyphenylene oxide [69] and some other reinforced polymeric foams [70].

In addition, Nishikawa et al [71] studied the tensile properties of foamed PP sheet. They found that the percent elongation of foamed PP sample was affected by the cell shape. The elongation increased with an increase in the aspect ratio of the cell shape in the foamed PP sheet. The tensile properties of microcellular foamed polycarbonate [72] were also investigated in the early work.

Many theoretical approaches were developed based on the experimental results of studying the structure-properties relationship of polymeric foams. For instance, one of the most famous and widely accepted constitutive models was developed by Gibson and

Ashby [**73**]. This constitutive model relates the relative tensile properties to the relative density of the convectional foams. The tensile modulus and the tensile strength could be related to the relative foam density in the following equations:

$$\frac{E_f}{E_p} \approx C_1\left(\phi\frac{\rho_f}{\rho_p}\right)^2 + C_1'(1-\phi)\left(\frac{\rho_f}{\rho_p}\right) \tag{2.2}$$

$$\frac{\sigma_f}{\sigma_p} \approx C_5\left(\phi\frac{\rho_f}{\rho_p}\right)^{\frac{3}{2}} + C_5''(1-\phi)\left(\frac{\rho_f}{\rho_p}\right) \tag{2.3}$$

where $E_f$ is tensile modulus of the foams, $E_p$ is tensile modulus of the unfoamed polymer, $\sigma_f$ is the tensile strength of the foams, $\sigma_p$ is tensile strength of the unfoamed polymer, $\rho_f$ is the density of the foam, $\rho_p$ is the density of the unfoamed polymer, $\phi$ is the fraction of sold in cell struts and $C_1, C_1', C_5$ and $C_5'$ are constants representing the microstructure of the foams. These constitutive models would be able to assist engineers to predict the mechanical properties by knowing the relative density of the polymeric foams.

Researchers tried to compare these constitutive models to the experimental data on different polymeric materials. Fu et al [2] investigated the structure-property relationship of microcellular poly (methyl-methacrylate) (PMMA) foams. This study proved that the Gibson and Ashby's model perfectly related the relative tensile modulus and relative density of microcellular PMMA foams. However, the Gibson and Ashby's model underestimated the mechanical strength of the microcellular PMMA foams. Thus, an empirical formula was proposed to correlate the tensile strength relationship based on the experimental data. Overall, the mechanical properties of those microcellular foams have not been extensively studied. Most of this research tried to relate the mechanical

properties of the foams with their relative density without looking at the effect of other processing parameters and cell morphologies of the foams.

Other analytical models were also developed to simulate the mechanical property polymeric foams. Wimberly et al [74] evaluated a linear finite element analysis model for predicting the mechanical behaviour of extruded low density PPO/PS foams. However, the linear finite element model shows very different to the experimental data. That leads to conclusions about the inability of a linear model to predict the mechanical behaviour of cellular foamed materials.

Recently, the tensile behaviours of varies unfoamed TPO composites were investigated by Lee et al [75], Mehta et al [27], Mishra et al [24] and Liu et al [76]. However, the relationship of cell morphologies and tensile mechanical properties of cellular TPO foams with such specific composition of PP/Elastomer have not being reported in the literature.

### 2.4.2 Elastic Recovery Tests of Polymeric Foams

Polymer foams are intensively used on packaging, space filling and collision (energy absorption) regions in the automotive industry due to its high energy absorption capability. The materials used in these applications are needed to withstand the compressive loads for varying periods of time. It is desirable that the foamed materials can perform the requirements during compressive loading and recover fully upon load removal. Therefore, it is crucial to study the elastic recovery behaviour of these polymeric foams in order to minimize the material usage for various engineering applications.

The elastic recovery behaviour of polymeric materials is rarely reported. Zitzumbo et al [**78**] studied the elastic recovery of semi-crystalline polymers including LDPE and HDPE. They designed an optoelectronic system to investigate the recovery of polymeric samples. They found that the recovery process of polymers develops in two stages. The initial stage recovery occurred very rapidly based on the Hookean and the second stage was very slow and controlled by the inelastic and plastic components of the material. Talal et al [**79**] studied the elastic recovery of cellular polyurethane, polyethylene and polyimide foams. They found that the elastic recovery increased as the original compressive strain and the duration of compression increased. They also found that the elastic recovery is improved by introducing a cellular structure in the materials. However, the effects of cell morphologies on elastic recovery of cellular TPO foams have not being studied before.

### 2.4.3 Impact Properties of Polymeric Foams

Impact test is used to test a materials ability to resist high-rate or shock loading. For instance, a plastic bumper subjected to shock impact loading during a collision. The impact test determines how much energy the materials absorb in fracturing a test piece at high velocity. Various tests have been devised to measure the ability of material to withstand impact loading. There are two major types of impact tests: pendulum and drop weight. Izod, Charpy and tensile impact are the most common of the pendulum type of impact tests.

The effect of cell morphology on impact resistance of polymeric materials is rarely reported. Doroudiani et al [80] investigated the effect of cell morphology on the impact

strength of Polystyrene foams. They found that the cell size does not affect the impact strength of the foams. However, the impact strength was dominated by the relative density of the foam. They also concluded that the plastic and viscoelastic deformation in the cell walls is the major source of energy dissipation in these materials. Barlow et al [81] investigated the effect of foam density on the impact strength of microcellular polycarbonate foams. They found that the impact strength of these foams appears to be a strong function of both relative foam density and the cell size. The impact strength increased with the relative foam density and also increased with increasing cell size at a given density of the microcellular PC foams. Bledzki et al [82] studied the effect of processing parameters of injection molded PP, PC/ABS foams. They found that the physical and chemical blowing agent strongly affected the impact characteristics of microcellular foams. By increasing the chemical blowing agent content in the PP, the cell density and cell size increases, resulting in the Charpy notched impact strength of the foams decrease up to 33%. Tovar-Cisneros et al [83] investigated the effect of mold temperature on morphology and impact strength of injection molded HDPE foams. They found that the impact strength increased with increasing skin thickness. The unfoamed skin layer works as an absorbtion layer of the direct impact. Other research had also examined the impact strength of polystyrene [84, 85], polyethylene [86, 87, 88] foams. However, the effects of cell morphologies on impact resistance of cellular rubber toughen TPO foams have not being studied before.

Researchers also developed the numerical models to predict the impact strength of polymeric materials under various impact conditions. Duan et la [89] examined the impact resistance of ABS and PBT materials by conducing multiaxial impact test. They

developed a finite element model to simulate the impact testing by using the computer. They found that the result obtained from the finite element model has a good fit on the experimental data. The model successfully simulated the impact conditions and calculated the impact resistance of the specific polymers. Other analytical models were also developed to simulate the impact loading on polymers. Sherwood et al [90] developed a constitutive model to simulate the energy absorbing polyurethane foam under impact loading. However, none of the models are able to simulate the effect of cell morphology on impact strength of polymeric foams.

# Chapter 3
# Processing, Characterization and Mechanical Properties of TPO Microcellular Foams

## 3.1 Introduction

The TPO thermoplastic material has been increasingly used in the automotive industry. The major applications include both exterior and interior plastic parts, such as bumper fascias, claddings and wire insulation, because of its excellent weatherability, low density and low cost. By using cellular TPO foamed materials on these applications, material, fuel and cost reduction could be further improved. Thus, this is crucial to study the mechanical properties of various microcellular TPO foams. In this chapter, the investigations on the processing, characterization and mechanical properties of microcellular TPO foams were presented. The microcellular TPO foams were successfully processed under various processing parameters. Three key processing parameters (saturation pressure, foaming temperature and foaming time) which affect the final foam morphology were identified. The foam morphology of these microcellular

TPO foams which were processed under various processing parameters was characterized. The effects of final foam morphology on mechanical properties of thesis microcellular TPO foams were also investigated. Finally, the relationship between the foam morphology and mechanical property was correlated. The investigation of this study would help engineers to process the microcellular TPO foams with different foam morphology to suit their specific engineering applications and to achieve material and weight reduction.

## 3.2 Experimental

### 3.2.1 Experimental Materials

The TPO materials were composed of different ratios of PP and engage (rubber). The PP7805 (80 dg/min MFI) and Engage 8130 (13 dg/min MFI) were supplied by Exxon and DuPont respectively. The PP and engage were blended by a twin screw extruder to the desired combinations. The number suffix of the TPO indicates the percentage of PP in the resultant TPO composite. For instance, the TPO70 examined in this study consisted of 70% of PP and 30% Engage. Three different TPO composites (TPO90, TPO70 and TPO50) were examined in this study. The solubility and diffusivity data of PP and engage were measurement by Microcellular Plastics Manufacturing Laboratory in the University of Toronto. The solubility and diffusivity data of three different TPO composites were interpolated from the data of PP and engage as summarized in Table 3-1.

The TPO material blended with ingredient called DTPO also investigated in this study. The DTPO blends consist of PP, engage, and mineral filler. The composite was

blended by a twin screw extruder to the desired combinations. In DTPO, the ratio between the PP and engage is 7:3. The DTPO material was supplied by Decoma International Inc. and this is the commercial TPO material currently used in automotive industries.

The TPO materials were hot compression molded into 3 mm thick panels by using a hydraulic heated press machine (Carver Inc.) for 5 minutes under 5 tons of pressure at 200°C. The final TPO specimens were obtained by punching an ASTM (D638-03, Type V) die on the TPO panel. The detail dimension of the TPO samples was shown in Figure 3-2. The physical blowing agent mainly used in this study was $N_2$ supplied by BOC Inc.

### 3.2.2 Crystallization Behaviour Measurements

The thermal behaviour of TPO materials was exmained by using a differential scanning calorimetry (DSC, TA Inc. Q2000) in a flowing nitrogen atmosphere. Each of the TPO specimens was first heated from 40°C to 200°C at the rate of 5°C/min in order to remove the previous thermal history. This was followed by cooling from 200°C to 40°C at the rate of 5°C/min. Finally, the specimen was heated back up to 200°C at 5°C/min.

### 3.2.3 Processing of Microcellular Foams

Microcellular foaming experiments were performed in a two-stage batch process. Figure 3-3 shows the schematics of batch foaming process. In the first stage, the TPO samples were saturated in the pressure chamber with $N_2$ gas under room temperature. A syringe pump (ISCO Model 206D) was used to increase the gas cylinder pressure to the desired saturation pressures of 13.8MPa (2000psi) and 27.6MPa (4000psi). The

saturation times for all different TPO composites were approximately 3 days at 13.8MPa and 27.6MPa saturation pressures. For the second stage, the gas-saturated samples were foamed by removing the samples from the pressure chamber. The foaming step was carried out by putting the gas-saturated samples in a heated hydraulic press in which the platens are heated to the desired foaming temperatures for specified foaming times. A previous study had also used a heated hydraulic press to foam microcellular polymeric materials [91]. The combination of pressure and temperature changes resulted in the rapid solubility drop in the samples, inducing cell nucleation and cell growth. All specimens were foamed less than five minutes after being taken out of the pressure chamber. Afterwards, the samples were quenched in cold water to fix the microstructure to form the final TPO foams.

### 3.2.4 Sample Characterization

The TPO foam morphology was characterized by utilizing a scanning electron microscope (SEM, JEOL JSM-6060). The samples were cooled in liquid nitrogen and fractured to produce a clean and intact surface with minimum plastic deformation. They were then gold or platinum coated by using a sputter coater to enhance the conductivity of the TPO samples. The average cell size and cell density were analyzed by utilizing the ImageJ software from National Institutes of Health, USA. The cell density was calculated as the number of cells per unit volume with respect to the unfoamed polymer. The cell density was calculated from ImageJ software by using the following equation (3.1):

$$N = \left(\frac{n}{A}\right)^{3/2} \times \frac{\rho_P}{\rho_f} \tag{3.1}$$

where $n$ is the number of cells in the defined area $A$, and $\rho_p$ and $\rho_f$ are the density

of the unfoamed and foamed polymer, respectively.

The foam density was measured by the buoyancy method. This can be done by measuring the volume and weight of the foamed sample. There is a standard measuring procedure from America Standard for Testing and Materials (ASTM) D792-00 "Standard Test Methods for Density and Specific Gravity (Relative Density) of Plastics by Displacement" to measure the density of the materials [62]. By following the ASTM method, the density of the material was measured by using the density determination kit on the digital balance. The density of the material was determined by comparing the weight of the foamed sample in air and in water. According to ASTM D792, the following equation was used to determine the relative density ($\varphi$) of the foamed samples:

$$\varphi = \frac{w(air) * \rho(H_2O)}{0.99983[w(air) - w(H_2O)]} + 0.0012 g/cm^3 \quad (3.2)$$

where $\varphi$ is the relative density of the foamed sample, $w(air)$ is the weight of the foamed sample in air, $w(H_2O)$ is the weight of the foamed sample in water, and $\rho(H_2O)$ is the density of the water.

Equation 3.2 was used for the foamed samples with the density less than 1g/cm$^3$. Other fluids can also be used to determine the relative density of the foam by using Equation 3.2 when the density of the fluid is known.

### 3.2.5 Mechanical Testing

The tensile mechanical properties of microcellular TPO foams were tested following the ASTM D638 on an Instron 4465 mechanical testing machine at room temperature without using the extensometer. The capacity of the load cell is 5kN. The displacement

rate of the crosshead was 10mm per minute [92]. A pair of 5kN wedge action grips were used to hold the samples. After each testing, the imprint pattern on the samples showed that the slippage in the grip during the testing was kept to a minimum. Therefore, the effect of slippage in the grip and the deflection on the cross head on strain rate was neglected in this study. TPO foam samples used for tensile testing had a thickness ranging from 3mm to 4mm, depending on the expansion ratio of the sample under various foaming conditions. Figure 3-2 shows the dimension of the microcellular TPO foamed sample for the tensile test. The tensile strength was calculated as the load force divided by the initial cross-sectional area of the specimen. The strain was calculated as the elongation divided by the initial length of a specimen. Three tensile properties were determined from the resultant stress-strain curves for each foaming condition: modulus of elasticity, tensile strength and strain at break. The modulus of elasticity was obtained by calculating the slope of the stress-strain curves in the elastic region. The elongation at break of a sample was calculated in terms of percent elongation. A minimum of five specimens were tested for each set of foaming conditions. The average value of each foaming condition was reported in this study.

## 3.3 Results and Discussion

Closed cell TPO foams with average cell sizes in the microcellular level were obtained. The effect of processing conditions on the foam morphologies was investigated. The foam morphologies were characterized in terms of their average cell density, average cell size and foam density. A detailed discussion is provided on the effect of each processing condition: saturation pressure, foaming time and foaming temperature, as well

as the effect of TPO composition. The mechanical properties such as elastic modulus, tensile strength, and elongation at break are presented for different cell morphologies of the microcellular TPO foams.

### 3.3.1 Crystallization Behaviour of TPO Materials

The thermal behavior of TPO materials was examined. The thermal behaviour (in terms of melting temperature, crystallization temperature, and heat of fusion and percentage crystallinity) of various TPO materials is summarized in Table 3-2. Table 3-2 shows that both melting and crystallization temperatures of various TPO materials are not influenced by the percentage content of engage and additive in the TPO materials. Therefore, the melting and crystallization temperature of various TPO materials is dominated by the thermal behaviour of the PP.

However, the heat of fusion of various TPO materials was influenced by the composition of the TPO material. The heat of fusion decreased with the PP content in the material. As the PP content in the material decreased, the degree of crystalline in the polymer matrix decreased, causing the heat of fusion to decrease. Furthermore, the heat of fusion of DTPO was decreased by addition of additive. The heat of fusion of DTPO decreased 20% as compare to the TPO70.

The crystallinity of TPO was estimated by using the heat of fusion (209J/g) of 100% crystalline PP [93-95]. In Table 3-2, the crystallinity decreased from 46.4% to 24.5% as the PP content decreased from 100% to 50% in the TPO material. There was an additional 10% decrease in crystallinity for the materials with 10% additive. Since the gas solubility in the material matrix increased as the crystallinity decreases, the material with

low crystallinity is desirable to foam by using batch foaming method. Therefore, the formability of DTPO and TYC735X could be relatively higher than TPO90 and TPO70. Table 3-3 shows the heat of fusion and the crystallinity of the PP phase in TPO materials. The heat of fusion of the PP phase in TPO materials was calculated by removing the contribution of the rubber phase in the weight and the enthalpy so that the heat of fusion of PP remained only with respect to the weight of the PP. By doing so, the crystallinity of PP phase in various TPO materials was constant at approximately 50% as shown in the Table 3-3. Therefore, this indicated that the crystallinity of PP phase was not influenced by the percentage content of engage in TPO materials.

### 3.3.2 Effect of Saturation Pressure on Cell Morphology

In order to study the effect of saturation pressure on the cell morphologies, the other two processing parameters were fixed. The foaming temperature of 150°C was selected to ensure the foaming temperature is below the melting point of these TPO composites. Figure 3-4 shows that the cell density slightly increased as the saturation pressure increased from 13.8MPa to 27.6MPa. As the saturation pressure increased, the solubility of $N_2$ in the TPO matrix also increased at room temperature. This resulted in an overall increase of $N_2$ gas content in the saturated polymer-gas mixture. The increased amount of gas in turn increased the number of nucleation sites and therefore the average cell density was increased as well [2, 91]. Thus, the increased cell density proved that the solubility of the gas under various pressures was a major factor in controlling the foam nucleation. In general, the cell density of various TPO materials remains in the order of $10^9$-$10^{10}$cells/cm$^3$. Therefore, the effect of saturation pressure on cell density was not

significant in this case.

The effect of saturation pressure on the average cell size was shown in Figure 3-5. It can be observed that the average cell size of TPO50 slightly decreased as the saturation pressure increased. Due to the fact that the number of nucleation sites increased as the pressure increases, the increased cell density resulted in the decrease of average cell size. Previous studies report that the average cell size decreased with increasing saturation pressure for microcellular PMMA [96], polystyrene [97] and PMMA-polystyrene composite [98] foams. However, the effect of saturation pressure on average cell size was not noticeable for TPO70, TPO50 and DTPO.

Figure 3-6 shows that the relative foam density decreased as the saturation pressure increased. It was found that as the saturation pressure increases, the amount of $N_2$ content in the polymer matrix also increases, which leads to a higher volume expansion, causing the density of the TPO foams to decrease. As the saturation pressure doubled from 13.8MPa to 27.6MPa, the volume expansion ratio of microcellular TPO foams increased approximately 5-10% at long foaming time. As a result, the effects of saturation pressure on foam density of microcellular TPO foams are significant as clearly shown in these experiments. In order to minimize the deterioration of the mechanical properties of microcellular TPO foams, the highest saturation pressure (27.6MPa) was selected for the other experiments since the relative density of microcellular TPO foams was minimized.

### 3.3.3 Effect of Foaming Time on Cell Morphology

The effects of foaming time on the cell morphologies of microcellular TPO foams are presented in Figure 3-8 - Figure 3-9. The effect of foaming time on average cell

density was shown in Figure 3-7. The cell density first slightly increased at early foaming stage. This demonstrates that the cell nucleation can be slightly improved by heating the sample above the glass-transition temperature upon the rapid depressurization for various TPO materials. The cell density reaches the maximum at a specific foaming time depending on the foaming temperature and TPO compositions and then remains constant. For TPO50, the cell density slightly decreased at longer foaming time due to cell coalescences. As the cells continue to grow, some eventually meet each other to form a large cell, resulting in the increases of cell size and the decreases of cell density. However, the cell density of various TPO materials remains in the order of $10^9$-$10^{10}$cells/cm$^3$. Therefore, the effect of foaming time on cell density is not significant.

As shown in Figure 3-8, the average cell size of various TPO materials slightly increased with the foaming time. As the foaming time increases, the viscosity of the polymer decreases and as the diffusivity of the gas from polymer matrix increases cell growth is promoted. This phenomenon illustrates that the cell nucleation stage was dominant during the early foaming stage and the cells continue to grow during continuous exposure of the samples to heat. At 150°C foaming temperature, the average cell size grew approximately 65% for TPO90, 150% for TPO70, 450% for TPO50 and 270% for DTPO in the first 60s of foaming time. In addition, the rate of cell growth reduces with the increases of foaming time. According to the dynamics of foam growth [**10**], the rate of cell growth decreases as the concentration of $N_2$ in the gas-polymer matrix decreases and the cell grows larger and larger. For TPO70, TPO50 and DTPO, much of the cell growth takes place within the first 60s of foaming at lower foaming temperature. Beyond this time, the cell size and the microstructures of the foams do not

appear to change significantly.

Analyzing the graphs in Figure 3-9, it can be seen that the foam density of microcellular TPO70 foams decreased as the foaming time increased, since the volume expansion ratio increased as the cell size increased. Similar results were observed for TPO90, TPO50 and DTPO. Therefore, the foaming time is a major factor in controlling the relative density of the TPO foams [**2**].

### 3.3.4 Effect of Foaming Temperature on Cell Morphology

The effects of foaming temperature on the cell morphologies of microcellular TPO foams are presented in Figure 3-7 - Figure 3-9. To study the effects of foaming temperature, the foaming time and saturation pressure were fixed at 40 seconds and 27.6MPa, respectively.

Figure 3-7 shows the effect of foaming temperature on the cell density of the microcellular TPO foams. Figures 3-10 shows some SEM micrographs of TPO70 processed at 30s of foaming time and various foaming temperatures. For TPO70, the cell density did not change notably when the foaming time was fixed at 30s. By observing Figure 3-7, the cell density remains in the order of $10^9$-$10^{10}$cells/cm$^3$ for various TPO materials. Therefore, the effect of foaming temperature on cell density is not significant.

Figure 3-8 shows the effect of foaming temperature on average cell size. The average cell size increased as the foaming temperature slightly increased from 130°C to 170°C. This phenomenon arose because the mobility of the polymer chains increased and the polymer viscosity decreased [**63**]. Furthermore, the movement of $N_2$ gas was more active at high temperatures, resulting in the promotion of cell growth [**51**]. Similar results

can be observed for TPO90 and TPO50 in Figure 3-8.

Figure 3-9 shows the effects of foaming temperature on the relative foam density of the microcellular TPO foams. The relative foam density decreased as the foaming temperature increased, reaching a minimum decrease of approximately 0.76 at 170°C for TPO70, 0.9 at 180°C for TPO90, 0.8 at 150°C for TPO50 and 0.85 at 170°C for DTPO. These results were consistent with the slight increase in both the average cell size and cell density as mentioned before.

As the foaming temperature further increases, the relative foam density increases. For instance, the relative foam density of TPO70 increased from the minimum of 0.76 at 170°C to 0.85 at 180°C. The reason for this phenomenon is that, as the foaming temperature increases too much beyond the melting point of the polymer, the mobility of the polymer chains increases while the chain stiffness and viscosity decrease. This means that $N_2$ gas molecules diffused out of the polymer matrix instead of supporting the desired cell nucleation and growth [**63**]. As a result, the cells in the foam structure collapse as the foaming temperature increases too much beyond the melting point of the polymer material. Similar results are observed for TPO90, TPO50 and DTPO in Figure 3-9. Overall, the optimal foaming temperature was found to be at 170°C in order to obtain the maximum high volume expansion ratio of the foams.

### 3.3.5 Effect of the TPO Composition on Cell Morphology

The effects of TPO composition on the cell morphologies of microcellular TPO foams are presented in Figure 3-7 - Figure 3-9. The average cell size slightly increases as the rubber content in the TPO composite increases. Since the interface between PP and

rubber phase is relatively week, the energy needed to grow the cells in the interface is much less than in the matrix of the materials. As a result, the cell size increases as the rubber content increases. In addition, the increased amount of rubber phase in the TPO matrix also reduced the stiffness and viscosity of the material which in turn increases the average cell size in the microstructure.

Analyzing the graphs in Figure 3-9, the relative foam density of TPO foams decreased from the minimum 0.9 to 0.75 as the PP content in the TPO composite decreased from 90% to 70%, respectively. However, the relative foam density of TPO50 increased to the minimum of 0.8. This is due to the cell density of TPO50 reduced in the order of $10^9$cells/cm$^3$ which affects the overall volume expansion of the microcellular foamed TPO50. Overall, the cell morphologies of microcellular TPO foams vary with the TPO composition under the same processing parameters. However, the effects of processing parameters on the cell morphologies of the different TPO composites share a similar trend.

### 3.3.6 Effect of Processing Parameters on Cell Morphology

The effect of processing parameters on relative foam density is shown in Figure 3-9. Microcellular foam material was used to minimize material consumption for various engineering applications. The relative foam density of the microcellular foam describes the amount of material that has been consumed compared to the unfoamed material. Thus, a desired relative foam density of the microcellular TPO foams can be obtained by altering processing parameters. As seen in Figure 3-9, by drawing a horizontal line parallel to the x-axis at the desired relative foam density, the desired relative foam density

of microcellular TPO foams can be produced by various combinations of foaming time and foaming temperature. Table 3-4 shows the desired weight reduction of TPO materials can be achieved by different combination of foaming time and foaming temperature. Similarly, various relative foam densities of microcellular TPO foams can be achieved by drawing a vertical line parallel to the y-axis at the desired foaming time on Figure 3-9. In this manner, a set of constant relative foam densities of microcellular TPO foams can be achieved by altering the processing parameters to suit the requirements of different applications.

### 3.3.7 Effect of Foaming Conditions and Cell morphology on Mechanical Properties

The effect of foaming time and foaming temperature on the engineering stress-strain curves of microcellular TPO foams is shown in Figures 3-11 and Figures 3-12 respectively. In order to study the effect of foaming time in Figures 3-11, the foaming temperature was fixed at 150°C. Figures 3-12 studies the effect of foaming temperature where the foaming time was fixed at 30s. The error of these stress-strain curves for each foaming condition was less than 10%.

The foaming time and its effect on the engineering stress-strain curve of Microcellular TPO foams can be observed from Figures 3-11. More additional graphs illustrated in Figure 3-13 - Figure 3-15 show the effect on elastic modulus, tensile strength and the elongation at break for TPO90, TPO70, TPO50 and DTPO. The mechanical properties such as elastic modulus and tensile strength decreased with foam density. These results were expected since a decrease in relative foam density means that

the actual material per unit volume decreases and the material reduce its weight. However, the elongation at break of the TPO foams increases as the foam density decreases at first. One explanation for this phenomenon is that it is a result of the small bubbles blunting the crack tips which increased the energy needed to propagate the crack [**51**]. These results show that the toughness of the resultant TPO foams was improved by introducing microcellular structures with high cell density in the material. The elongation at break decreased at longer foaming times since the $N_2$ gas molecules would diffuse out of the polymer matrix under extended foaming time.

By observing Figures 3-12(b), the elastic modulus and the tensile strength decrease as the foaming temperature increase for microcellular TPO70 foams. Similar results are observed for TPO90, TPO50 and DTPO. In general, the elongation at break increases as the foaming temperature increases. However, as the foaming temperature further increased, the elastic modulus, tensile strength and relative foam density increased quickly. This is due to the foaming temperature increasing too much beyond the melting point of the polymer as discussed before.

The effects of TPO composition on the elastic modulus, tensile strength and the elongation at break of TPO foams can be observed from Figure 3-13 - Figure 3-15. The mechanical properties such as elastic modulus and tensile strength decreased, as the PP content in the TPO composite deceased. By comparing the unfoamed TPO composites, the elastic modulus decreased from 400MPa (TPO90) to approximately 80MPa (TPO50) and the tensile strength decreased from 20MPa (TPO90) to approximately 6MPa (TPO50). These results were expected since the PP act as a plastic segment which contributes most of the mechanical strength of the TPO composites. By comparing

TPO90 and TPO50, the tensile modulus and tensile strength decreased as much as four times as PP content decreased 40%. As a result, the mechanical properties of the TPO composites are very sensitive to the PP content in the materials. Therefore, the percentage content of PP has to be carefully selected in order to maximize the mechanical properties of microcellular TPO foams.

By comparing TPO70 and DTPO, the tensile modulus of DTPO is approximately 10% higher than TPO70. This is attributed to the addition of mineral-filler in the material. The mineral-filler increased the friction and creates more residual stress in the molecular chain, resulting in higher stress needed to deform the material. This results shows that the modulus of elasticity can be improved by addition of an ingredient such as mineral-filler in TPO materials. However, the effect of mineral filler on the tensile strength was not noticeable.

From observing Figure 3-15, the elongation at break increased as the PP content in the TPO composites decreased. These results show that the elastomeric segment contribute the elastomeric properties. Therefore, the elongation at break increases with the content of elastomer in the TPO composite. Overall, the results prove that the TPO composites could improve the mechanical properties such as impact properties and scratch resistance as compare to the materials such as pure PP.

The graphs in Figures 3-16 - Figures 3-18 show the effect of relative foam density of the microcellular TPO foams on tensile modulus, tensile strength and elongation at break. It was observed that the tensile modulus and tensile strength decreased non-linearly as the relative foam density decreased. The tensile modulus and tensile strength values decreased approximately by half for TPO90, TPO70, TPO50 and DTPO, as the relative

foam density decreased from 1 (unfoamed) to the minimum.

For TPO70, comparing the unfoamed and foamed materials, the tensile strength decreased approximately 25% as the relative foam density decreased 25% from 1.0 to 0.75 as shown in Figures 3-17. Although this observation shows a one-to-one reduction ratio in tensile strength and relative foam density, once the material is foamed, the tensile strength decreased approximately only 13% as the relative foam density decreased 22% from 0.96 to 0.75. The rate of decrease in tensile strength reduced significantly after the material was foamed. Similar results were observed for TPO90 and TPO50. For DTPO, Both tensile modulus and tensile strength did not change notably from the relative foam density of 0.92 to 0.84. These results show that the weight reduction of TPO materials can be achieved without sacrificing much on the mechanical properties by introducing microcellular structure in TPO materials. Furthermore, the elongation at break increased linearly as the relative foam density decreased. The elongation at break of TPO70 increased from 27% to 45% as the relative foam density decreased from 1 to 0.75 as shown in Figures 3-18(b). Similar results were observed in TPO90 and TPO50 in Figures 3-18. For DTPO, the maximum elongation at break obtained at the high foam density region. The elongation at break remains similar to the unfoamed polymer as the relative foam density measures below 0.92. This may be due to the addition of residual stress in the molecular chain as it increases the elongation at break at high foam density. However, this residual stress reduced as the foam density decreases. Overall, these results show that the elasticity was improved by introducing a microcellular foam structure in the TPO materials.

By analyzing the foaming and mechanical behaviour of various TPO composites, the

TPO material with the PP to engage ratio of 7:3 is the optimal composition of the TPO material. In foamability, the TPO70 obtained the minimum relative density which is the maximum weight reduction of the materials. In mechanical properties, the TPO70 obtained the minimum rate of reduction of tensile strength as the foam density of the material decreases, as well as maintained a reasonable tensile modulus and tensile strength for automotive applications. Therefore, the TPO materials with PP to engage ratio of 7:3 was selected to further examine the effect of cell morphology on mechanical properties of the cellular TPO foams. In summary, the results obtained from this study show that a desired relative foam density and cell density with associated mechanical properties of four different TPO composites can be obtained by carefully altering the processing parameters as according to the structure-property relationships.

## 3.4 Constitutive Model for Microcellular TPO Foams

The structure-mechanical property of microcellular TPO foams was experimentally obtained in the pervious section. In this section, constitutive models were proposed to correlate the structure mechanical relationship of microcellular TPO foams. These constitutive models can help engineers predict the mechanical property of microcellular TPO foams prepared with different processing parameters.

The constitutive models proposed in this study were based on the constitutive models developed by Gibson and Ashby. The constants in the models were altered to fit the constitutive models in the experimental data. The proposed constitutive models relate the tensile modulus and tensile strength to the relative foam density of the microcellular TPO foams and were presented in the following sub-sections in detail.

### 3.4.1 Effect of Relative Foam Density on Tensile Modulus

The relative tensile modulus is defined as the tensile modulus of the foams over the tensile modulus of the unfoamed polymer. Figures 3-16 shows the effect of relative foam density on relative tensile modulus of microcellular foamed (a) TPO90, (b) TPO70, (c) TPO50 and (d) DTPO. The tensile modulus was found to be very closely related to the relative density of the foams. The dots plotted on the figures are the experimental data obtained in the previous section.

As shown in the Figures 3-16 the proposed constitutive models for microcellular TPO90 foams plotted in solid line in the Figures 3-16(a) are shown as follows:

TPO90:
$$\frac{E_f}{E_p} \approx 0.6\left(0.8\frac{\rho_f}{\rho_p}\right)^2 + (0.2)\left(\frac{\rho_f}{\rho_p}\right) \tag{3.3}$$

The constants $C_1 = 0.6$, $C_1' = 1$ and $\phi$ is 0.8 were used to fit the experimental results. However, the proposed constitutive model only, can predict the structure-tensile modulus relationship up to the relative foam density of 0.98. The relative tensile modulus significantly increased from the relative foam density of 0.98 to 1.

The proposed constitutive models for microcellular TPO70, TPO50 and DTPO foams were presented in Equation 3.4, Equation 3.5 and Equation 3.6 respectively as follows:

TPO70:
$$\frac{E_f}{E_p} \approx 0.75\left(0.8\frac{\rho_f}{\rho_p}\right)^2 + (0.2)\left(\frac{\rho_f}{\rho_p}\right) \tag{3.4}$$

TPO50:
$$\frac{E_f}{E_p} \approx 0.85\left(0.9\frac{\rho_f}{\rho_p}\right)^2 + (0.1)\left(\frac{\rho_f}{\rho_p}\right) \tag{3.5}$$

DTPO:
$$\frac{E_f}{E_p} \approx 0.70\left(0.8\frac{\rho_f}{\rho_p}\right)^2 + (0.2)\left(\frac{\rho_f}{\rho_p}\right) \tag{3.6}$$

The constants $C_1 = 0.75$, $C_1' = 1$ and $\phi$ is 0.8 were used for microcellular TPO70 foams. The constants $C_1 = 0.85$, $C_1' = 1$ and $\phi$ is 0.9 were used for microcellular TPO50 foams and the constants $C_1 = 0.70$, $C_1' = 1$ and $\phi$ is 0.8 were used for microcellular DTPO foams to fit the experimental data. These proposed constitutive models fit very well with the experimental data.

### 3.4.2 Effect of Relative Foam Density on Tensile Strength

The relative tensile strength is defined as the tensile strength of the foams over the tensile strength of the unfoamed polymer. Figures 3-17 show the effect of relative foam density on relative tensile strength of microcellular foamed (a) TPO90, (b) TPO70, (c) TPO50 and (d) DTPO. Similarly, the tensile strength of microcellular TPO foams was closely related to the relative density of the foams. The dots plotted on the figures were the experimental data obtained from the pervious section. The following equation is the constitutive model proposed for microcellular TPO90 foams as plotted in Figures 3-17(a):

TPO90:
$$\frac{\sigma_f}{\sigma_p} \approx 0.9\left(0.8\frac{\rho_f}{\rho_p}\right)^{\frac{3}{2}} + (0.2)\left(\frac{\rho_f}{\rho_p}\right) \tag{3.7}$$

The constants $C_5 = 0.9$, $C_5' = 1$ and $\phi$ is 0.8 were used to fit the experimental results. Similarly, this proposed constitutive model only, is able to predict the structure-tensile strength relationship up to the relative foams density of 0.98. The relative tensile strength

increased rapidly from the relative foam density of 0.98 to 1.

For TPO70, the proposed constitutive model (Equation 3.8) based on Gibson and Ashby's model was plotted as the dash line in Figure 3-22(b):

$$\frac{\sigma_f}{\sigma_p} \approx \left( 0.8\frac{\rho_f}{\rho_p} \right)^{\frac{3}{2}} + (0.2)\left( \frac{\rho_f}{\rho_p} \right) \tag{3.8}$$

The constants $C_5 = C_5' = 1$ and $\phi$ is 0.8 were used to fit the experimental results. However, Equation 3.8 underestimated the tensile strength of microcellular TPO70 foams at a low density region. This is due to the fact that the constitutive model developed by Gibson and Ashby was based on the experimental data obtained from conventional foams, which have the cell sizes ranging approximately from 50μm to 100μm. As a result, this model underestimated the mechanical performance of microcellular foams. Therefore, the empirical formula was proposed according to the experimental data of this:

TPO70:
$$\frac{\sigma_f}{\sigma_p} \approx 0.75\left( 0.8\frac{\rho_f}{\rho_p} \right)^{\frac{1}{2}} + (0.2)\left( \frac{\rho_f}{\rho_p} \right) \tag{3.9}$$

The formula was plotted as the solid line in Figure 3-27(b) and it fit the experimental results very well.

Finally, the proposed constitutive models for microcellular TPO50 and DTPO foams were shown in Equation 3.10 and Equation 3.11 respectively as follows:

TPO50:
$$\frac{\sigma_f}{\sigma_p} \approx \left( \frac{\rho_f}{\rho_p} \right)^{\frac{3}{2}} \tag{3.10}$$

DTPO:
$$\frac{\sigma_f}{\sigma_p} \approx \left( 0.8\frac{\rho_f}{\rho_p} \right)^{\frac{3}{2}} + (0.2)\left( \frac{\rho_f}{\rho_p} \right) \tag{3.11}$$

The constants $C_1 = C_1' = 1$ and $\phi$ is 1 were used for microcellular TPO50 foams and the constants $C_1 = C_1' = 1$ and $\phi$ is 0.8 were proposed to fit the experimental data for microcellular DTPO foams. These proposed constitutive models fit the experimental results very well.

## 3.5 Conclusion

In this chapter, a two-stage batch process was used to prepare closed cell microcellular TPO foams. The effects of processing parameters on the cellular morphologies of microcellular TPO foams were investigated. The experimental results show that the effect of processing parameters on average cell size and cell density of microcellular TPO foams was not significant. The relative foam density of the microcellular TPO foams was inversely proportional to saturation pressure, foaming temperature and foaming time. A minimum relative foam density of 0.75 was obtained under a saturation pressure of 27.6MPa for TPO70. Higher saturation pressures are necessary to further decrease the relative foam density of the microcellular TPO foams.

The mechanical properties of the microcellular TPO foams are directly related to the processing parameters which vary the cell morphology. The results show that the tensile strength of TPO70 decreased only approximately 13% as the relative foam density decreased 22%. Similar results were observed on other three TPO composites. Therefore, the weight reduction of TPO material can be achieved without sacrificing much of the mechanical properties by introducing microcellular structure in TPO materials. Under the same processing parameters, the cell morphologies and mechanical properties of TPO foams vary with the TPO composition. However, the results show that the effects of

processing parameters on the cell morphologies and mechanical properties of the different TPO composites share a similar trend.

The constitutive models were proposed to relate the tensile mechanical property to the relative density of microcellular TPO foams. The mechanical property was very closely related to the relative density of the foams. For TPO70, the constitutive models developed by Gibson and Ashby underestimated the tensile strength of the microcellular TPO foams. Therefore, a new constitutive model was proposed for microcellular TPO70 foams. Overall, the proposed constitutive models fit the other microcellular TPO foams very well.

In summary, the microstructure of TPO foams can be controlled effectively by carefully altering the foaming parameters. Lightweight TPO material for various applications can be achieved with various foam densities and cell densities producing diverse mechanical properties of microcellular TPO foams.

Table 3-1: The solubility and diffusivity of various TPO materials.

| Materials | Solubility ($g_{N2}$/ $g_{polymer}$) | Diffusivity ($cm^2/s$) |
|---|---|---|
| PP 7805 | 0.02200 | $1.03869 \times 10^{-06}$ |
| TPO90 | 0.02036 | $0.99843 \times 10^{-06}$ |
| TPO70 | 0.01708 | $0.91794 \times 10^{-06}$ |
| TPO50 | 0.01380 | $0.83743 \times 10^{-06}$ |
| Engage 8130 | 0.00560 | $0.636174 \times 10^{-06}$ |

Table 3-2: Thermal behaviour of TPO materials.

| Material | Melting Temperature (°C) | Crystallization Temperature (°C) | Heat of Fusion (J/g) | Percentage Crystallinity (%) |
|---|---|---|---|---|
| PP | 166 | 135 | 97 | 46.4 |
| TPO90 | 166 | 130 | 88 | 42.1 |
| TPO70 | 166 | 131 | 73 | 34.9 |
| TPO50 | 165 | 128 | 51 | 24.5 |
| DTPO | 166 | 134 | 54 | 25.8 |
| TYC735X | 166 | 130 | 59 | 28.2 |

Table 3-3: Thermal behaviour of TPO materials with respect to PP phase only.

| Material | Heat of Fusion (J/g) | Percentage Crystallinity (%) |
|---|---|---|
| PP7805 | 102 | 49 |
| TPO90 | 98 | 47 |
| TPO70 | 105 | 50 |
| TPO50 | 103 | 49 |

Table 3-4: The effect of foaming parameters on weight reduction of TPO70.

| Percent Weight Reduction | Foaming Temperature (°C) | Foaming Time (s) |
|---|---|---|
| 5% | 130 | 25 |
| | 150 | 15 |
| | 170 | 5 |
| 10% | 130 | 32 |
| | 150 | 23 |
| | 170 | 15 |
| 15% | 130 | 50 |
| | 150 | 35 |
| | 170 | 22 |
| 20% | 130 | N/A |
| | 150 | N/A |
| | 170 | 35 |

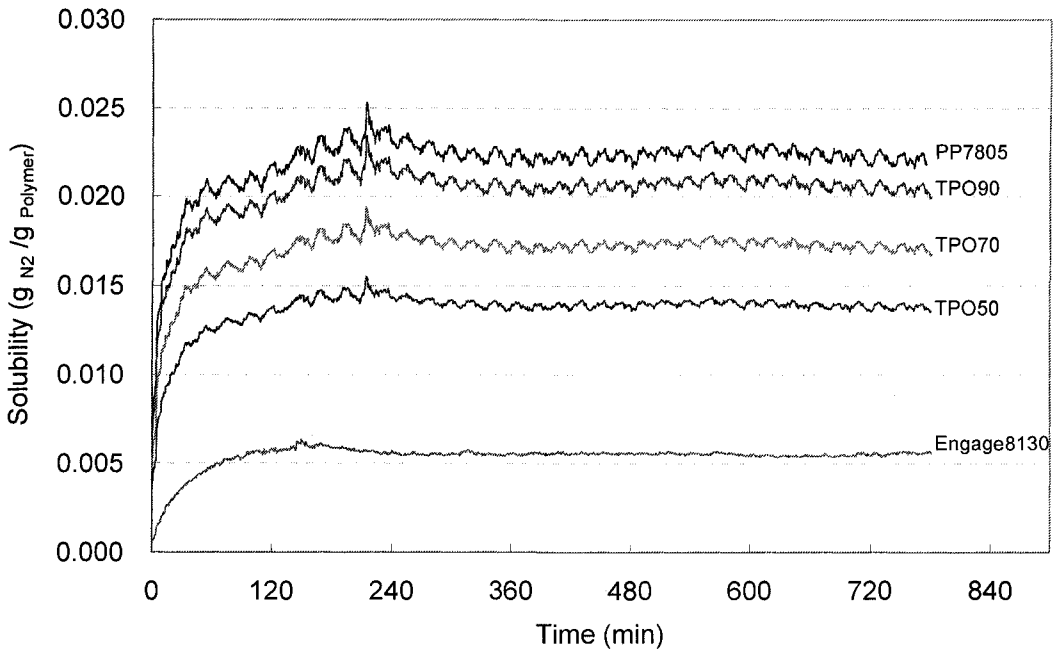


Figure 3-1: The dimension of the TPO samples (ASTM Type V)

| D638 | Type V (mm) |
|---|---|
| W | 3.18 |
| L | 9.53 |
| WO | 9.53 |
| LO | 63.5 |
| G | 7.62 |
| D | 25.4 |
| R | 12.7 |

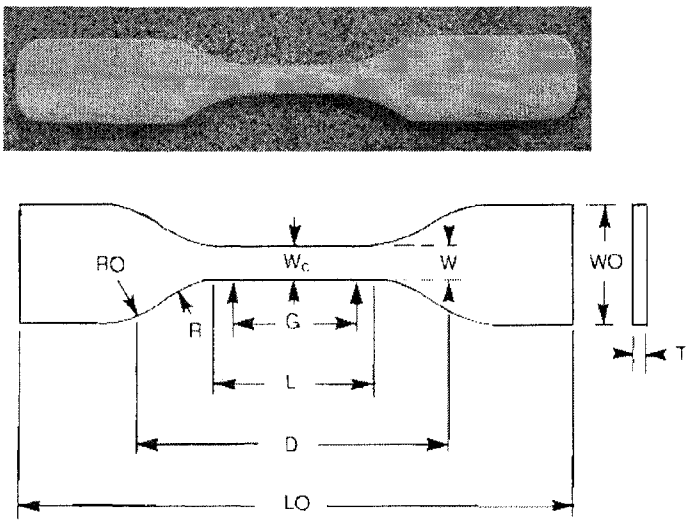


Figure 3-2: The dimension of the TPO samples (ASTM Type V)

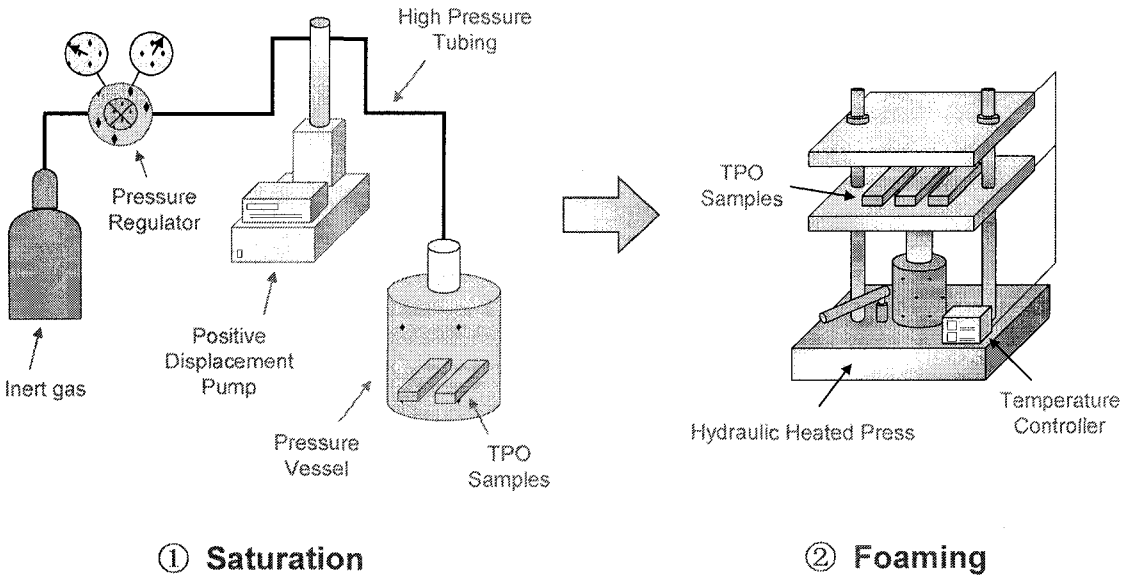


Figure 3-3: The schematics of batch foaming process

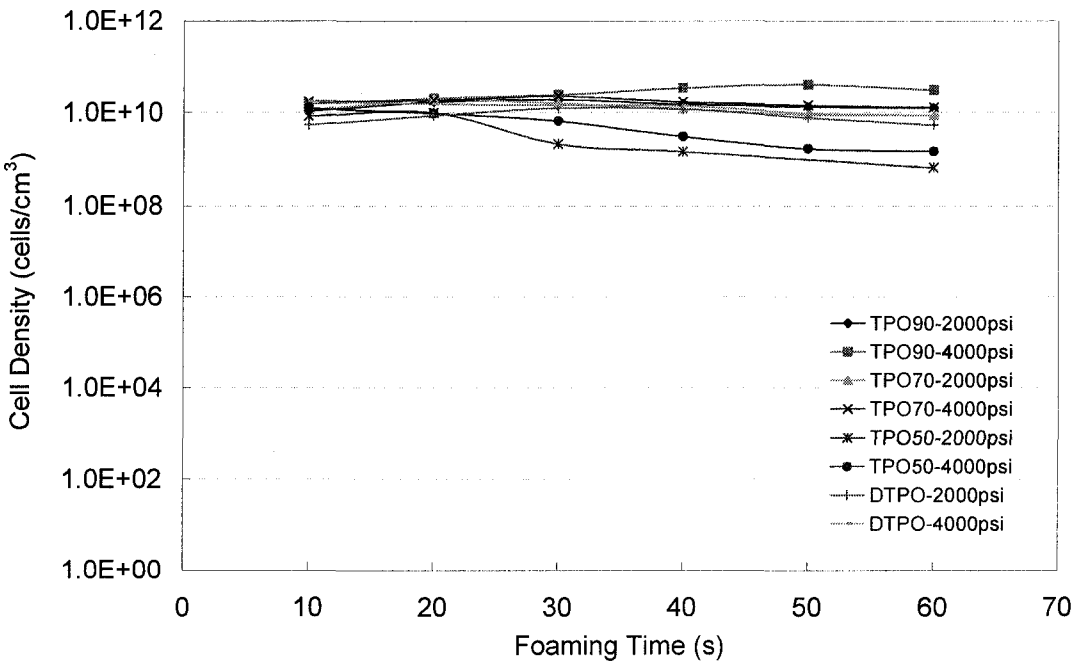


Figure 3-4: Effect of saturation pressure and foaming time on the cell density of microcellular foamed TPO90, TPO70, TPO50 and DTPO. (Foaming Temperature: 150°C)

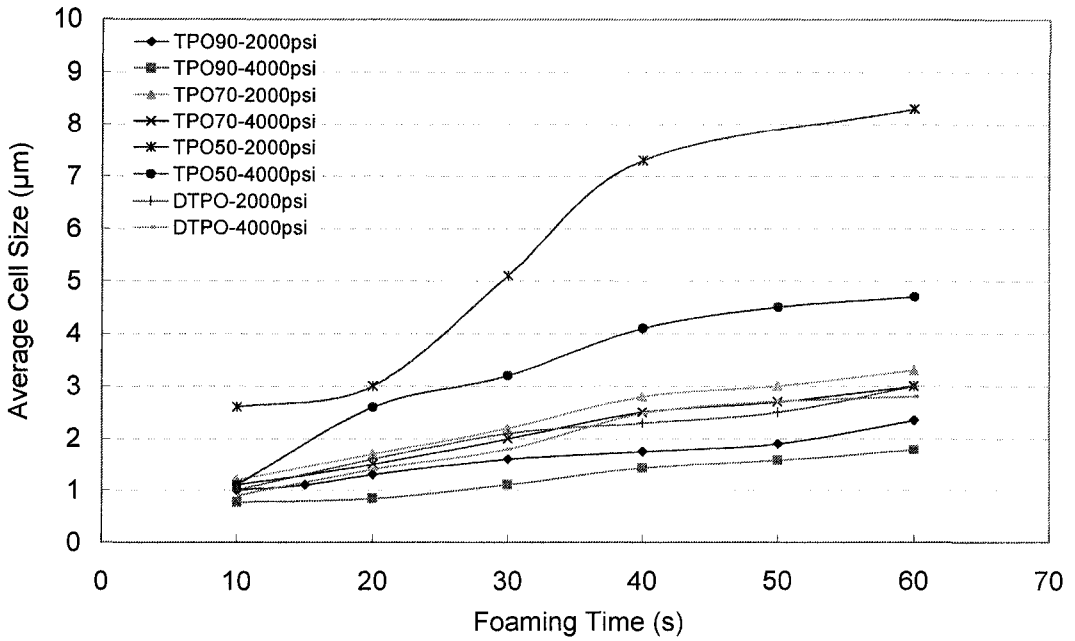


Figure 3-5: Effect of saturation pressure and foaming time on the average cells size of microcellular foamed TPO90, TPO70, TPO50 and DTPO. (Foaming Temperature: 150°C)

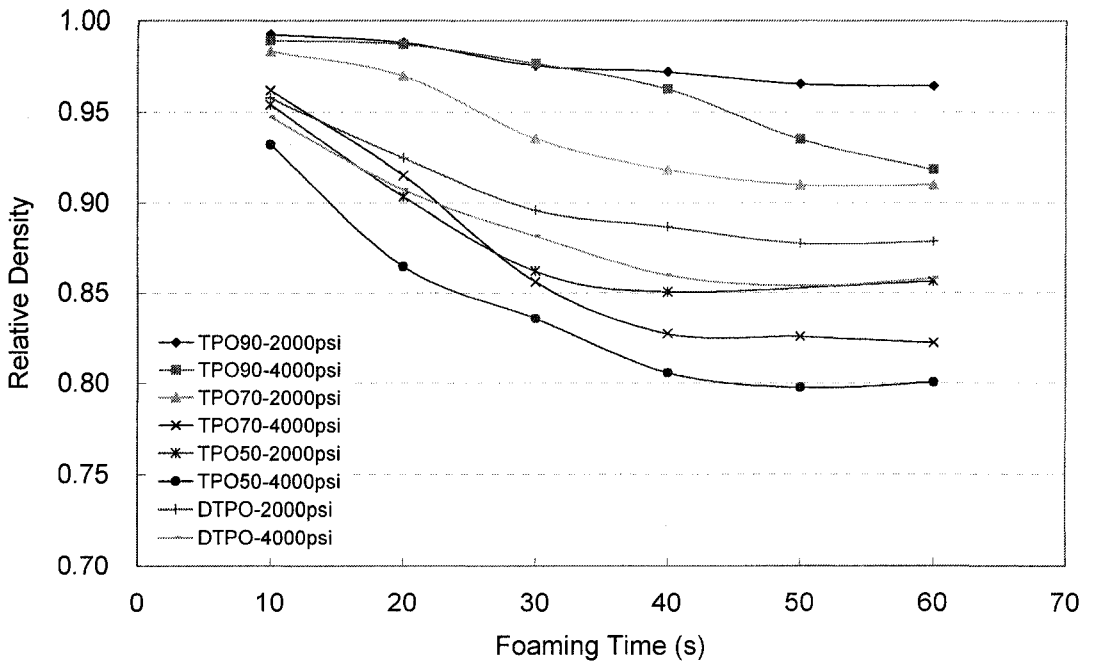


Figure 3-6: Effect of saturation pressure and foaming time on the relative density of microcellular foamed TPO90, TPO70, TPO50 and DTPO. (Foaming Temperature: 150°C)

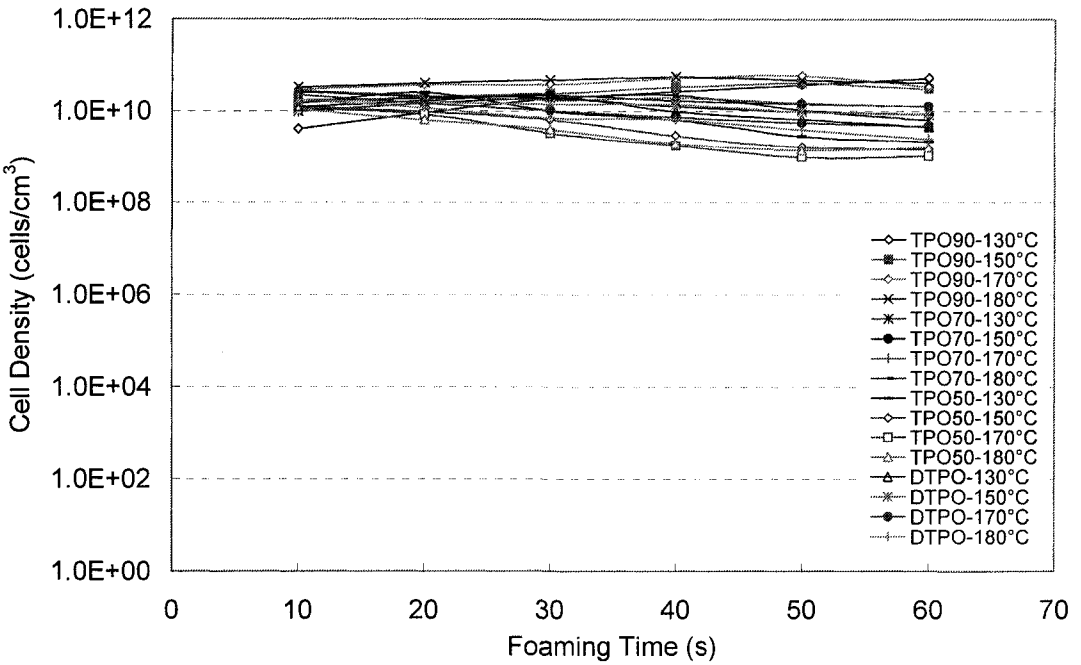


Figure 3-7: Effect of foaming temperature and foaming time on the cell density of microcellular foamed TPO90, TPO70, TPO50 and DTPO. (Saturation Conditions: 27.6MPa at RT)

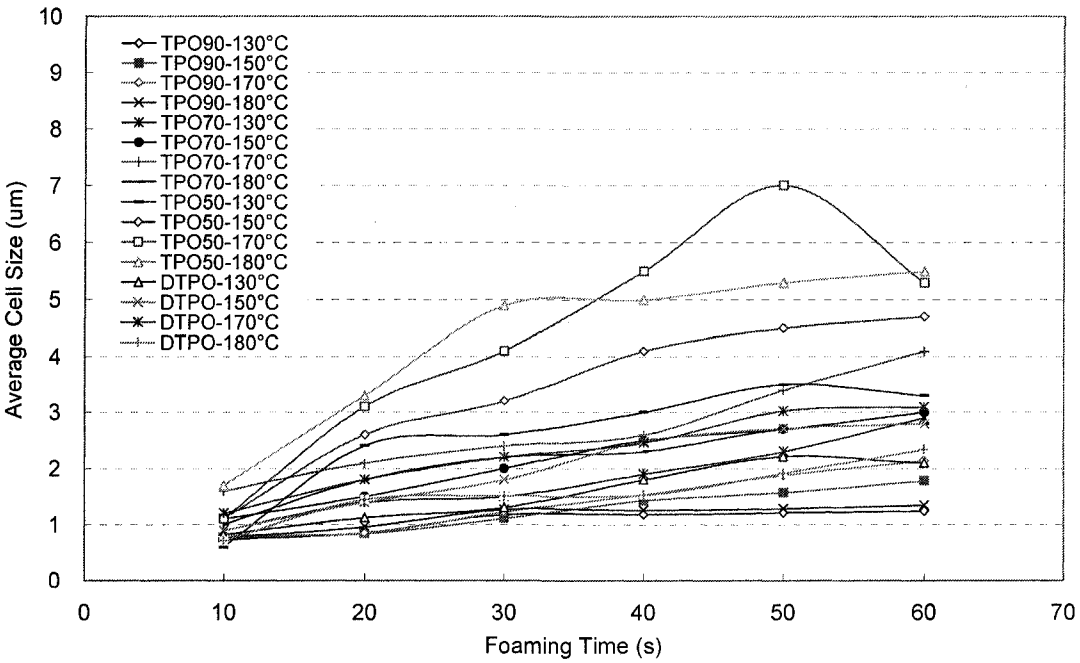


Figure 3-8: Effect of foaming temperature and foaming time on the average cell size of microcellular foamed TPO90, TPO70, TPO50 and DTPO. (Saturation Conditions: 27.6MPa at RT)

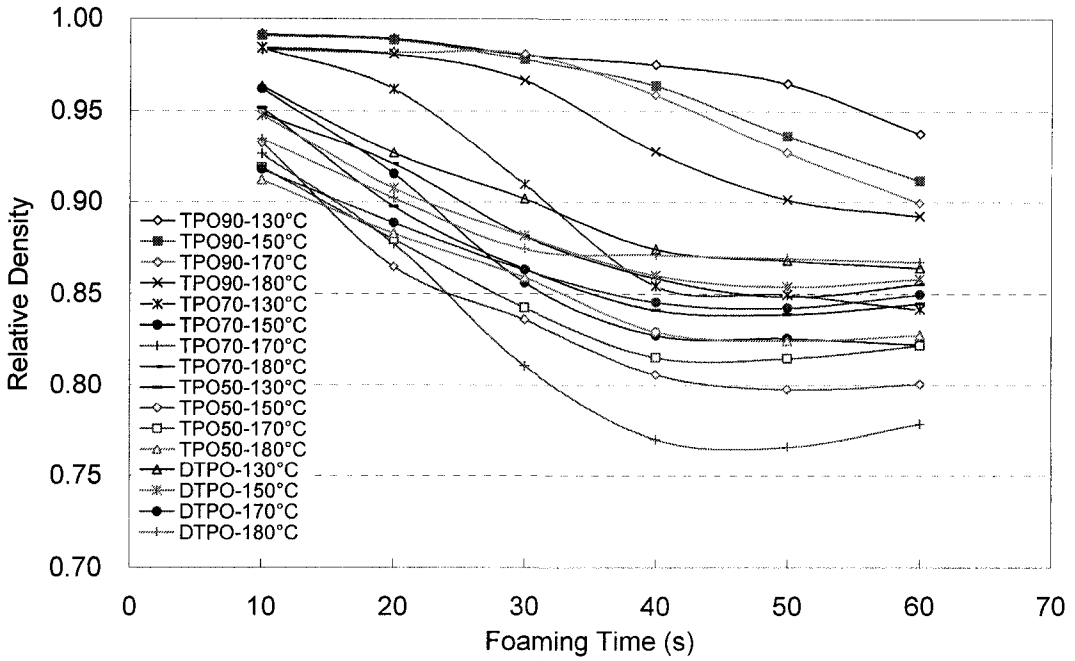


Figure 3-9: Effect of foaming temperature and foaming time on the relative density of microcellular foamed TPO90, TPO70, TPO50 and DTPO. (Saturation Conditions: 27.6MPa at RT)

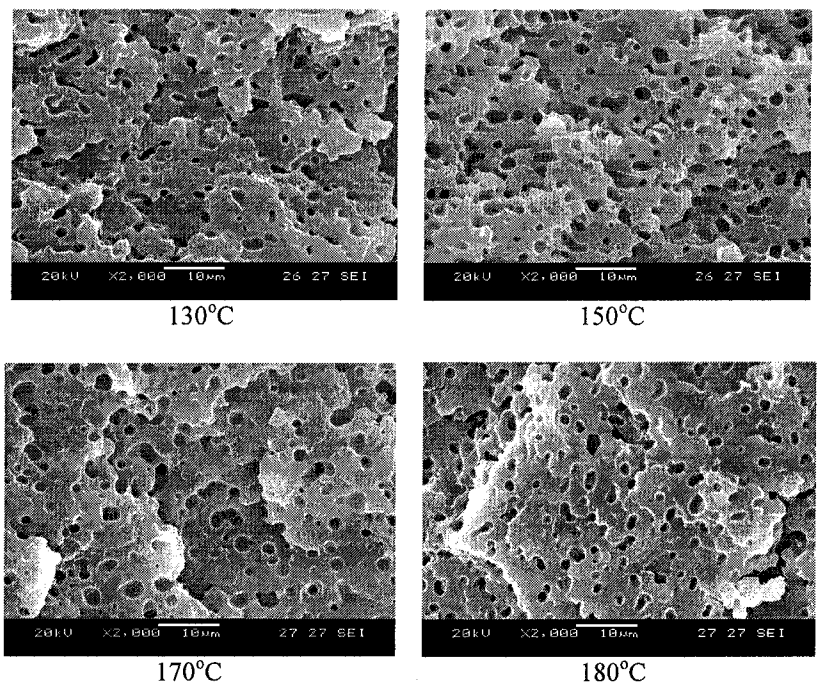


Figures 3-10: SEM micrographs for various foaming temperatures of microcellular foamed TPO70. (Saturation Conditions: 27.6MPa. Foaming Time: 30 seconds)

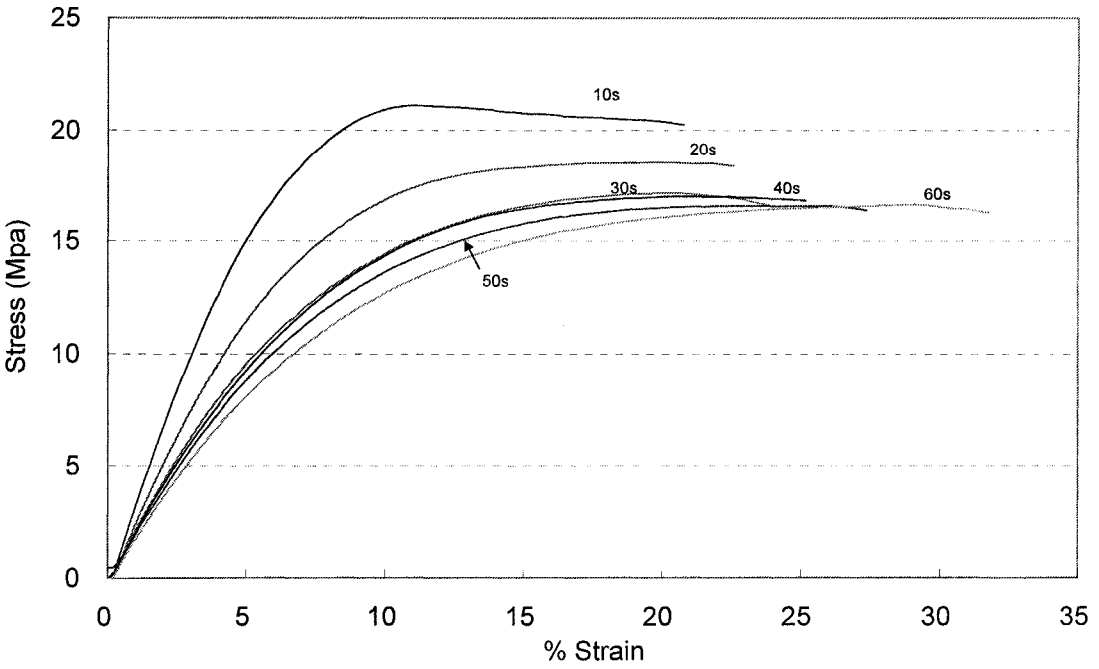


(a)

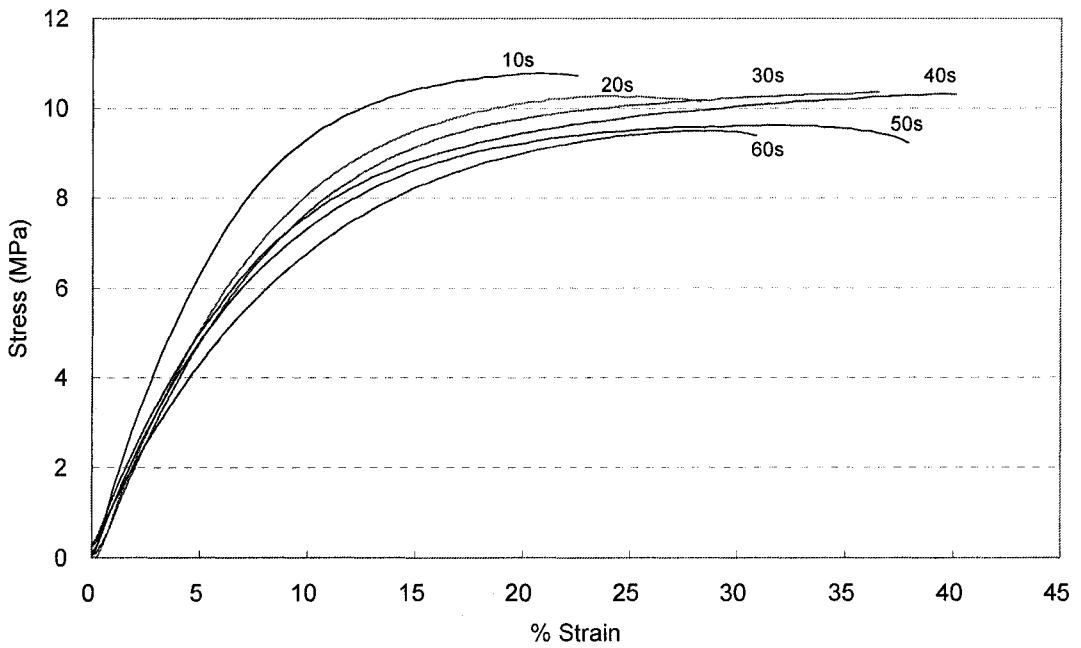


(b)

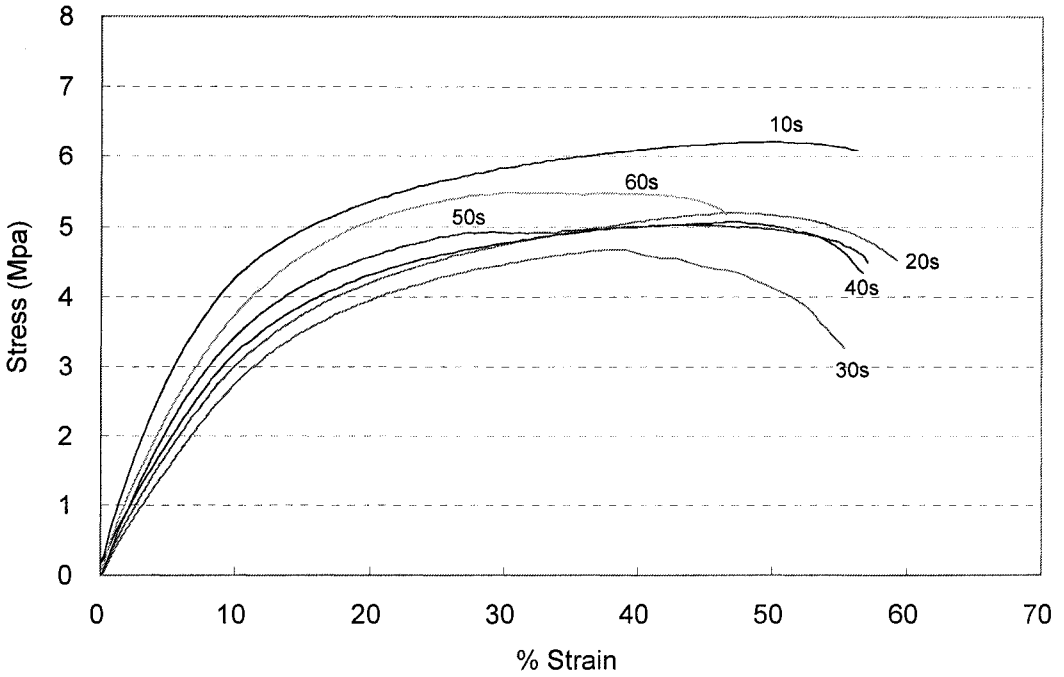


(c)

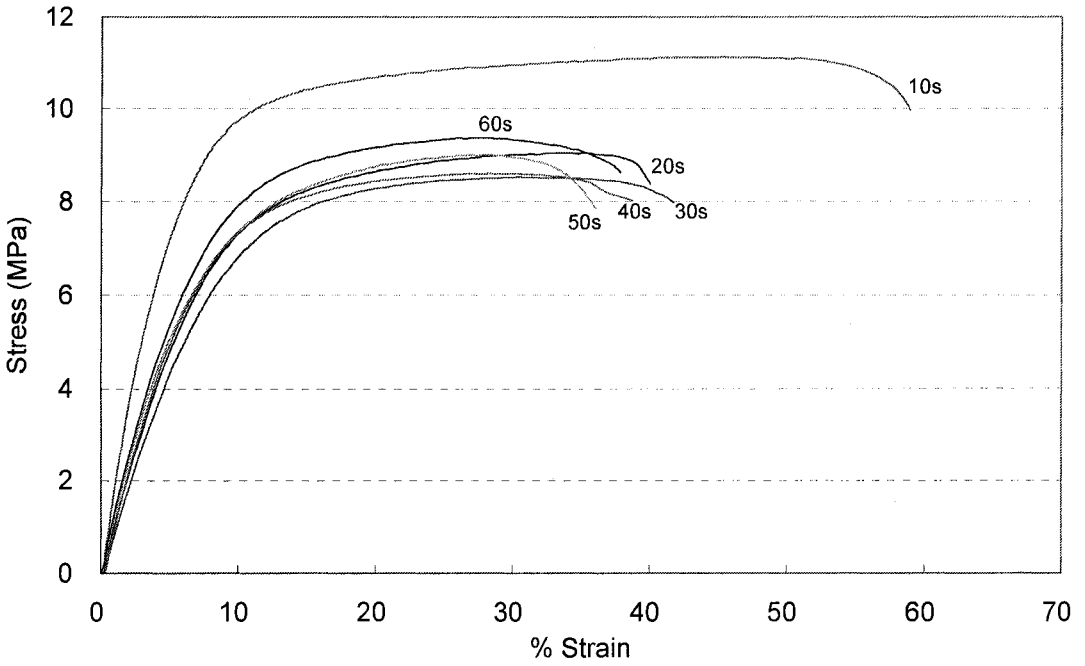


(d)

Figures 3-11: Effect of foaming time on the engineering stress-strain curves of microcellular foamed (a) TPO90, (b) TPO70, (c) TPO50 and (d) DTPO.
(Saturation Conditions: 27.6MPa at RT, Foaming Temperature:150$^{O}$C)

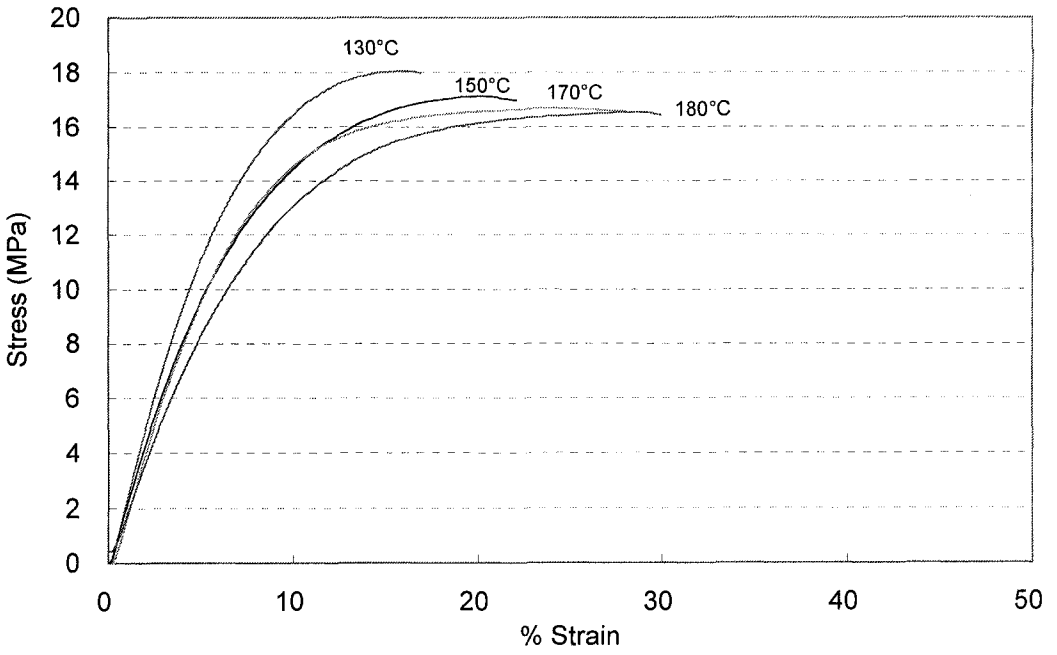


(a)

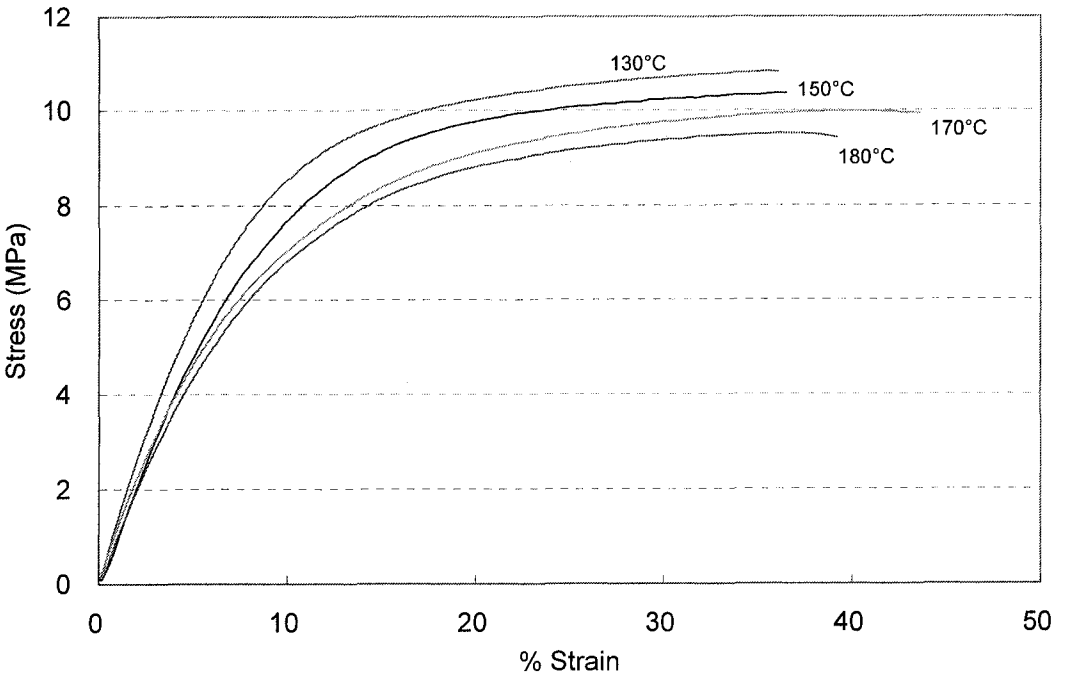


(b)

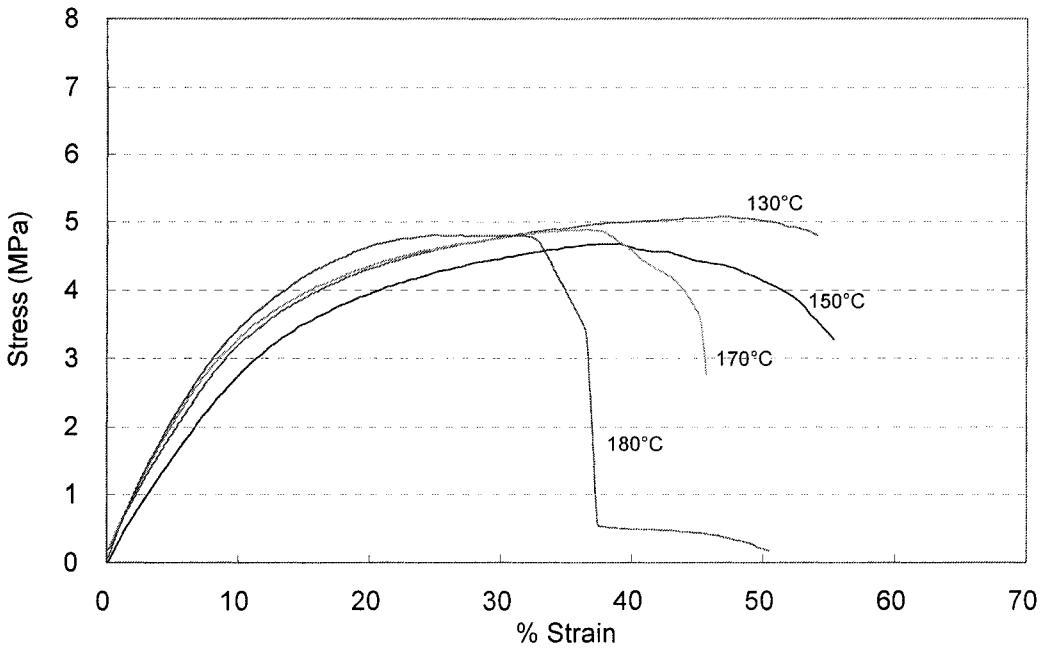


(c)

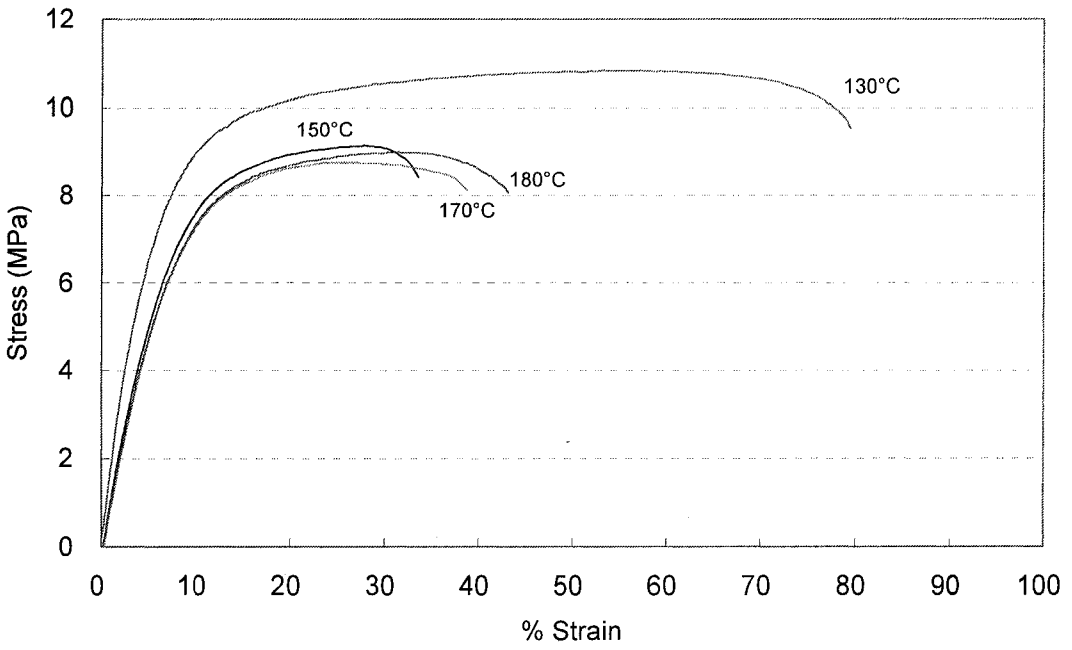


(d)

Figures 3-12: Effect of foaming temperature on the engineering stress-strain curves of microcellular foamed (a) TPO90, (b) TPO70, (c) TPO50 and (d) DTPO.
(Saturation Conditions: 27.6MPa at RT. Foaming time: 30s)

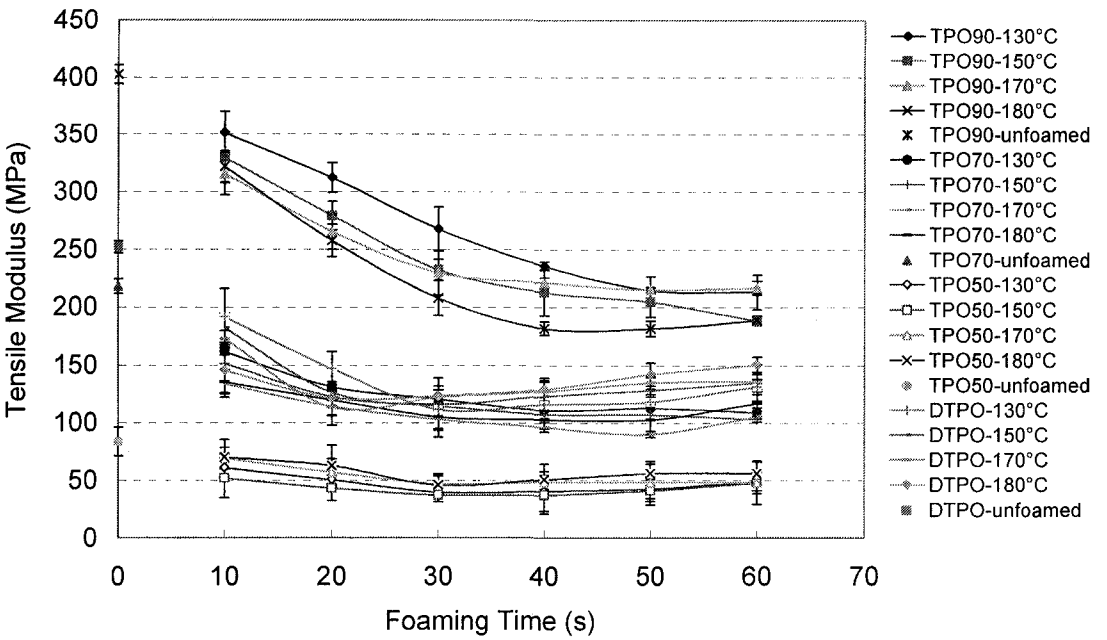


Figure 3-13: Effect of foaming temperature and foaming time on the tensile modulus of microcellular foamed TPO90, TPO70, TPO50 and DTPO. (Saturation Conditions: 27.6MPa at RT)

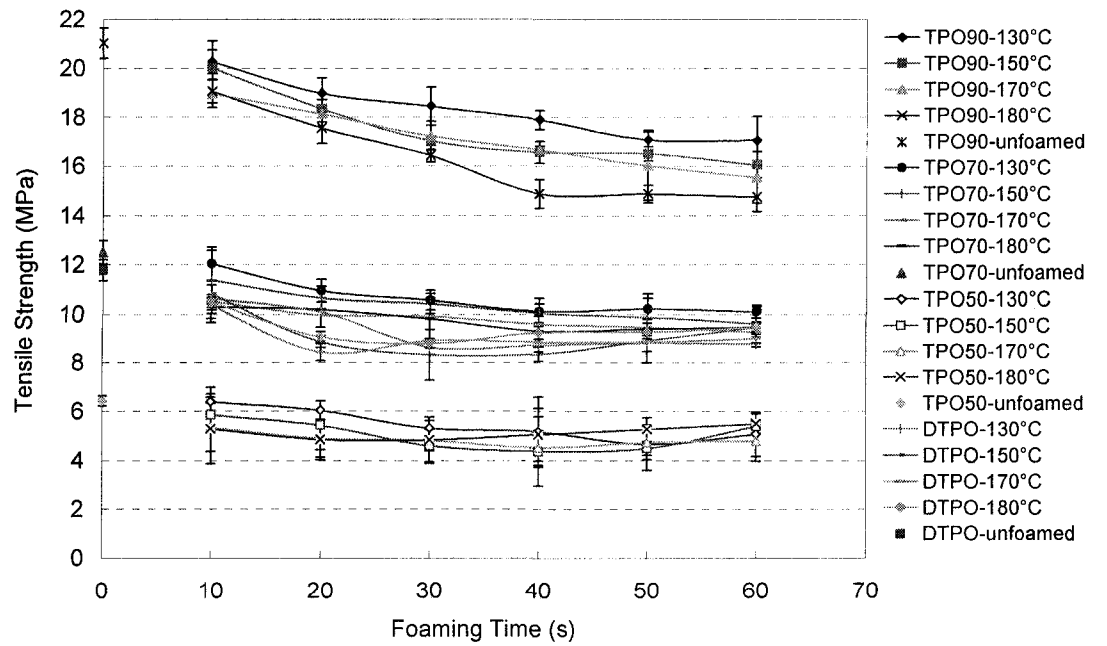


Figure 3-14: Effect of foaming temperature and foaming time on the tensile Strength of microcellular foamed TPO90, TPO70, TPO50 and DTPO. (Saturation Conditions: 27.6MPa at RT)

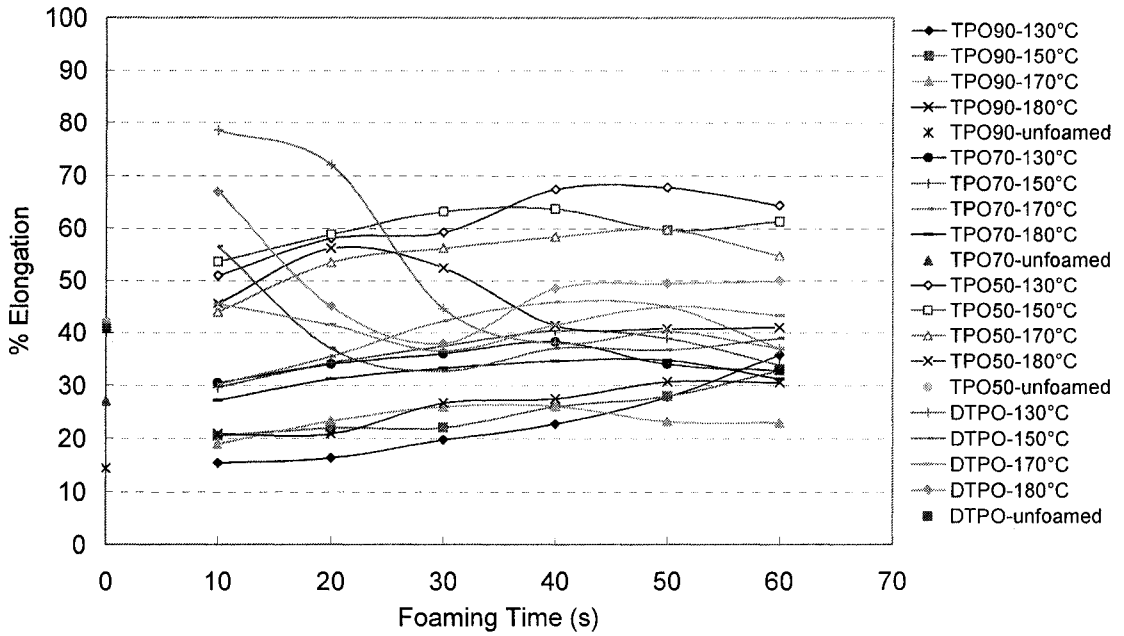


Figure 3-15: Effect of foaming temperature and foaming time on the percent elongation of microcellular foamed TPO90, TPO70, TPO50 and DTPO. (Saturation Conditions: 27.6MPa at RT)

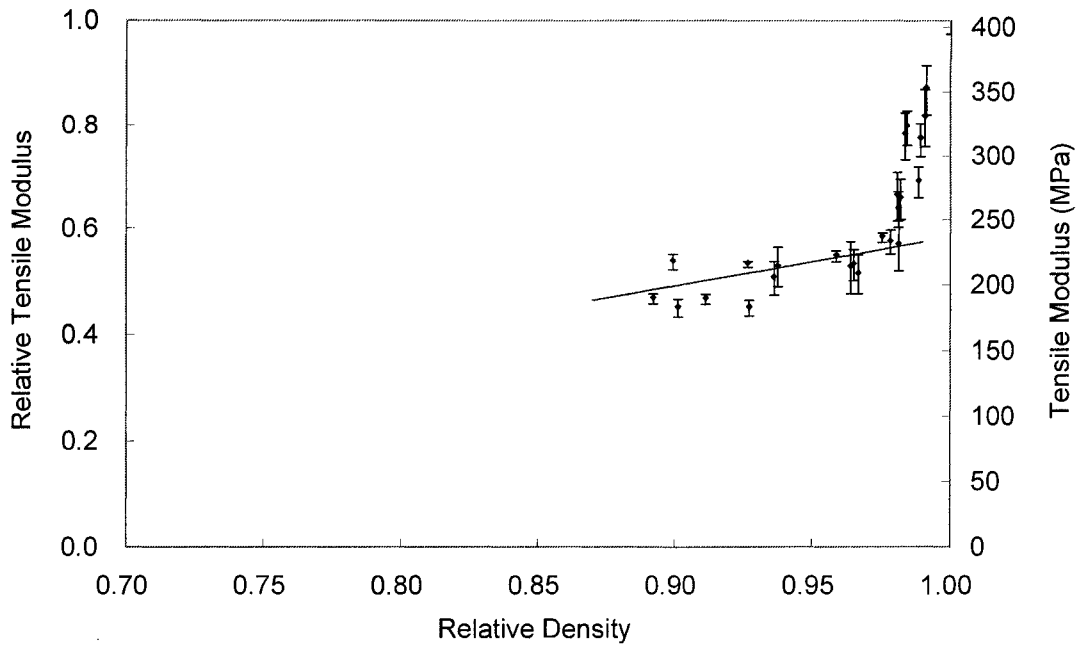


(a)

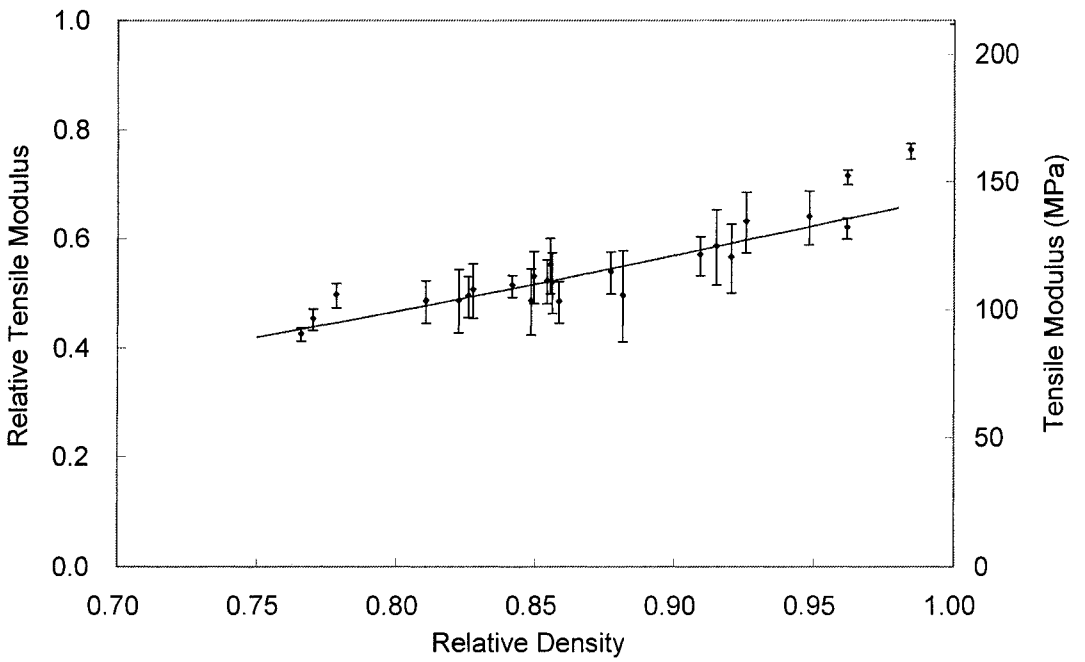


(b)

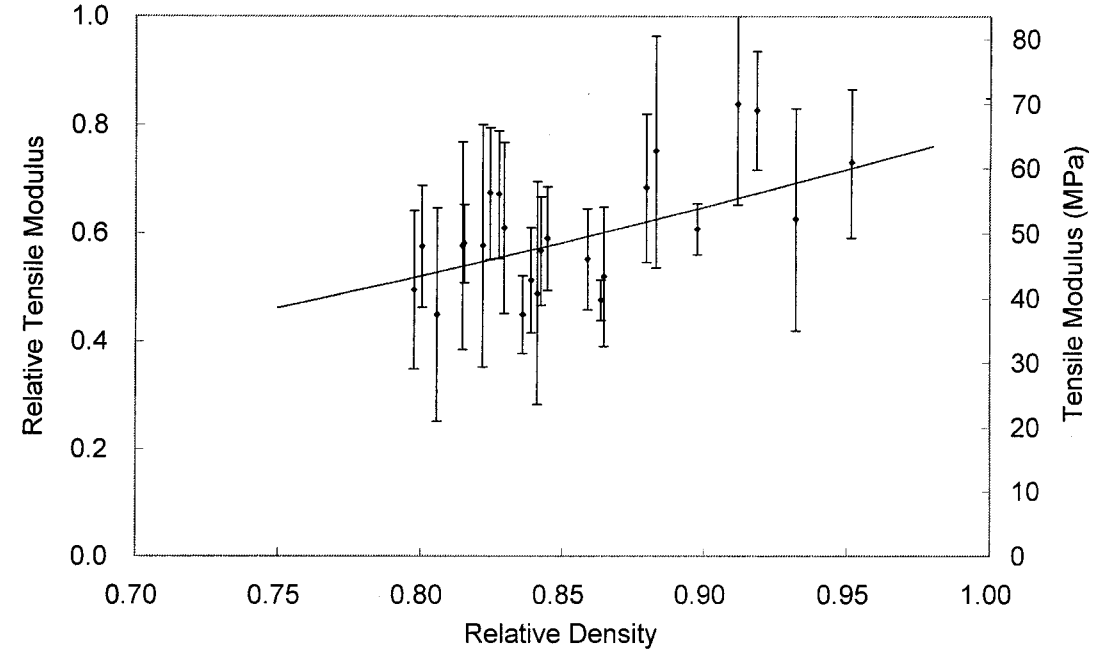


(c)

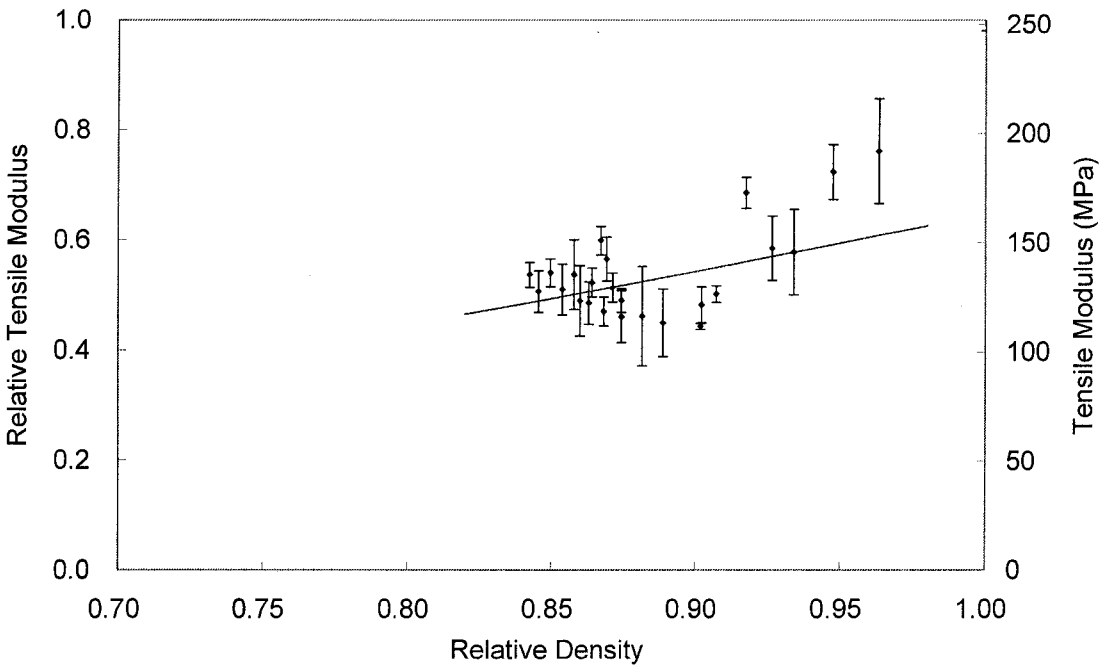


(d)

Figures 3-16: The effect of relative foam density on relative tensile modulus (a) TPO90, (b) TPO70, (c) TPO50 and (d) DTPO

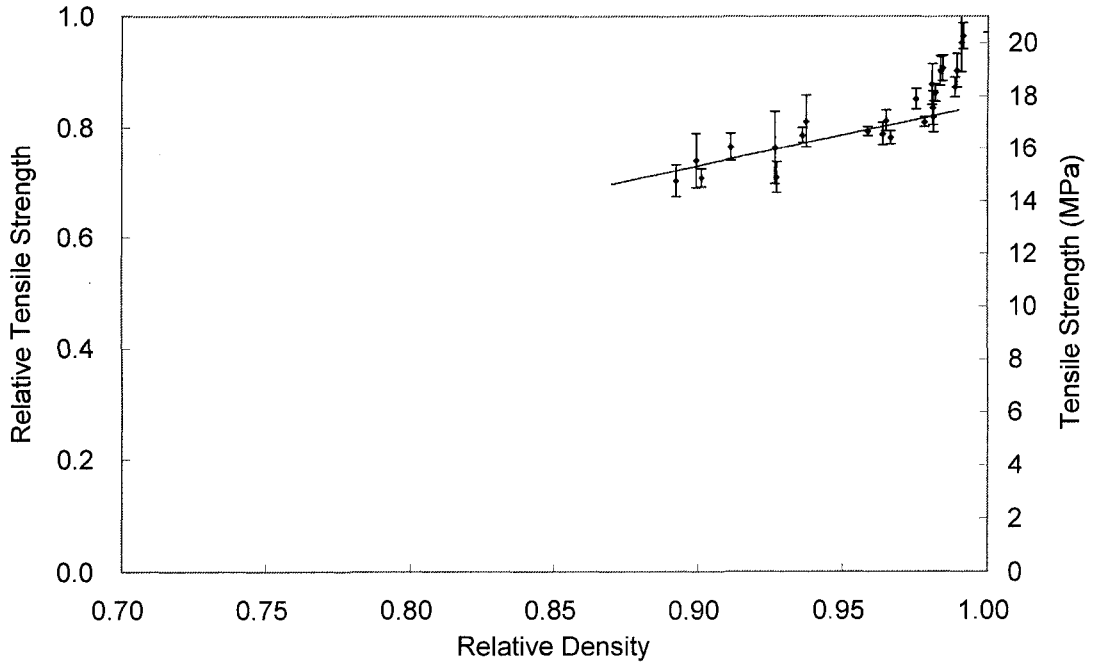


(a)

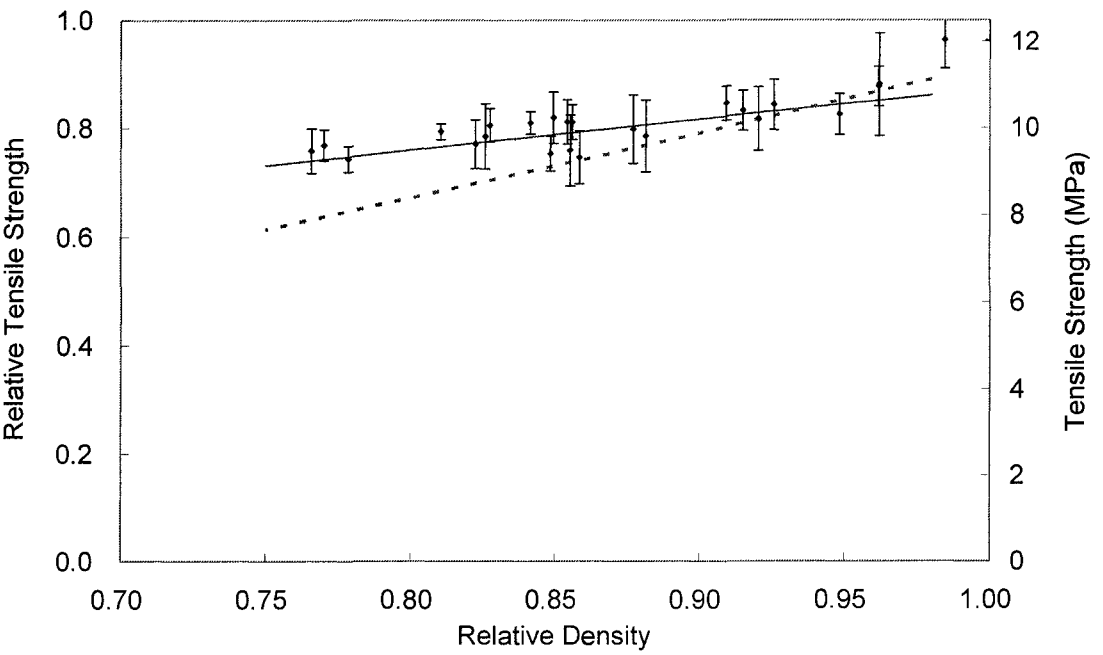


(b)

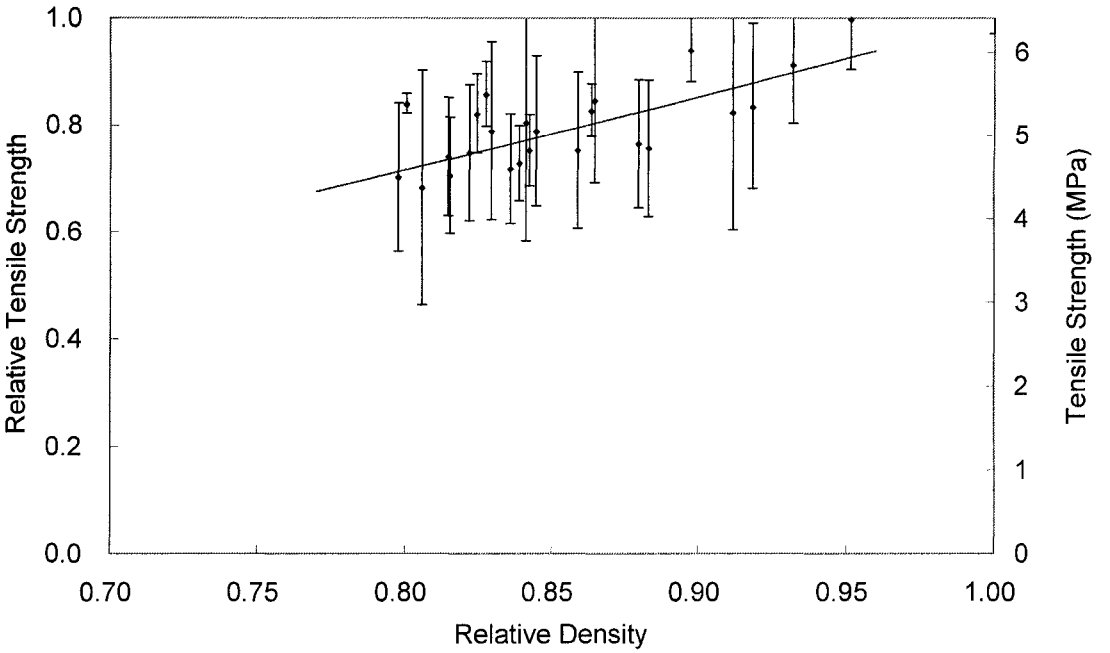


(c)

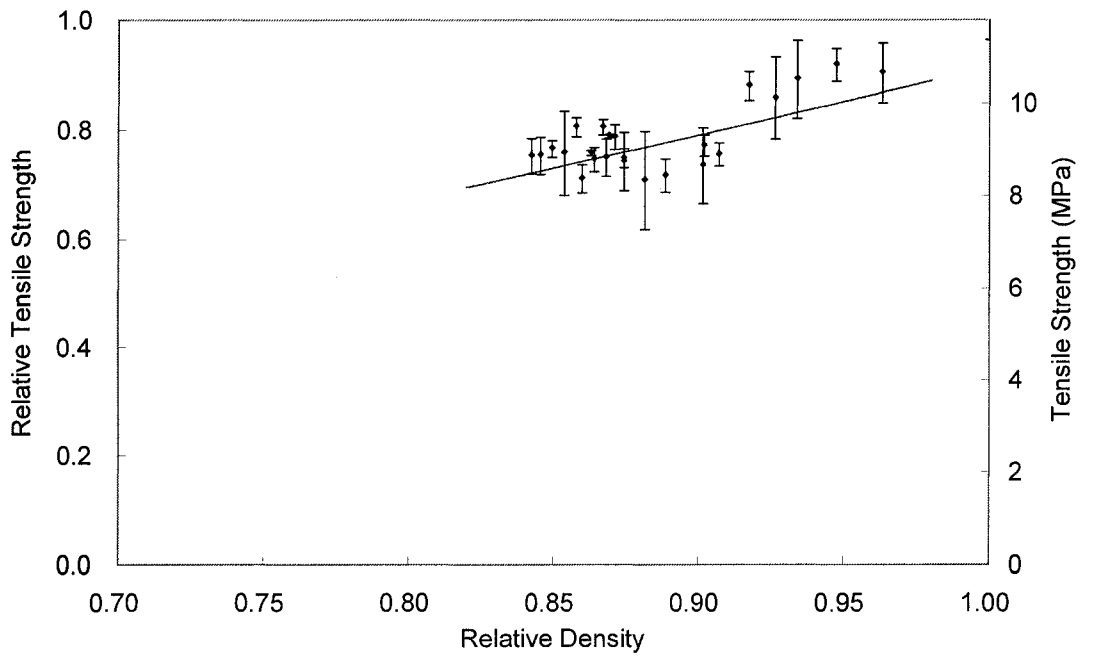


(d)

Figures 3-17: The effect of relative foam density on relative tensile strength of (a) TPO90, (b) TPO70, (c) TPO50 and (d) DTPO

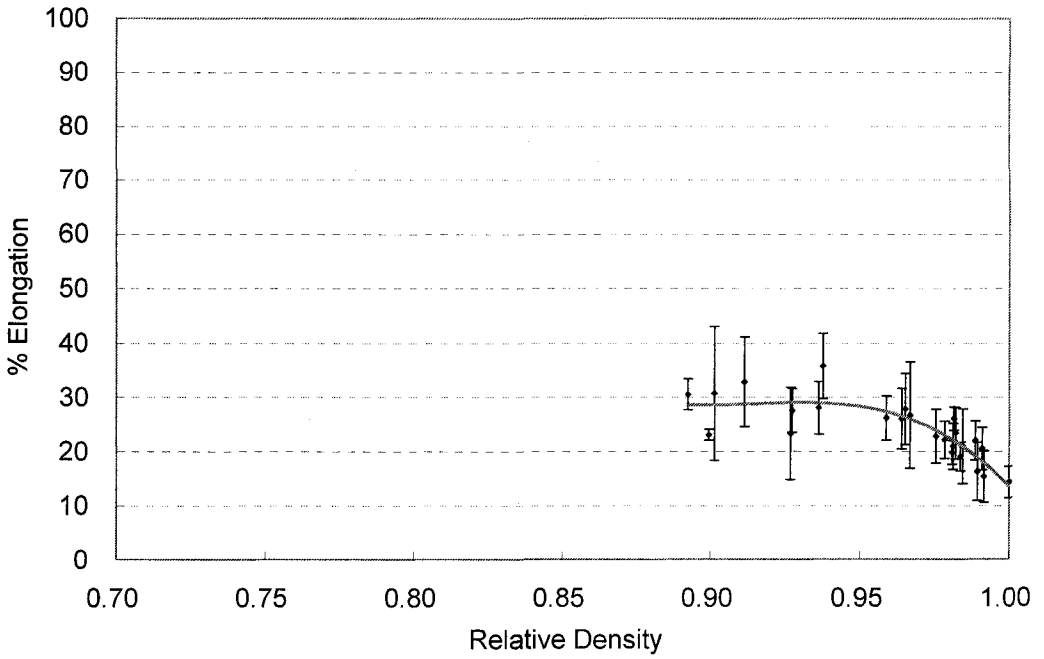


(a)

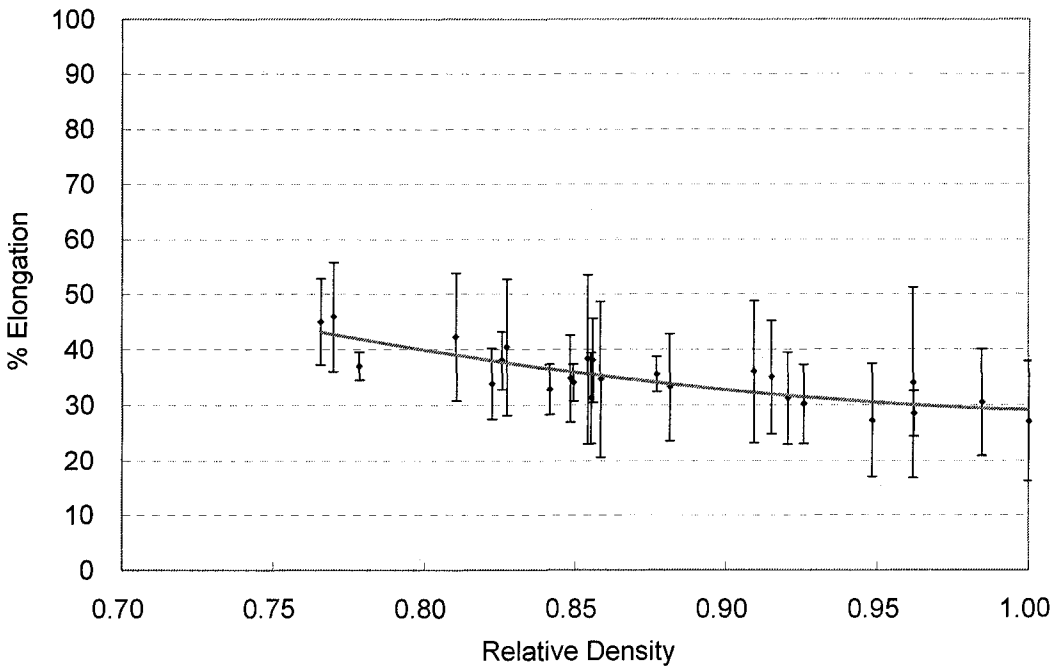


(b)

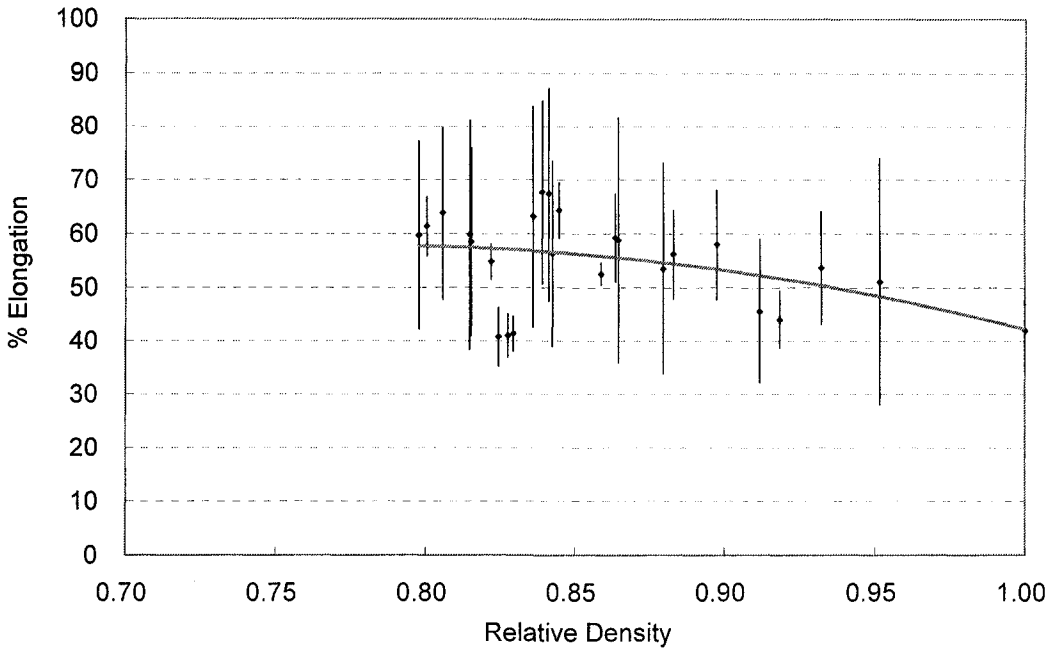


(c)

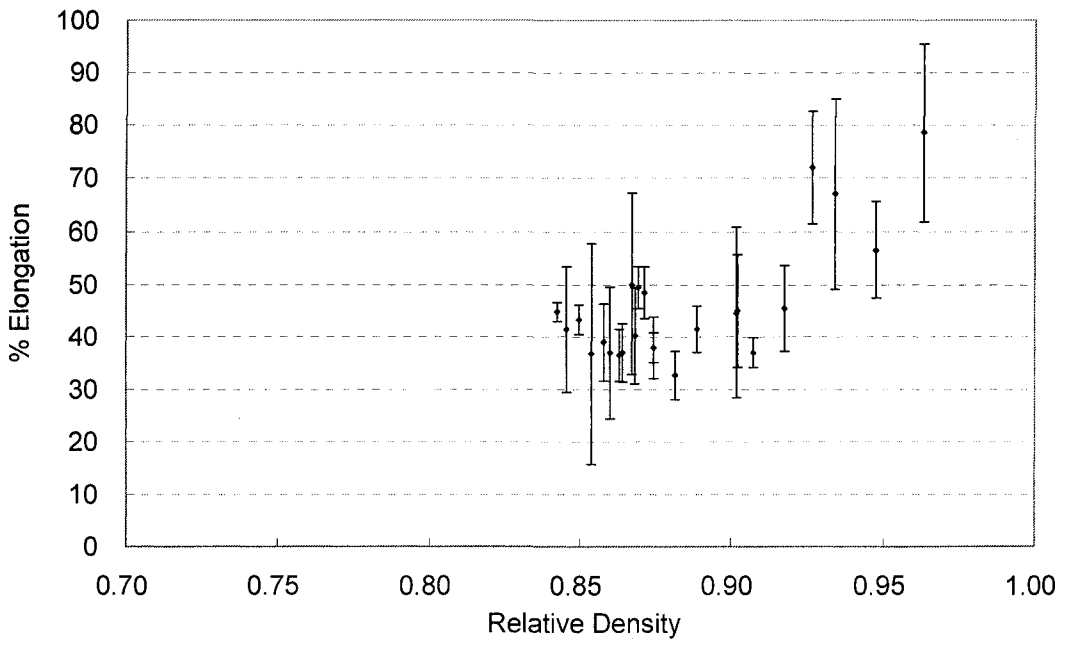


(d)

Figures 3-18: Effect of relative density on the percent elongation of microcellular foamed (a) TPO90, (b) TPO70, (c) TPO50 and (d) DTPO.

# Chapter 4
# Elastic Recovery of Microcellular TPO Foams

## 4.1 Introduction

Polymer foams are intensively used on packaging, space filling and collision (energy absorption) regions in the automotive industry due to its high energy absorption capability. The materials used for these applications are needed to withstand the compressive loads for some periods of time. It is desirable that the foamed materials can perform the requirements during compressive loading and recover fully upon load removal. Therefore, it is crucial to study the elastic recovery behaviour of these polymeric foams in order to achieve the purpose of minimizing the use of materials for various engineering applications.

In this chapter, the processing, morphology characterization and elastic recovery testing of microcellular TPO foams were investigated. The microcellular TPO foamed samples which meet the ASTM standard were successfully processed by batch foaming process under various processing conditions. The foam morphology of these microcellular TPO foams processed under various process parameters was characterized.

The effects of foam morphologies on elastic recovery of microcellular TPO foams were examined. Finally, the relationship between the foam morphology and elastic recovery of microcellular TPO foams was correlated.

## 4.2 Experimental

### 4.2.1 Experimental Materials

The materials examined in this chapter were PP and TPO. The unfoamed engage material was also examined to compare with the microcellular PP and TPO foams. The PP7805 and engage8130 were supplied by Exxon and DuPont respectively. The TPO material composed of 90% TPO70 and 10% mineral filler was called the TYC735X. The final TPO (TYC735X) composite was blended by a twin screw extruder to the desired combination and it was supplied by Basell. It had a density of 0.96 g/cm$^3$ and an MFI of 25 dg/min. Similar to DTPO, the TYC735X is also one of the commercial TPO materials currently used in automotive industries.

The materials were hot compression molded in a die by using a heated hydraulic press (Carver Inc.) for 10 minutes under 5 tons of pressure at 200°C for PP and TPO and 150°C for engage. The dimension of the final TPO specimens obtained from the die met the ASTM D395 Type II standard [77]. All specimens have cylindrical shape with the thickness of 6mm and the diameter of 13mm. The detail dimension of the samples was shown in Figure 5-10. The physical blowing agent used in this study was nitrogen ($N_2$) supplied from BOC Inc.

### 4.2.2 Processing of Microcellular TPO Foams

The two-stage batch foaming process was utilized to prepare the microcellular PP and TPO foams. In the first stage, the samples were saturated in the pressure chamber with $N_2$ gas at room temperature for 2 weeks. In the second stage, the foaming step was carried out by removing the gas-saturated samples from the pressure chamber and then put in a heated hydraulic press in which the platens were heated to the desired foaming temperatures at a specified foaming time. The combination of pressure and temperature changes resulted in the rapid solubility drop in the samples, inducing cell nucleation and cell growth. All specimens were foamed less than five minutes after being taken out of the pressure chamber. Afterwards, the foamed cell structure was stabilized by quenching the samples in cold water. Five foamed specimens for each foaming condition were prepared for cell morphology characterization and elastic recovery testing.

### 4.2.3 Foam Characterization

Similar to Chapter 3, the morphology of microcellular PP and TPO foams was characterized by utilizing a scanning electron microscope (SEM, JOEL JSM-6060). Before taken to the SEM, the specimens were cooled in liquid nitrogen before fractured and then platinum-coated to enhance conductivity. The ImageJ software from National Institutes of Health, USA was used to analyze the SEM images. The cell density was calculated as the number of cells per unit volume with respect to the unfoamed polymer by using Equation 3.1. The foam density was measured by the density measurement kit. The relative foam density was calculated as the ratio of the foam density to the density of unfoamed materials.

### 4.2.4 Elastic Recovery Testing

The elastic recovery testing measured the ability of the material retains elastic properties after prolonged action of compressive stresses. According to ASTM standard D395 [77], the elastic recovery in the direction of compression at constant strain has been defined in terms of compression set, $C_B$. The compression set expressed as the percentage of original deflection had not been recovered after release is shown as follows:

$$C_B = \left( \frac{t_o - t_i}{t_o - t_n} \right) \times 100 \tag{4.1}$$

where, $t_0$ is the original thickness of the specimen, $t_i$ is the thickness of the specimen after release and $t_n$ is the thickness of the original compressive deformation on the apparatus. According to Equation 4.1, the specimen at first has the compression set of 100% upon release from the apparatus and then a zero compression set would be obtained as the specimen fully recovered to its original dimensions.

The original thickness of each foamed specimen was measured before the elastic recovery testing. All of the thickness measurements were made by digital caliper. The thickness of a specimen was determined by averaging out the three thickness values obtained from measuring on each side. The thickness of the foamed samples varied from 6mm to 6.2mm and were dependent on the foaming conditions.

The compression set apparatus was designed following the requirements of ASTM standard D395 method B: compression set under constant deflection in air. Figure 4-2 shows the compression set apparatus used in these experiments. The apparatus consisted of two heat-treated alloy steel plates, four high strength alloy steel bolts and nuts. Each of the steel plates had the thickness of 20mm. These thick steel plates are needed in order to

ensure minimum deflection during the compression stage. The surface of the steel plates had been grinded to mirror finish to maximize the accuracy of the testing.

The elastic recovery testing on the microcellular PP and TPO foams was conducted following the ASTM standard D395. Two specimens of each material were prepared at each foaming condition. These two specimens were subjected under elastic recovery testing at the original compressive strain of 10% and 25% respectively. These values were chosen by ASTM standard to ensure the data obtained would be spanning the linear elastic and plateau regions of the foamed materials. In the elastic recovery testing, the foamed specimens were placed between the steel plates and nuts were tightened to fix the plate securely in the desired position. The specimens were compressed at the desire original compressive strain at room temperature for 70 hours as according to ASTM standard. Once the time had elapsed, the specimens were removed from the apparatus. The thickness of each specimen was then immediately measured and recorded. The thickness of each specimen was recorded on an hourly basis in the first five hours upon the removal from the apparatus and then recorded on a daily basis for the first week to monitor the recovery behaviour of various microcellular PP and TPO foams.

## 4.3 Results and Discussion

The effects of the processing parameters (foaming time and foaming temperature) on cell morphologies (foam density, cell density and average cell size) of microcellular PP and TPO foams were presented. The effects of cell morphology on the elastic recovery at two set of original compressive strains were discussed in the following sub-sections in detail.

### 4.3.1 Effects of Processing Parameters on the Foam Morphology

The effects of foaming time and foaming temperature on the cell size, cell density and relative foam density of microcellular PP and TPO foams were presented in Figure 4-3 - Figure 4-5. By observing Figure 4-3, the average cell size slightly increased with foaming time for microcellular PP and TPO foams. This is attributed to the decreased viscosity of the polymer matrix causing the cell size to increases. The cell size did not increase much at the first 60s of foaming time. This is due to the slow rate of heat transfer in the heated hydraulic press on relatively thick TPO samples. The major foaming stage took place between 60s and 150s of foaming time as the cell size significantly increased 5 times for TPO foams. Beyond 150s, the foam structure does not appear to change significantly. Overall, the effect on cell size was not significant for both PP and TPO foams. The cell density for microcellular PP and TPO foams more or less remain in the range of $10^9$ - $10^{10}$cells/cm$^3$ as shown in Figure 4-4. With the cell size continuing to grow and the cell density remaining approximately $10^9$-$10^{10}$cells/cm$^3$, the volume of the specimens expands causing the relative foam density to decease as shown in Figure 4-5.

By observing Figure 4-5, the relative foam density decreased as the foaming temperature and foaming time increased. The minimum relative density of microcellular PP and TPO foams obtained at 170°C foaming temperature were both approximately 0.8, which is 20% weight reduction of the materials. These results were consistent with the increases in the average cell size with high cell density as mentioned before. In the next section, the effect of foaming parameters and cell morphologies on elastic recovery of microcellular PP and TPO foams was examined in detail.

### 4.3.2 Effect of Processing Parameters and Cell Morphology on Elastic Recovery

The elastic recovery behaviour at 10% and 25% of the original compressive strain of unfoamed PP, TPO and engage materials are shown in Figure 4-6 and Figure 4-7 respectively. The curves shown in these figures is called the elastic recovery curves of materials. These curves show that the unfoamed specimens recovered very rapidly at the few hours upon release from the compression set apparatus. As the polymer specimen was compressed, the polymer chains were pushed toward each other and forced into a new structural confirmation. Upon release, the polymer chain attempted to recover the original position in order to obtain the structural equilibrium. This initial part of elastic recovery curve dominated the full recovery process and this is called the first stage of the recovery curve. After the rapid recovery in the first stage, the rate of elastic recovery of the specimens significantly reduced beyond the first day. The curves show a relatively less recovery over a much longer time. This minimal elastic recovery is called second stage of recovery curve. The results show that the second stage of recovery contributed only approximately 10% of the full recovery process. For foamed materials, this secondary elastic recovery stage appears to be associated with the recovery of the cellular structure of the foamed specimen [78, 79].

At 10% original compressive strain, the minimum compression set for unfoamed PP, TPO and engage are approximately 70%, 60% and 10% respectively. In other word, the PP and TPO successfully recovered 30% and 40% of the original compressive strain. For engage, it recovered 90% of the original compressive strain. This is clear that the elastic

recovery was affected by the stiffness or the degree of crystallinity of the material. The elastic recovery decreased with the amount of crystal structure in the material. For instance, the engage is a rubbery material without crystal structure. The engage had recovered more than 90% of the original compressive strain.

By observing Figure 4-7, the compression set increased as the original compressive strain increased from 10% to 25%. The minimum compression set for PP, TPO and engage are increased to approximately 81%, 65% and 19% respectively. The reason is that when a specimen was subjected in a higher compressive strain, higher force was given to the molecular chains and the cell structure of the polymer, resulting in more regions in the molecular chains and cell structure subject to fail causing the cell wall to collapse and leaving permanent deformation. Eventually some of the polymer chains and cell structures became fixed in these new positions and were not be able to retain their original position upon release. Therefore, the elastic recovery decreased with original compressive strain.

The effect of foaming time on elastic recovery at 10% and 25% original compressive strain of microcellular PP foams was shown in Figure 4-8 - Figure 4-9 respectively. By observing the figures, the compression set decreased as the foaming time increases. At 10% original compressive strain, the minimum compression set of 58% was obtained at 90s of foaming time. This is due to the fact that the minimum relative density was obtained at 90s of foaming time as shown in Figure 4-5. As a result, the elastic recovery is very closely affected by the relative density of the foams. By comparing the PP foams to the unfoamed PP material, the compression set decreased from 75% to 58% of the original compressive strain. The decrease in compression set means more elastic recovery

was obtained. When the foam was compressed, the cells in the foams also compressed. The gas pressure inside the compressed cells increased which created an extra residual stress in the cell structure to force the cells back to its original dimension and position. Upon release, this extra residual stress improved the elastic recovery of the foamed materials. Therefore, there is an approximately 22% improvement in elastic recovery by introducing microcellular structure in the PP material.

The effects of foaming parameters on the elastic recovery at 10% and 25% original compressive strain of microcellular TPO foams are shown in Figure 4-10 - Figure 4-13. Similarly, the compression set decreased as the foaming time and foaming temperature increase. At 10% original compressive strain as shown in Figure 4-11, the compression set decreased from 61% (unfoamed) to the minimum 40% at 150s foaming time. As a result, there was an approximately 31% improvement in elastic recovery by introducing microcellular structure in the TPO material.

By observing Figure 4-8 and Figure 4-9, the compression set increased with the original compressive strain. The minimum compression set of microcellular PP foams increased from 59% to 71% as the original compressive strain increased from 10% to 25%. In other words, less elastic recovery was obtained as the original compressive strain increased. Similarly, the elastic recovery of microcellular TPO foams decreased as the original compressive strain increased as shown in Figure 4-11 and Figure 4-13. The minimum compression set at 170°C of foaming temperature increased from 40% to 55% as the original compressive strain increased from 10% to 25%. The reason of this increased in compression set is consistent to the unfoamed material that was discussed before.

Figure 4-14 shows the effect of foaming time on elastic recovery of microcellular PP and TPO foams. The figure shows that the compression set of microcellular PP foams reached the minimum at 90s foaming time on both 10% and 25% original compressive strain. The minimum compression set of microcellular PP foams at 10% and 25% original strain are 90% and 70% respectively. At 10% original compressive strain, the compression set decreased as the foaming time and foaming temperature increased. Since the relative density decreased as the foaming temperature and foaming time increased, the compression set decreased with the relative density. However, the effects of foaming parameters and cell morphology on compression set decreased as the original compressive strain increased from 10% to 25% as shown in Figure 4-14.

By rearranging the data, the effect of relative density on elastic recovery at 10% and 30% original compressive strains of microcellular PP and TPO foams are shown in Figure 4-15 and Figure 4-16 respectively. The results show that the elastic recovery increased as the relative density of microcellular PP and TPO foams decreased. By comparing Figure 4-15 and Figure 4-16, the compression set of microcellular PP foams increased by 25% as the original compressive strain increased from 10% to 25%. However, the difference in compression set of microcellular TPO foams as the original compressive strain increased was only 18%. This is attributed to the PP has the yield strain less than TPO materials which were toughed by addition of engage. At 25% original compressive strain, the PP was compressed beyond its yield strain, the molecule chain of the PP specimens subjected to plastic deformation, so that the molecule chain were not able to retain its original position upon release. Therefore, the elastic recovery of the PP material decreased as the original compressive strain increases.

In addition, the effect of cell wall thickness on elastic recovery of microcellular PP and TPO foams is shown in Figure 4-17 and Figure 4-18 respectively. The cell wall thickness is defined as the average distance between the cells. By observing the figures, the effect of cell wall thickness on the elastic recovery of the microcellular PP and TPO foams was not noticeable. In summary, the elastic recovery is significantly affected by the relative density of microcellular foams. The weight reduced PP and TPO with superior elastic recovery can be obtained by introducing microcellular structure in the materials.

## 4.4 Conclusions

In this chapter, the microcellular PP and TPO foams were successfully prepared under various foaming conditions by using batch foaming method. The effects of processing parameters on the cellular morphology and elastic recovery of microcellular PP and TPO foams were examined. The experimental results show that the average cell size increased with foaming time and foaming temperature. The cell density remained in the order of between $10^9$ and $10^{10}$ cells/cm$^3$ at various foaming conditions. For PP and TPO foams, the maximum weight reduction of 20% was obtained at 27.6MPa saturation pressure.

The elastic recovery curves of microcellular PP and TPO foams were successfully obtained in this study. The results show that a maximum of 22% and 31% improvement in elastic recovery was achieved by introducing microcellular structure in the PP and TPO materials respectively. Furthermore, the results also prove that the compression set increased with the original compressive strain. In other words, less elastic recovery was observed at a higher original compressive strain. Finally, the results show that the elastic

recovery is significantly affected by the relative density of the microcellular foams.

In summary, the cell morphology of microstructure of PP and TPO foams can be controlled effectively by carefully altering the foaming parameters. Light weight TPO with superior elastic recovery for compressive loading applications can be achieved by introducing cellular structure in the materials.

| Type | 1 | 2 |
|---|---|---|
| Thickness | 12.5 mm | 6mm |
| Diameter | 29 mm | 13mm |

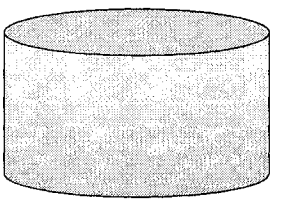

Figure 4-1: ASTM standard D395 (Type II) specimen.

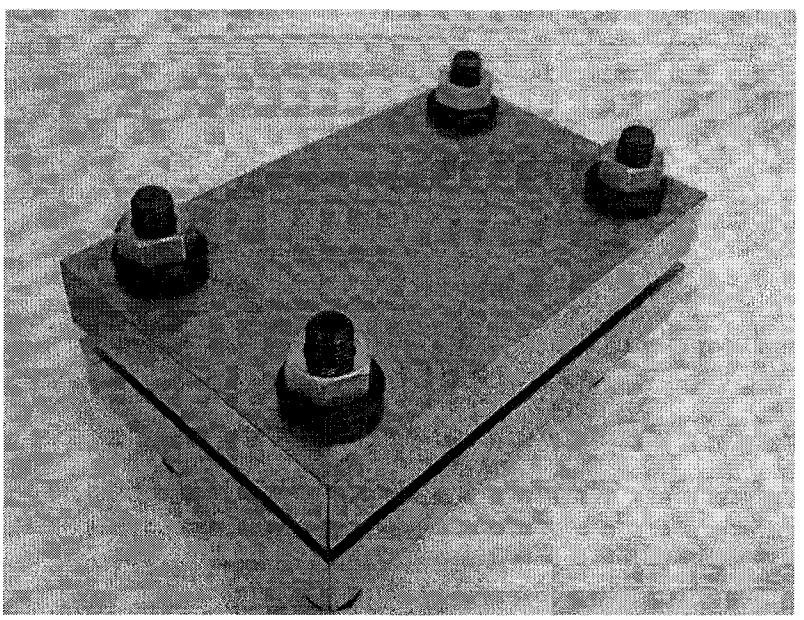

Figure 4-2: Compression set apparatus.

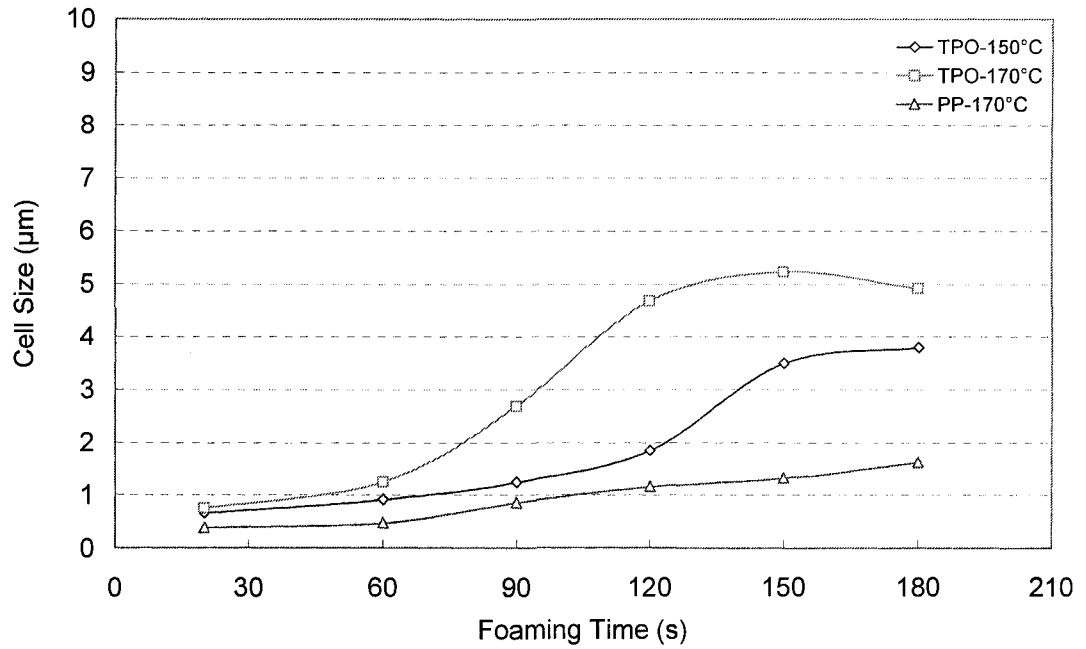


Figure 4-3: Effect of foaming temperature and foaming time on the cell size of microcellular foamed PP and TPO. (Saturation Conditions: 27.6MPa $N_2$ at RT)

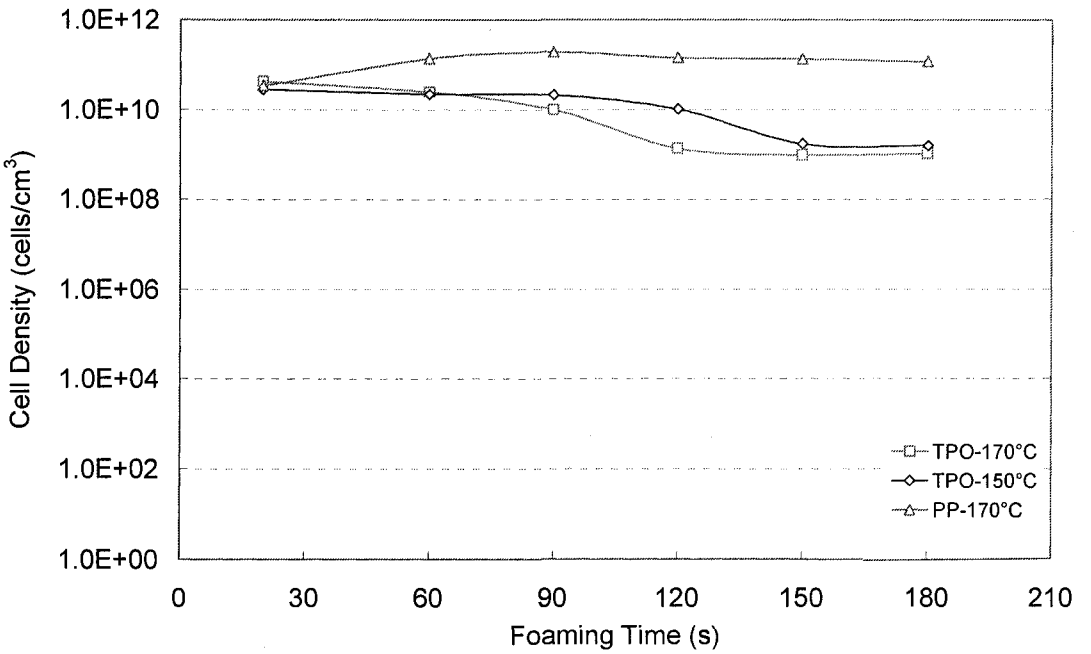


Figure 4-4: Effect of foaming temperature and foaming time on the cell density of microcellular foamed PP and TPO. (Saturation Conditions: 27.6MPa $N_2$ at RT)

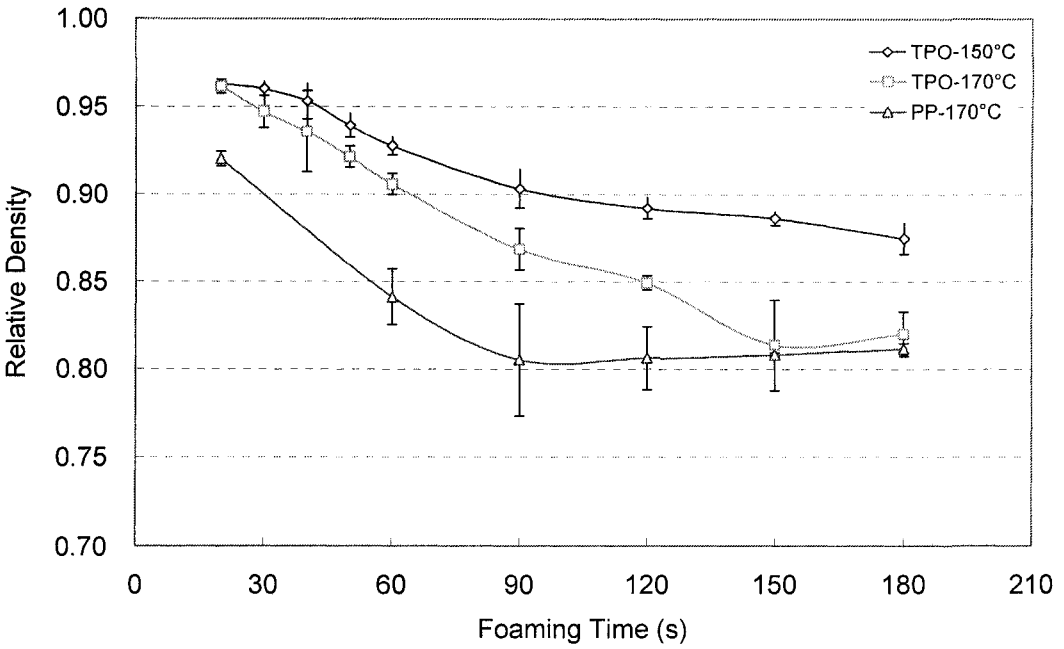


Figure 4-5: Effect of foaming temperature and foaming time on the relative density of microcellular foamed PP and TPO. (Saturation Conditions: 27.6MPa $N_2$ at RT)

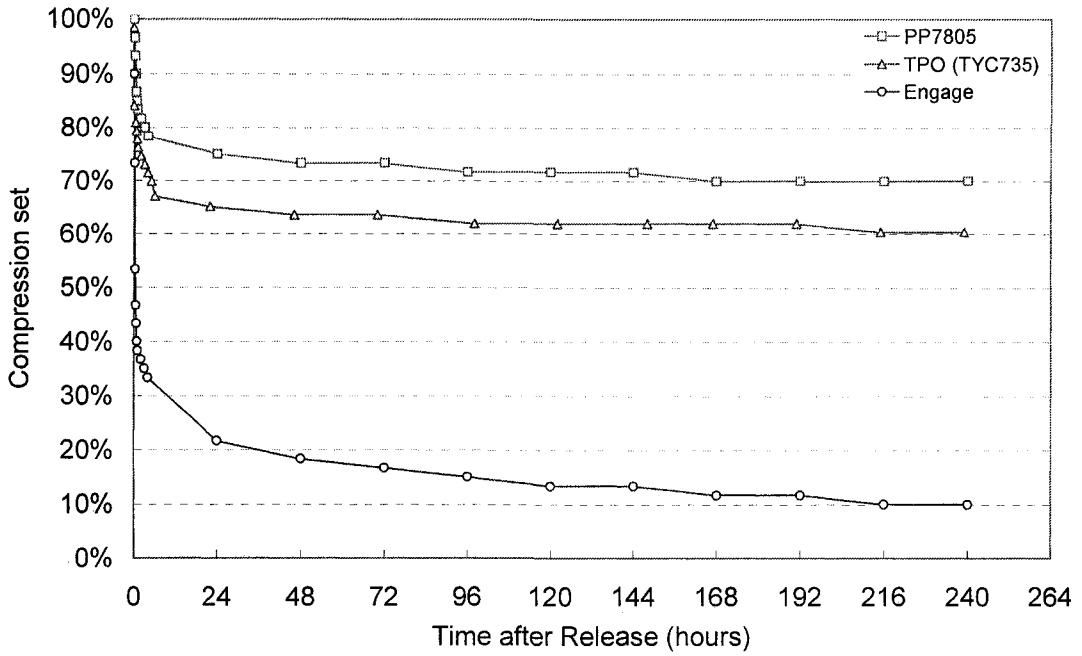


Figure 4-6: Unfoamed PP, Engage and TPO materials compressed at 10% strain for 70 hours at RT.

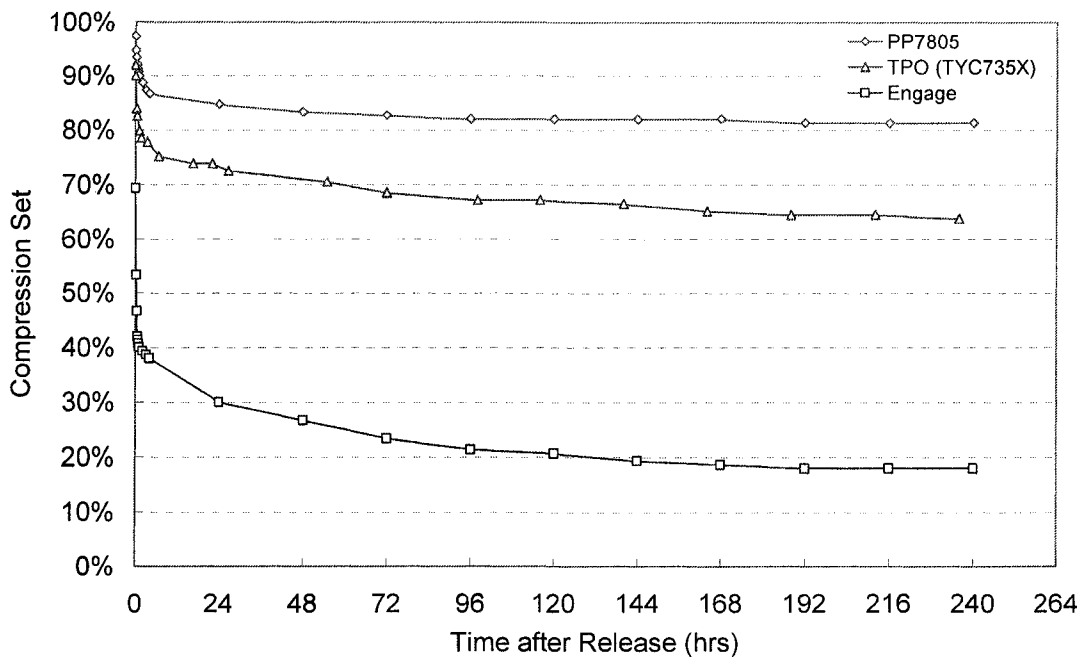


Figure 4-7: Unfoamed PP, Engage and TPO materials compressed at 25% strain for 70 hours at RT.

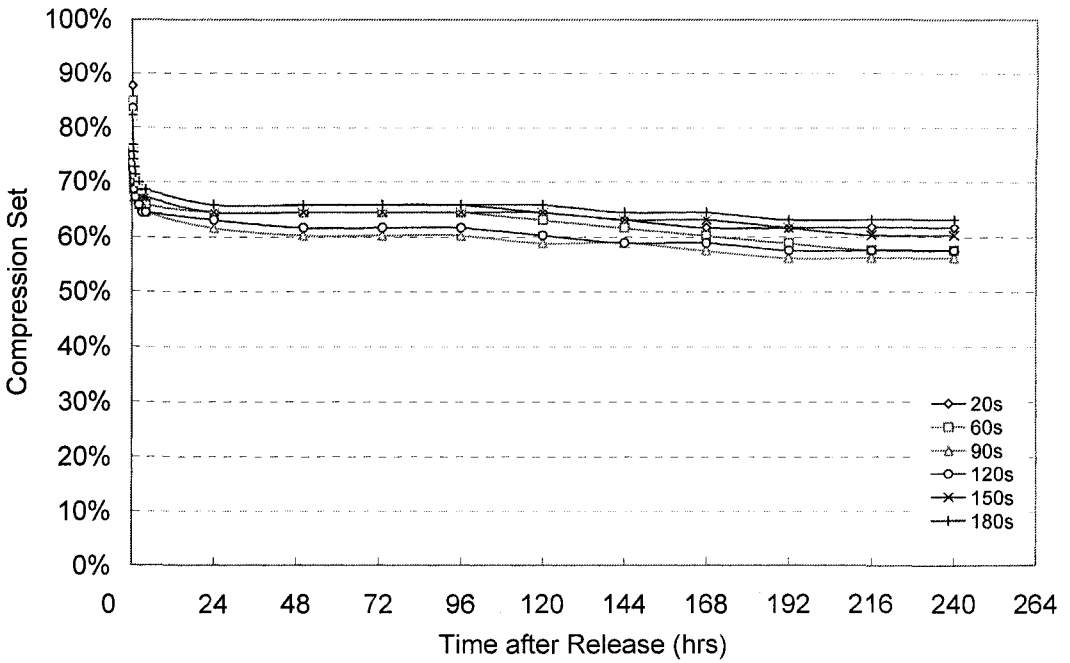


Figure 4-8: The effect of foaming time on compression set of microcellular PP foams compressed at 10% strain for 70 hours at RT. (Foaming Temperature: 170°C)

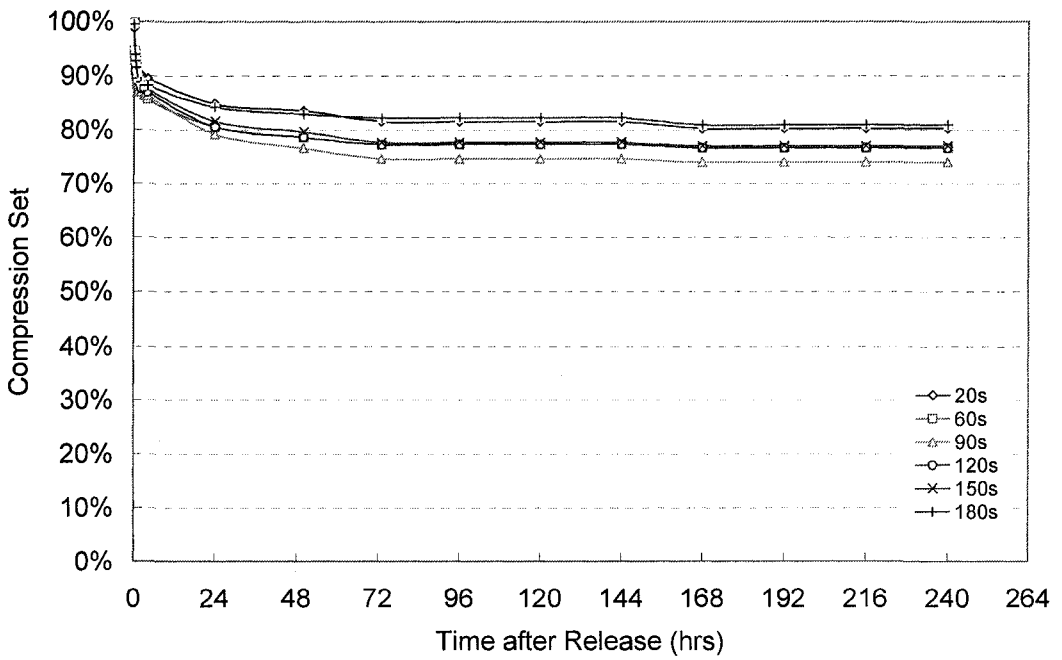


Figure 4-9: The effect of foaming time on compression set of microcellular PP foams compressed at 25% strain for 70 hours at RT. (Foaming Temperature: 170°C)

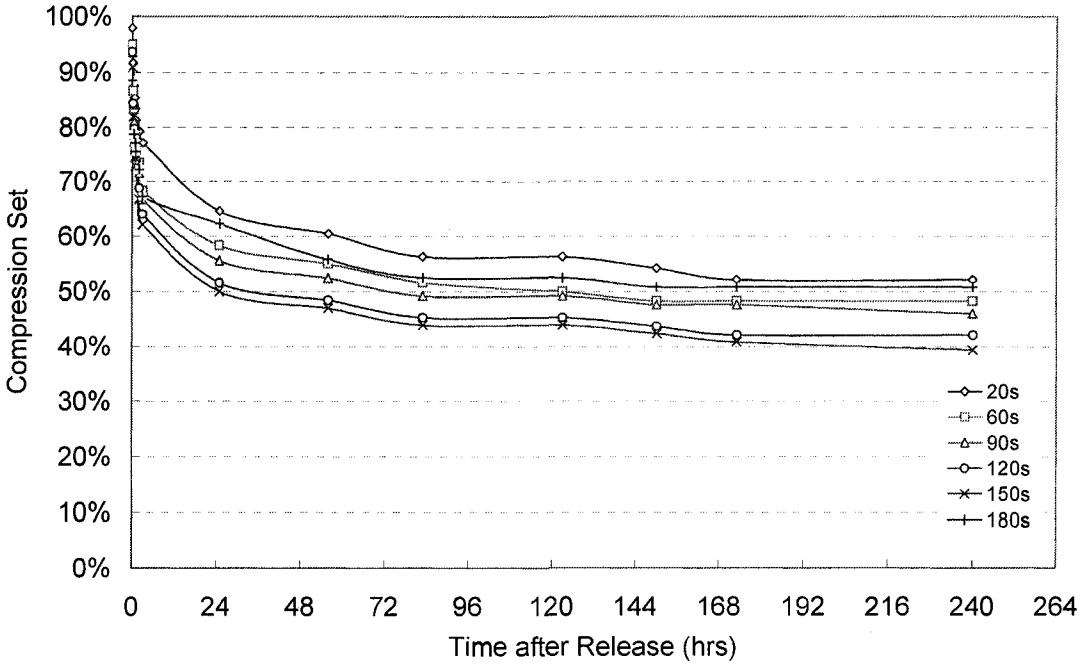


Figure 4-10: The effect of foaming time on compression set of microcellular TPO foams compressed at 10% strain for 70 hours at RT. (Foaming Temperature: 150°C)

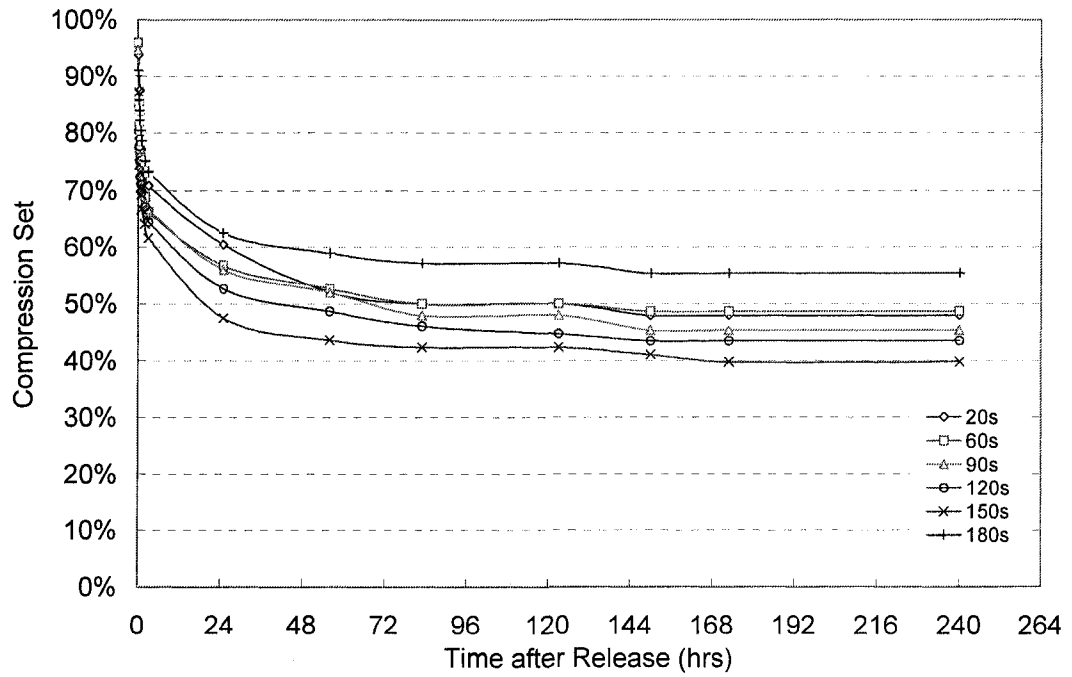


Figure 4-11: The effect of foaming time on compression set of microcellular TPO foams compressed at 10% strain for 70 hours at RT. (Foaming Temperature: 170°C)

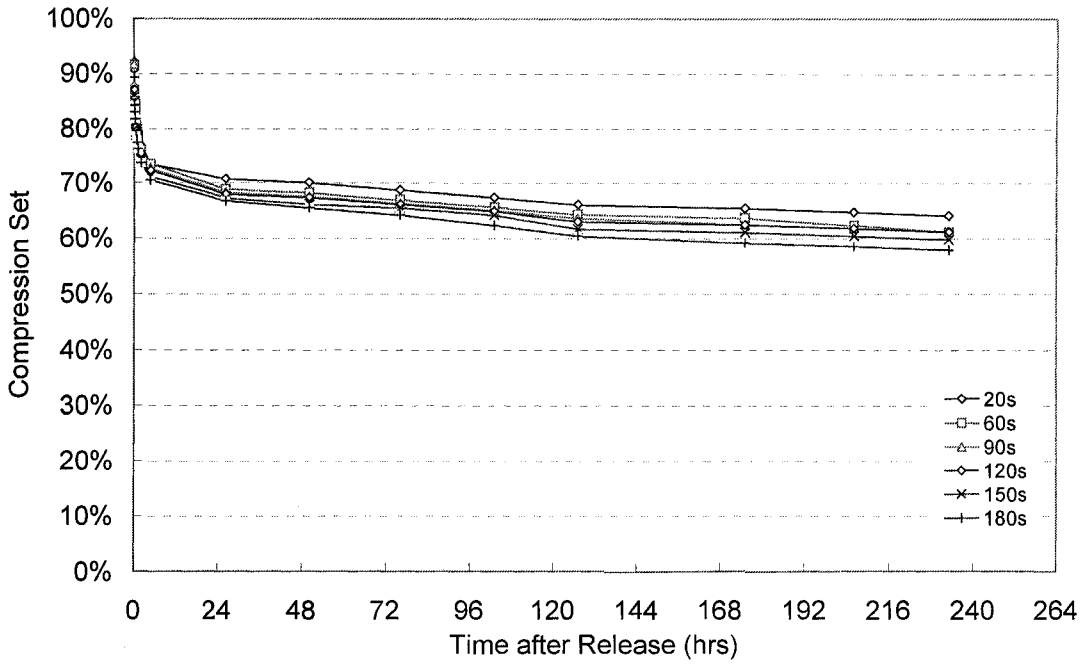


Figure 4-12: The effect of foaming time on compression set of microcellular TPO foams compressed at 25% strain for 70 hours at RT. (Foaming Temperature: 150°C)

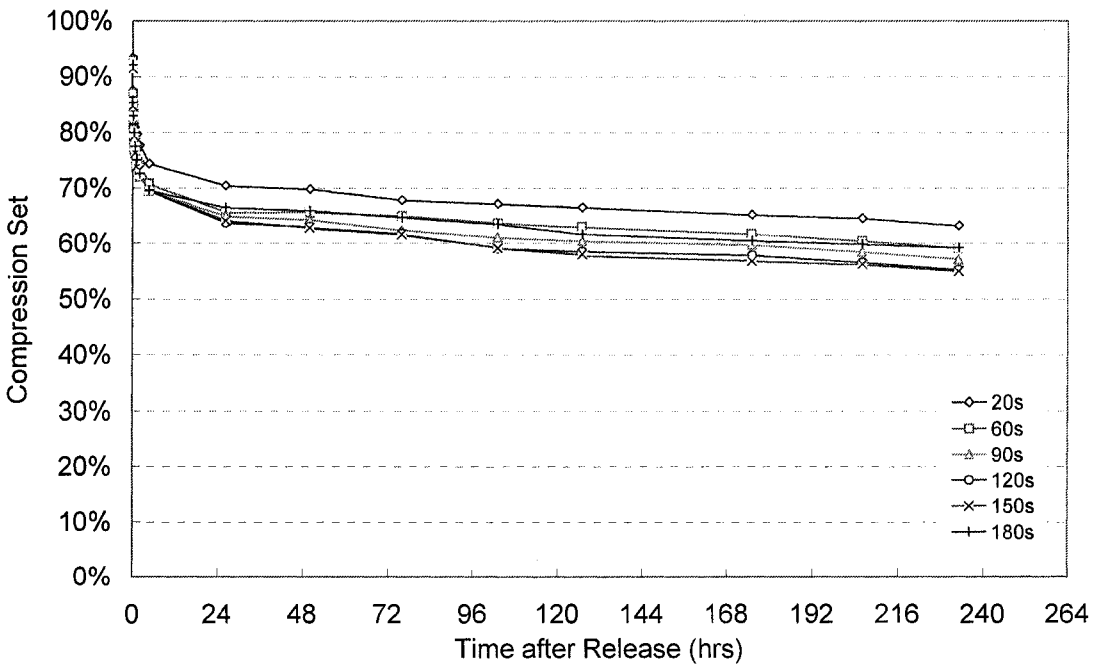


Figure 4-13: The effect of foaming time on compression set of microcellular TPO foams compressed at 25% strain for 70 hours at RT. (Foaming Temperature: 170°C)

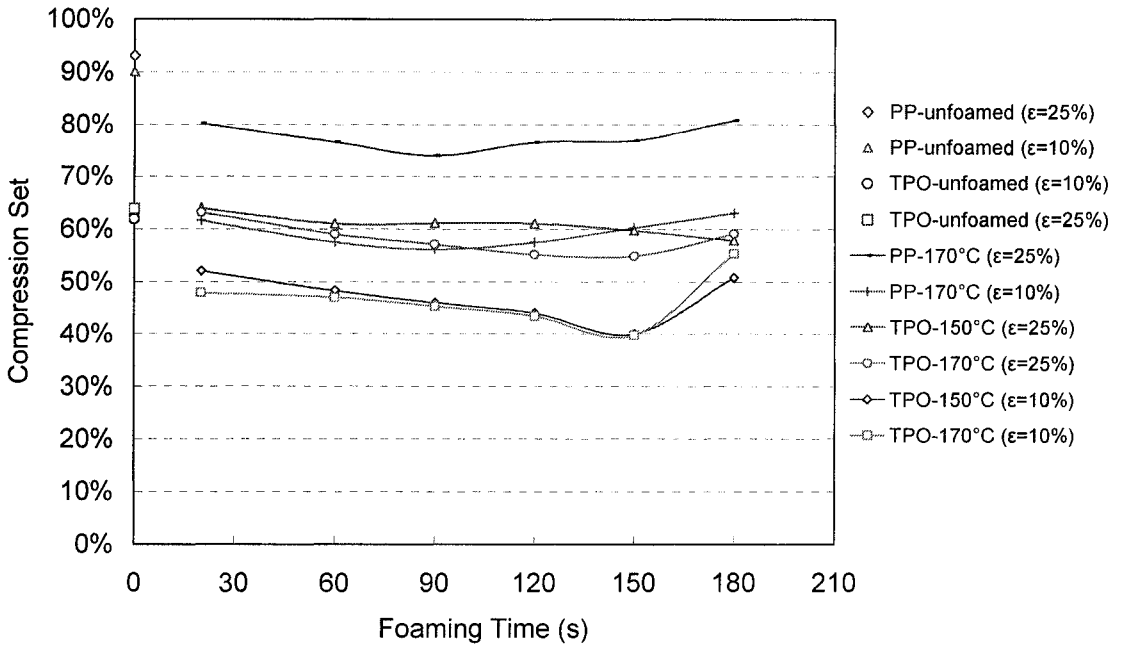


Figure 4-14: The effect of foaming conditions on compression set of microcellular PP and TPO foams.

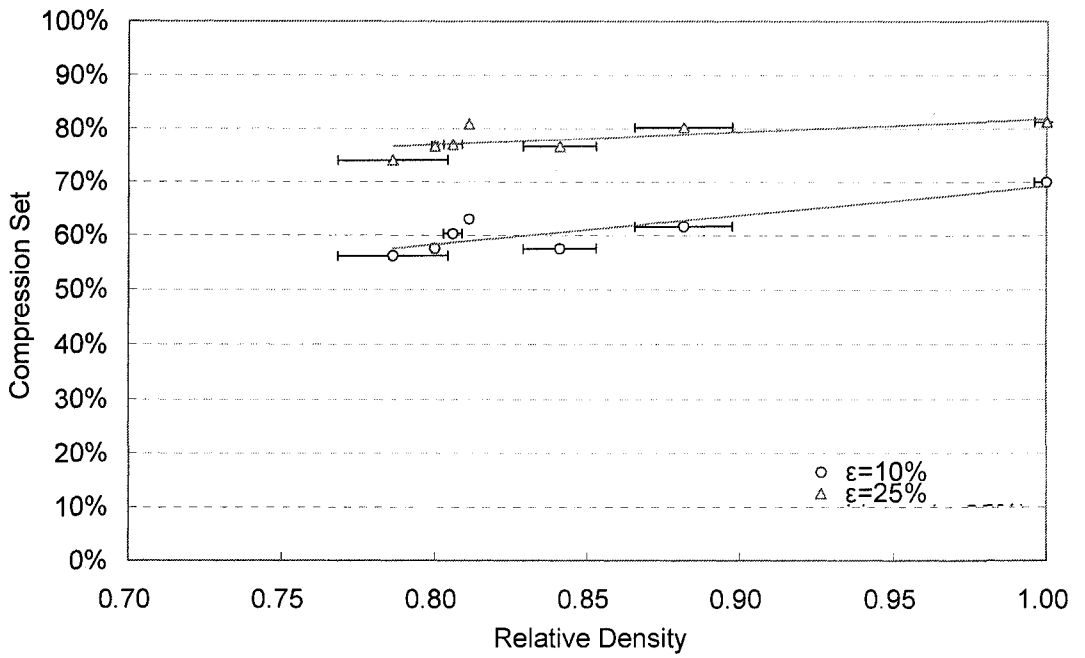


Figure 4-15: The effect of relative foam density on compression set of microcellular PP foams.

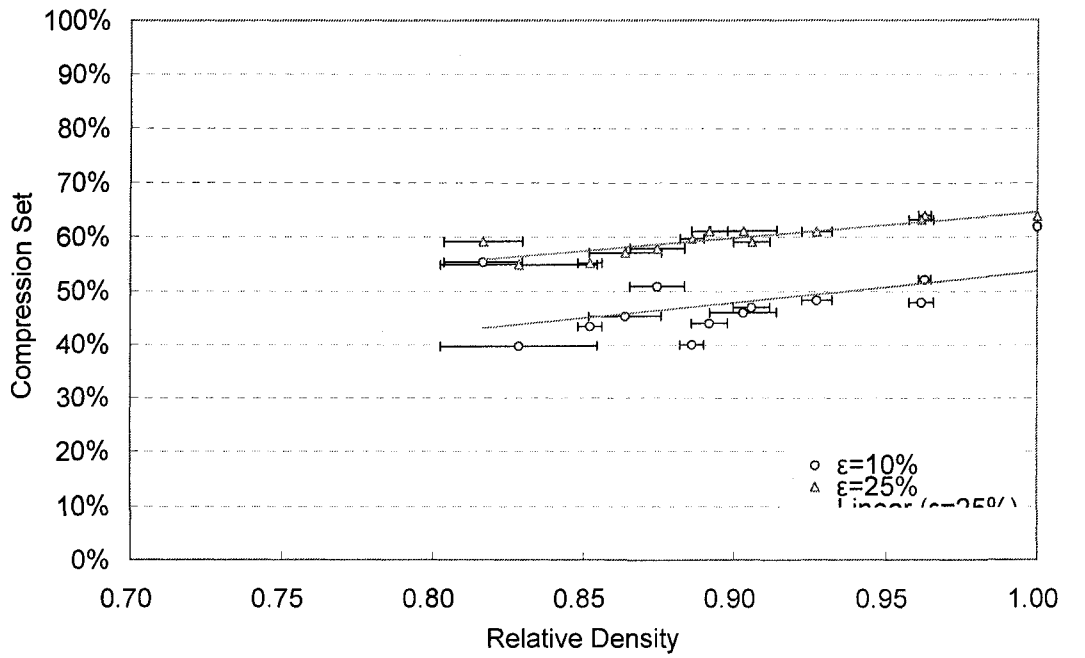


Figure 4-16: The effect of relative foam density on compression set of microcellular TPO foams.

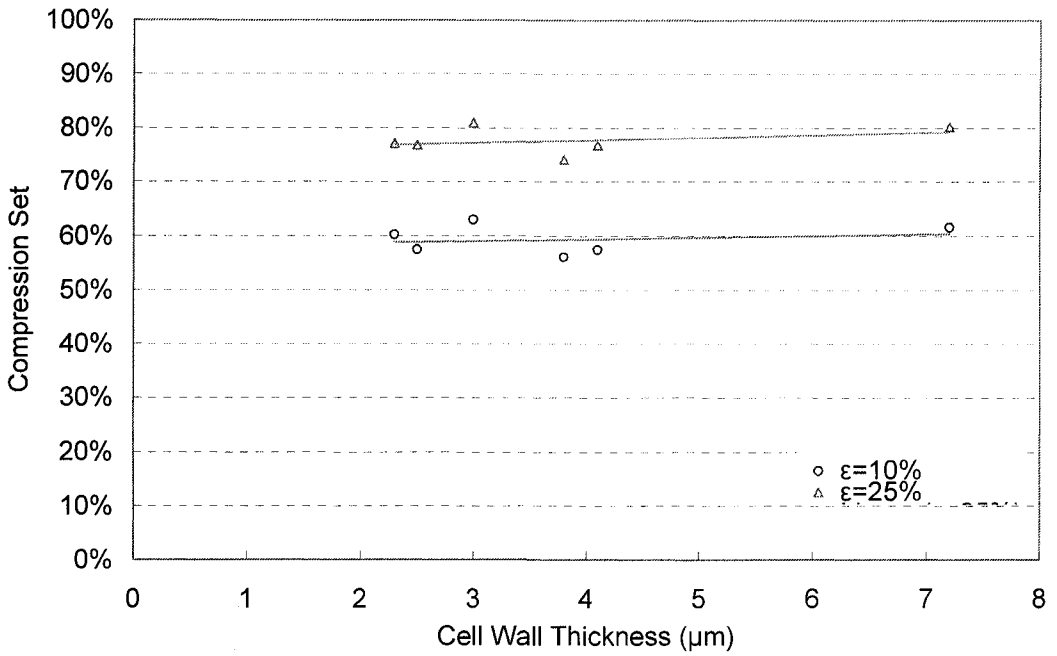


Figure 4-17: The effect of cell wall thickness on compression set of microcellular PP foams.

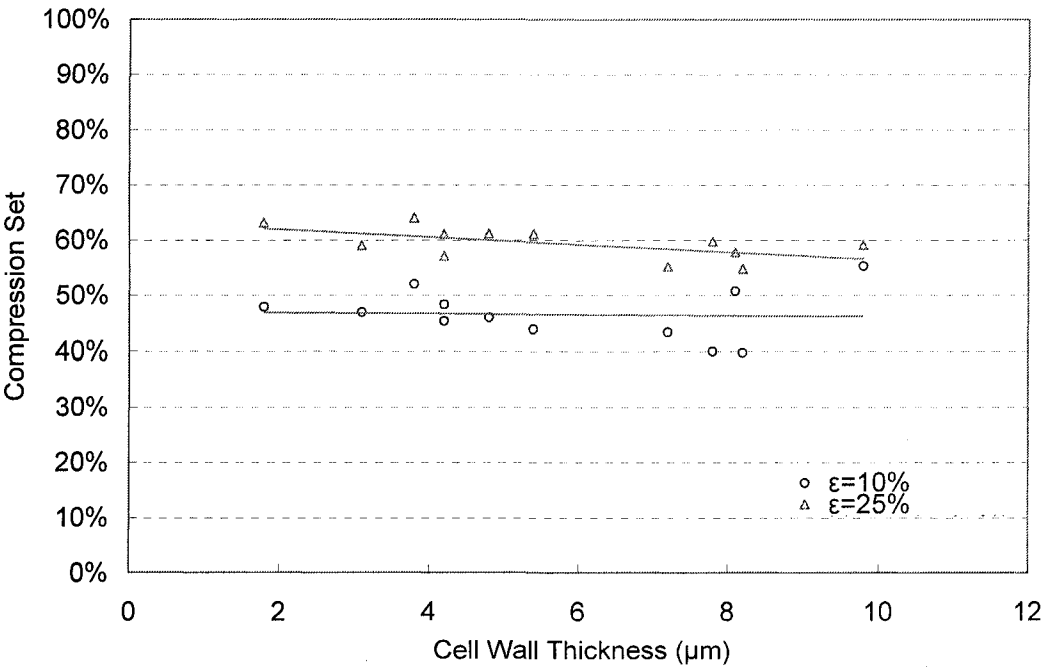


Figure 4-18: The effect of cell wall thickness on compression set of microcellular TPO foams.

# Chapter 5
# Mechanical Properties of Injection Molded TPO Foams

## 5.1 Introduction

The technologies of continuous foaming were employed rapidly to increase the productivity of polymeric foams. Thermoplastic foamed parts for automotive applications were successfully produced by an injection molding process. The cell morphology of fine-celled TPO foams was successfully controlled by alternating the processing parameters on the injection molding machine. However, characterization of the mechanical properties of fine-celled TPO foams produced by injection molding is necessary in order to optimize the TPO foams. In this chapter, the mechanical property of injection molded TPO foams with various cell morphologies that are suitable for automotive applications was examined. The results of this study help processing engineers to optimize the mechanical property of the injection molded TPO foams.

## 5.2 Experimental

### 5.2.1 Experimental Materials and the Processing of TPO Foams

The TPO material TYC735X was investigated in this chapter. The specimens of fine-celled TPO foams were processed and supplied from Microcellular Plastics Manufacturing Laboratory at the University of Toronto. The ASTM standard (D638 type IV) TPO foamed specimens and the 3mm thick foamed TPO plates were produced by a specially designed injection molding machine for tensile and impact testing respectively. This injection molding machine is capable of producing polymeric foams with various cell morphologies by altering the processing parameters. The information on the processing parameters of injection molded TPO foamed samples were listed on Table 6-1. There are three major controllable processing parameters (the amount of gas content in the molten gas/polymer mixture, with/without using the gas counter pressure and with/without opening the mold) can be altered in this injected molding machine. The physical blowing agent used was $N_2$ supplied by BOC Canada.

### 5.2.2 Mechanical Testing

The tensile mechanical testing was carried out according to ASTM D638 on an Instron 4465 mechanical testing machine at room temperature without using the extensometer. The displacement rate of the crosshead was 50mm per minute. The capacity of the load cell was 5kN. A pair of 5kN wedge action grips was used to hold the samples on the tester. After each testing, the imprint pattern on the samples showed that the slippage in the grips during the testing was kept to minimum. Therefore, the effect of

slippage in the grips and the deflection on the cross head on strain rate was neglected in this study. A minimum of five specimens were tested for each set of foaming conditions. The modulus of elasticity was determined by calculating the slope of the stress-strain curves in the elastic region. The strain was calculated from the displacement of the crosshead. The surface roughness of the samples was measured by using the surface roughness tester (Times Inc. TR200). The elastic modulus, tensile strength, and elongation at break of the foamed TPO specimens were characterized as a function of cell morphologies and surface roughness. The average value of each foaming condition was reported in this chapter.

The impact testing was carried out according to ASTM standard D5420 "Standard Test Method for Impact Resistance of Flat, Rigid Plastic Specimen by Means of a Striker Impacted by a Falling Weight" [99] by using a Gardner Impact tester (Qualitest IG-1142). This method determines the impact energy and impact resistance of rigid polymers. The impact energy defined as the minimum energy required to facture the TPO specimen. The impact resistance defined as the impact energy to fracture the sample per unit thickness. Failure was taken as any fracture in the sample that allowed light passage. A minimum 20 samples were tested for each processing condition. The average value of each foaming condition was reported in this chapter.

## 5.3 Results and Discussion

The effect of cell morphologies on mechanical properties of injection molded TPO foams was presented in this section. Table 6-1 listed the injection molded TPO foams which were processed under 8 different sets of processing conditions. Figure 5-1 shows

the engineering stress-strain curves of TPO foams prepared under these various set of processing conditions. The effects of the relative density, skin thickness, cell density and surface roughness on tensile properties and impact resistance were presented and discussed in the following sub-sections.

### 5.3.1 Effect of Skin Thickness on Mechanical Properties

The skin thickness is defined as the thickness of the unfoamed skin layer in the foamed specimen. The unfoamed skin layer existed in the foams which were produced by injection molding technique and other foaming techniques. As the molten gas/polymer mixture was injected into the mold, the rapid decreased of pressure in the mold caused the gas molecules on the surface to diffuse very quickly from the material. Therefore, no cells were nucleated in the regions close to the surface of the specimens. Thus, mechanical properties can be affected by the skin thickness of the polymeric foams.

Figure 5-2 - Figure 5-4 show the effects of skin thickness on tensile properties of injection molded TPO foams by observing the figures, the tensile modulus, tensile strength and percent strain increased with the skin thickness. The tensile modulus and tensile strength increased approximated 10%, as well, the percent strain increased rapidly from 100% to 600% as the skin thickness increases from 100μm to 500μm. These results were expected since the percentage of unfoamed region increases, the amount of material per unit area increases which cause the tensile properties of the foams to increase.

The effect of skin thickness on impact resistance is shown in Figure 5-5. By observing the figure, the impact resistance of injection molded TPO foams increased with the skin thickness. The impact resistance tripled as the skin thickness of the foams

increased from 90μm to 450μm. When the impact occurred directly on the face of the unfoamed skin layer, this solid unfoamed skin layer would work as an energy absorber in the first zone. The foamed structure in the core of the sample would be the second zone to absorb the impact energy. The thicker the skin layer, the more impact energy can be absorbed and harder to fracture. Therefore, the impact property increased with increasing the skin thickness of the foams.

### 5.3.2 Effect of Surface Roughness on Mechanical Properties

The effects of surface roughness on tensile properties of injection molded TPO foams were shown in Figure 5-6 - Figure 5-8. The error range of the tensile modulus and tensile strength on each processing condition vary from 1% to 10%. The tensile modulus and tensile strength did not change noticeably as the average surface roughness increased from 0μm to 2.5μm. This finding shows that the effect of surface roughness on tensile modulus and strength is negligible. However, the percent strain decreased as the surface roughness increased. The percent strain decreased significantly from 700% to 100% as the average surface roughness of the TPO foams increases from 0μm to 2.5μm. Similarly, the impact energy and impact resistance decreased as the surface roughness increased as shown in Figure 5-9. The impact resistance decreased from approximately 6kJ/m to 3kJ/m as the surface roughness increased from 0μm to 2.5μm. This is attributed to the stress concentration on the surface of the samples increased as the surface roughness increase. Therefore, less energy is needed to initiate cracks on the surface of the sample under impact loading, thus causing the percent strain and impact resistance to decrease. Therefore, the percent strain and impact resistance were also affected by the surface

roughness of the injection molded TPO foams.

### 5.3.3 Effect of Relative Density on Mechanical Properties

The effect of relative density on tensile property of injection molded TPO material is shown in Figure 5-10 - Figure 5-12. Similarly, both tensile modulus and tensile strength decreased with the relative density. By observing the figures, the tensile modulus decreased from 420MPa to 320MPa and the tensile strength decreased from 18MPa to 15MPa as the relative density decreases from 1 to 0.7%. This was attributed to the material reduction per unit volume of the foams. However, the tensile strength only decreased 16.7% as the weight of the material reduced by 30% as shown in Figure 5-11. Therefore, the introduction of the cellular structure by injection molding technique successfully improved the mechanical strength of the material. By observing Figure 5-12, the effect of relative density on the percent elongation was not noticeable.

The effects of relative density on impact resistance of injection molded TPO foams were shown in Figure 5-13. By observing the figures, the impact energy decreased with the relative density of the foams. The impact energy decreased by approximately half at 10% weight reduction of the TPO material. For the 25% weight reduction of foamed samples which produced without using gas counter pressure, the impact resistance further decreased down to one sixth of the unfoamed material.

By using gas counter pressure, the impact resistance remains at approximately 5kJ/m at 25% weight reduction of the foamed TPO materials. Since the foamed samples which had better surface roughness can be produced by using gas counter pressure, the stress concentration on the surface of the samples was reduced, causing the impact resistance to

increase.

For unfoamed TPO materials, the rubber treated as a second phase in the PP matrix contribute to the overall energy absorption in an impact loading. Thus, incorporating rubbery particles can toughen the unfoamed PP polymer. However, the interfacial adhesion between rubber phase and the PP phase is relatively weak. For TPO foams, the cells in the structure reduced the crack length between two regions of second phase rubber. As the crack of the cells is initiated by impact loading, less energy is required to propagate the crack. Therefore, the impact resistance of the TPO foams were significantly reduced compared to the unfoamed materials.

Overall, the results show that the impact resistance is very sensitive to the relative density, skin thickness and surface roughness. The cellular structure of the foams significantly reduced the ability of the TPO materials to withstand the shock loading.

## 5.4 Constitutive Model for Injection Molded TPO Foams

The constitutive model of the injection molded TPO foams was presented in this section. The structure-mechanical property of injection molded TPO foams was experimentally obtained in the pervious section. In this section, constitutive models were proposed to correlate the structure-mechanical relationship of injection molded TPO foams. These constitutive models can help engineers predict the mechanical property of microcellular TPO foams prepared with different processing parameters.

### 5.4.1 The Effect of Relative Density on Tensile Modulus

The effect of relative foam density on relative tensile modulus of injection molded

TPO foams was shown in Figure 5-10. Similarly, the tensile modulus found to be very closely related to the relative density of the foams. The dots were the data obtained experimentally from pervious section. The constitutive model based on Gibson and Ashby was proposed according to the experimental data of this:

$$\frac{E_f}{E_p} \approx 0.8\left(0.5\frac{\rho_f}{\rho_p}\right)^{1/2} + 0.6(0.5)\left(\frac{\rho_f}{\rho_p}\right) \tag{5.1}$$

The $C_1$= 0.8, $C_1'$= 0.6 and $\phi$ is 0.5 in Equation 5.1 were the constants to fit the experimental data. The formula was plotted as the solid line on the Figure 5-10. This constitutive model fits the experimental data very well.

### 5.4.2 The Effect of Relative Density on Tensile Strength

Figure 5-11 presented the effect of relative foam density on relative tensile strength of injection molded TPO foams. The dots plotted on the Figure 5-11 are the experimental results obtained in this Chapter. The proposed constitutive model based on Gibson and Ashby was plotted as the dash line on the figures and was shown in the following equations:

$$\frac{\sigma_f}{\sigma_p} \approx \left(0.9\frac{\rho_f}{\rho_p}\right)^{3/2} + (0.1)\left(\frac{\rho_f}{\rho_p}\right) \tag{5.2}$$

Where the constants $C_5$=1, $C_5'$=1 and $\phi$ is 0.9. The values of these constants were suggested based on the experimental data obtained from convectional foam.

By observing the Figure 5-11, the constitutive model (Equation 5.2) suggested by Gibson and Ashby underestimated the performance of the TPO foams. Similarly, this is due to the constants used in Equation 5.2 was estimated based on low density

conventional foams that had a relative density between 0.4 and 0.7. Since all the injection molded TPO foams had the relative density above 0.75, the constitutive model from Gibson and Ashby had underestimated the tensile strength of the injection molded TPO foams.

As a result, empirical formula was proposed according to the experimental data of this:

$$\frac{\sigma_f}{\sigma_p} \approx 0.8\left(0.8\frac{\rho_f}{\rho_p}\right)^{\frac{1}{2}} + (0.2)\left(\frac{\rho_f}{\rho_p}\right) \tag{5.3}$$

Where the constants $C_5$=0.8, $C_5'$=1 and $\phi$= 0.8. The formula was plotted as the solid line in Figure 5-11 and it fits the experimental data very well.

## 5.5 Conclusion

The mechanical properties and impact resistance of injection molded TPO foams were examined. The effects of relative density, skin thickness, cell density and surface roughness on tensile and impact properties of injection molded TPO foams were correlated. Several conclusions have been made in this chapter: 1) the tensile strength only decreased 16.7% at 30% weight reduction of injection molded TPO foams. Therefore, the tensile strength was successfully improved by introducing cellular structure in the TPO material by injection molding method. 2) The tensile properties and impact resistance increased with the skin thickness of the foams. 3) The percent strain was only affected by the surface roughness of the TPO foams due to the stress concentration on the surface of the foamed samples. 4) The impact resistance is very sensitive to the relative foam density, skin thickness and surface roughness of the foams.

5) For foamed TPO materials which is rubber toughened, the impact resistance is significantly decreased by the cellular structure. 6) The impact resistance and the surface roughness of the foams can be improved by using the gas counter pressure.

Table 5-1: Processing information of injection molded TPO foams.

| Run Number | $N_2$ Gas Content (%) | Relative Density | GCP | Mold Opening |
|---|---|---|---|---|
| 0 (unfoamed) | 0 | 1 | N/A | N/A |
| 1 | 0.5 | 0.90 | No | No |
| 2 | 0.5 | 0.85 | No | No |
| 3 | 0.5 | 0.70 | No | No |
| 4 | 0.5 | 0.75 | No | No |
| 5 | 0.5 | 0.90 | Yes | No |
| 6 | 0.5 | 0.85 | Yes | No |
| 7 | 0.5 | 0.70 | Yes | Yes |
| 8 | 0.5 | 0.75 | Yes | Yes |

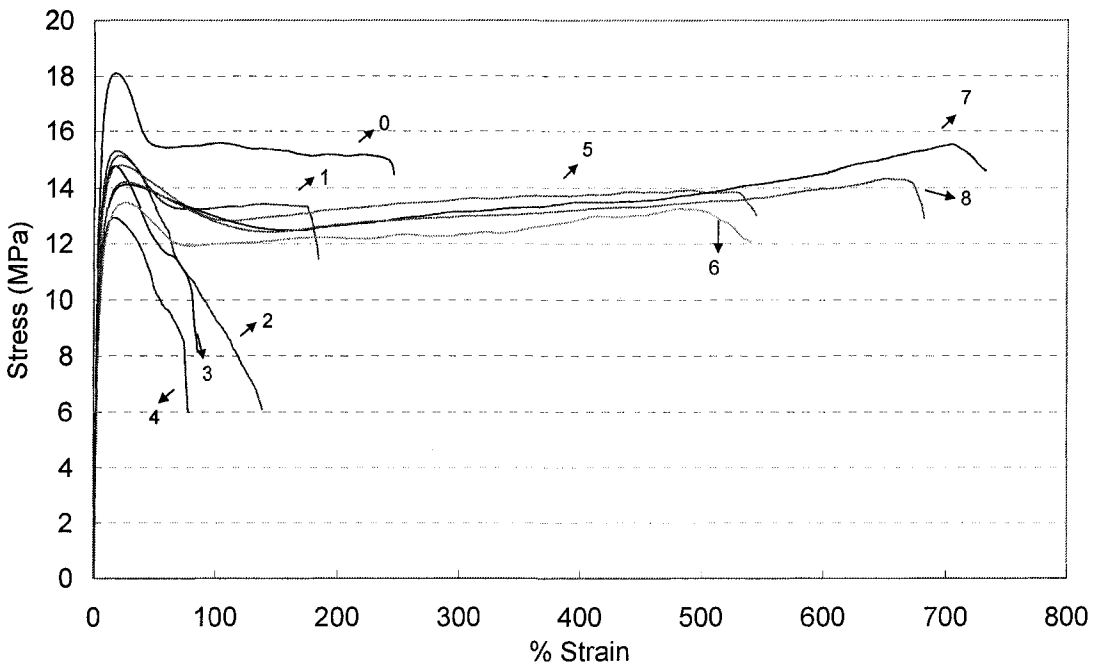


Figure 5-1: Engineering stress-strain curves of injection molded TPO foams.
(The number on each S-S curve represents the Run Number as refer to Table 5-1)

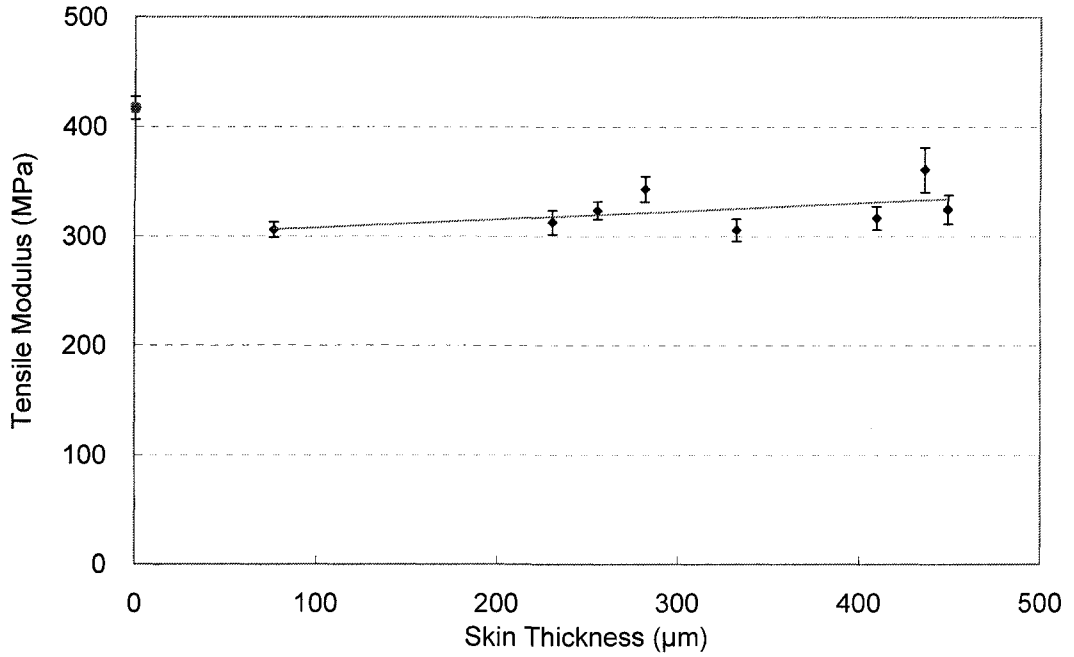


Figure 5-2: The effect of skin thickness on tensile modulus of injection molded TPO foams.

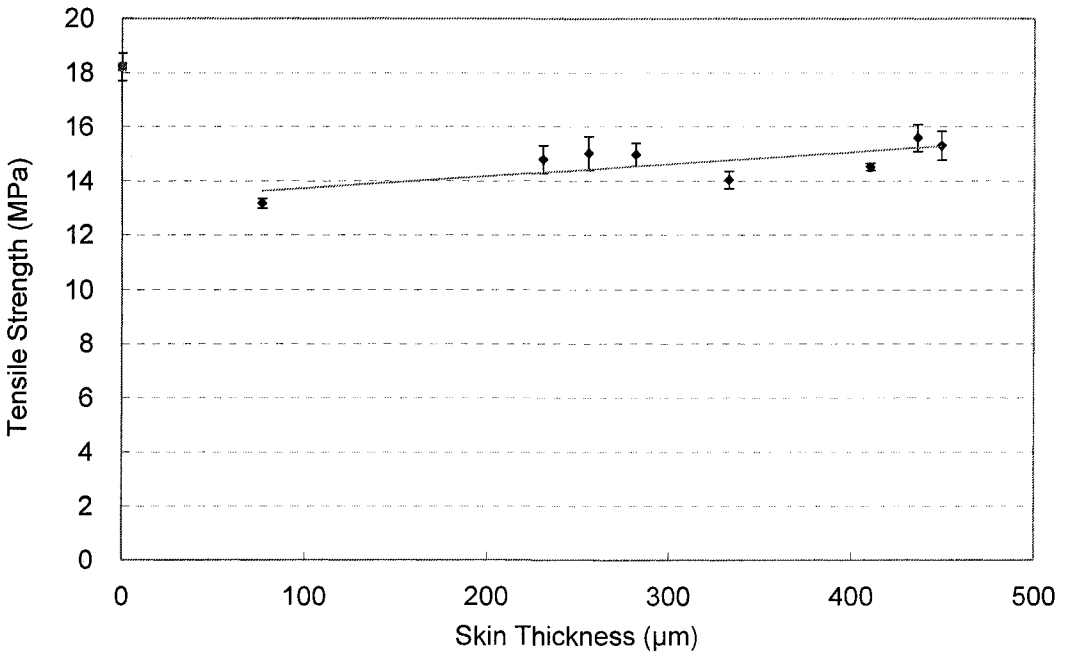


Figure 5-3: The effect of skin thickness on tensile strength of injection molded TPO foams.

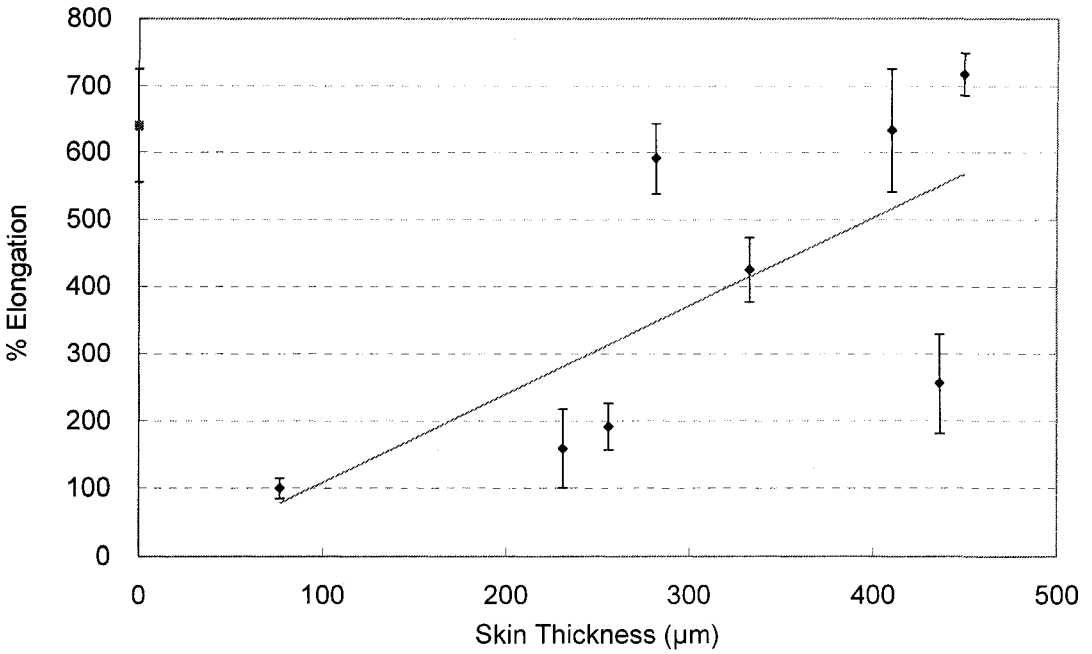


Figure 5-4: The effect of skin thickness on % elongation of injection molded TPO foams.

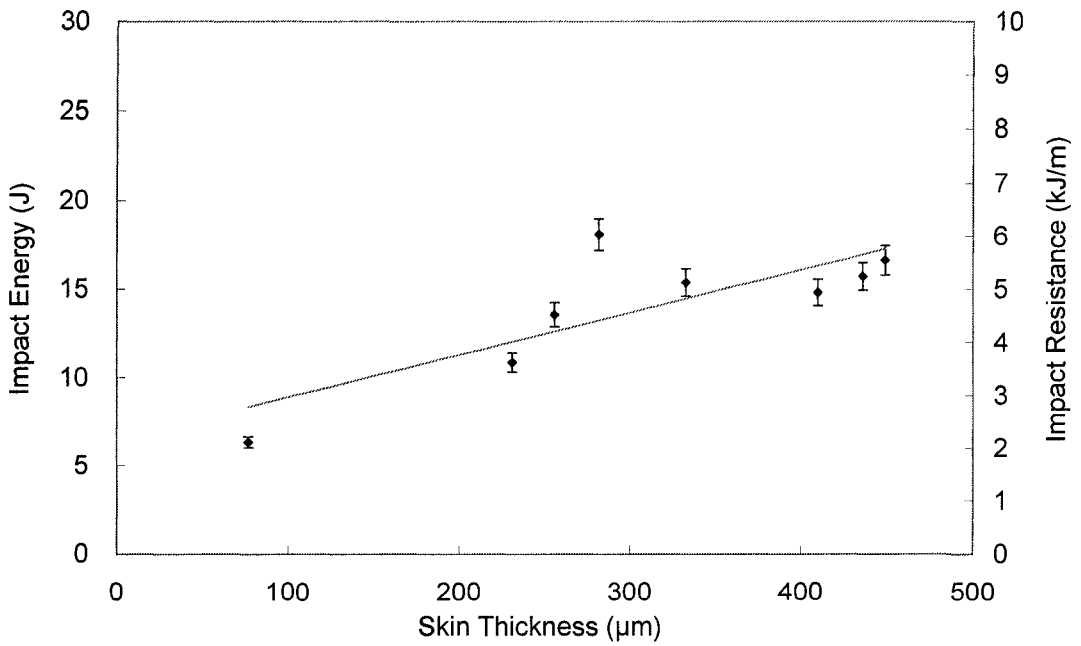


Figure 5-5: The effect of skin thickness on impact resistance of injection molded TPO foams.

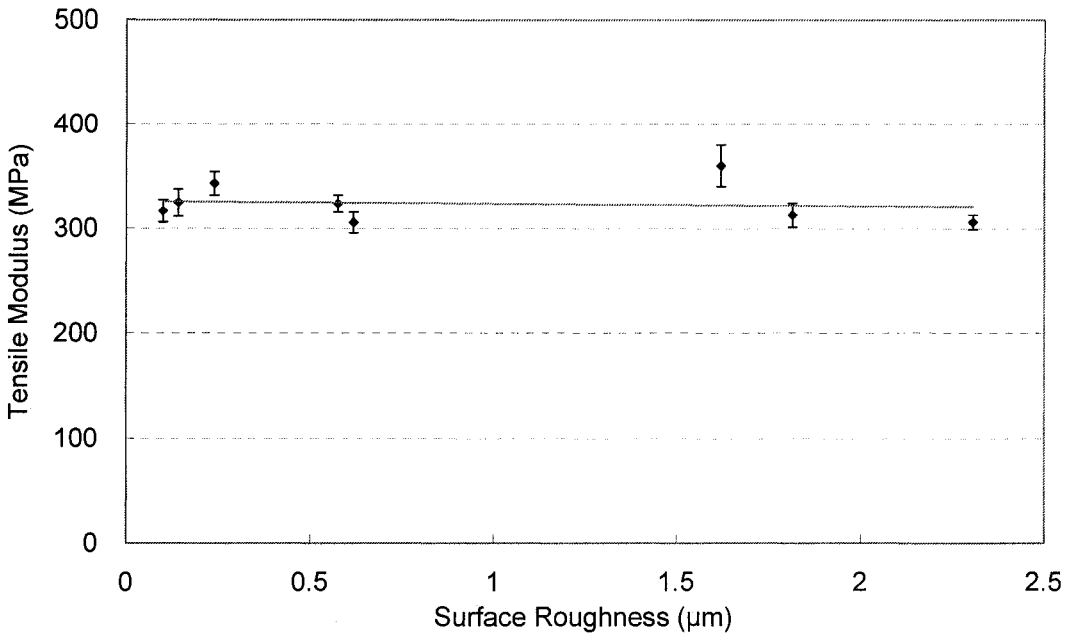


Figure 5-6: The effect of surface roughness on tensile modulus of injection molded TPO foams.

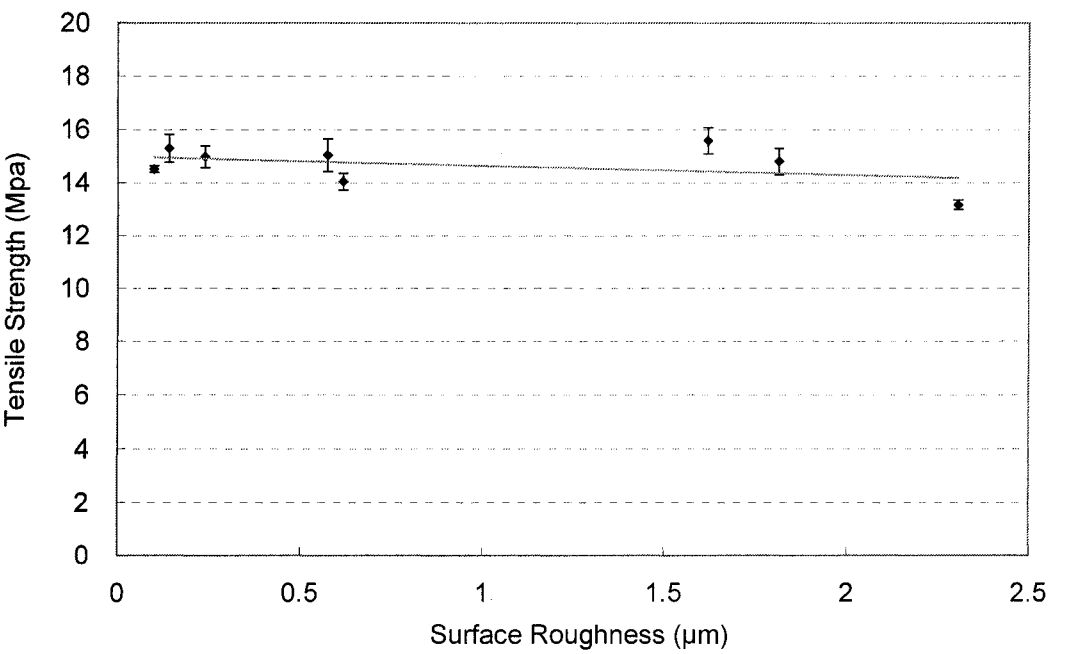


Figure 5-7: The effect of surface roughness on tensile strength of injection molded TPO foams.

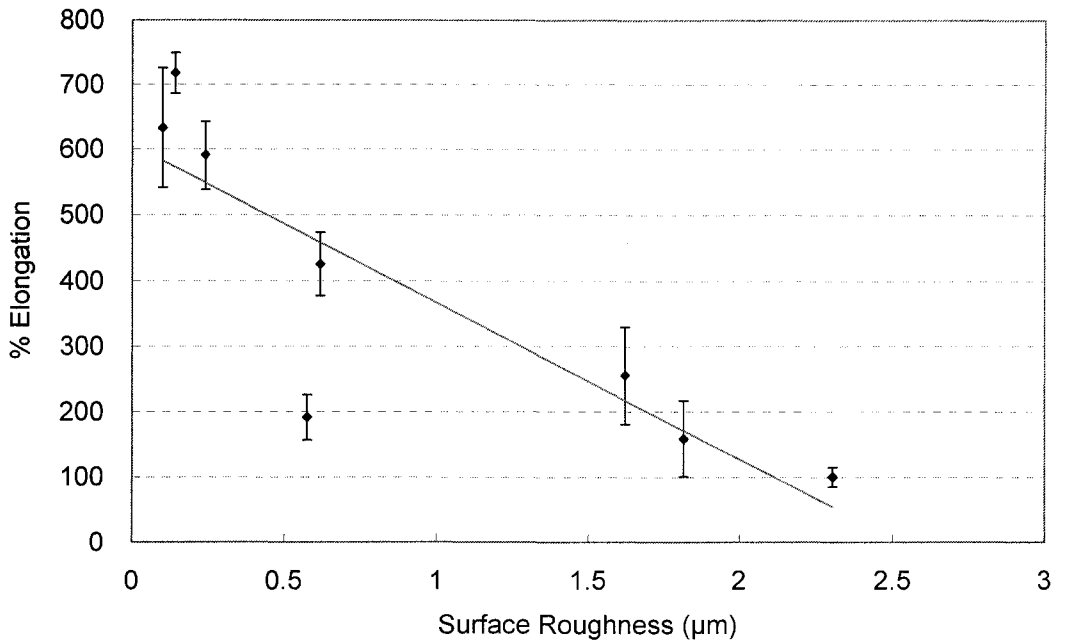


Figure 5-8: The effect of surface roughness on % elongation of injection molded TPO foams.

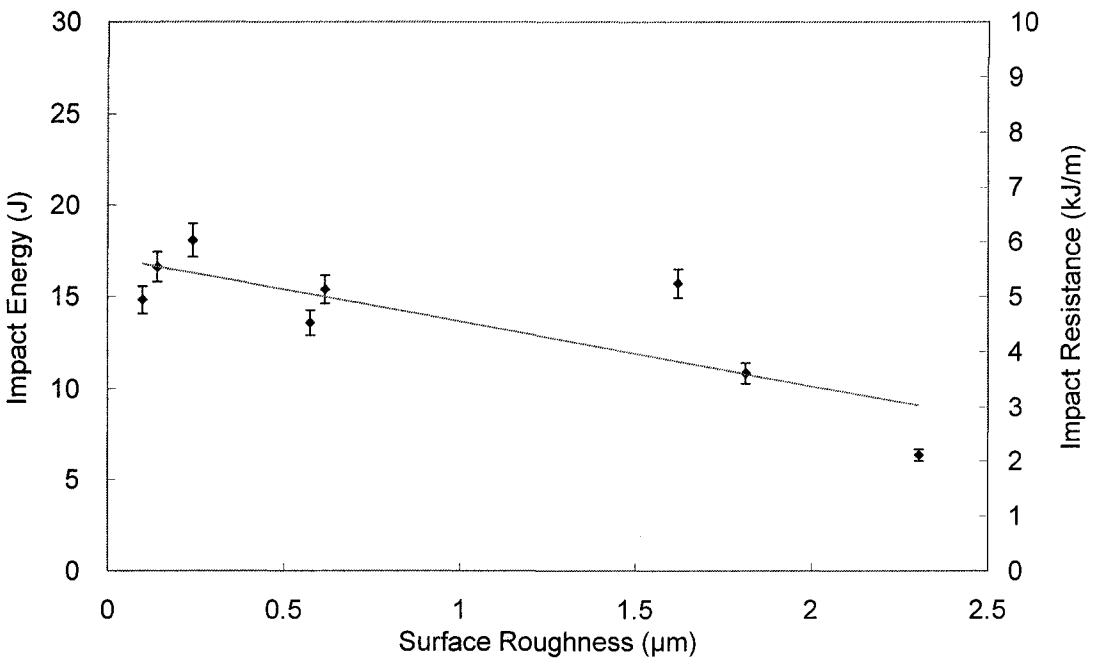


Figure 5-9: The effect of surface roughness on impact resistance of injection molded TPO foams.

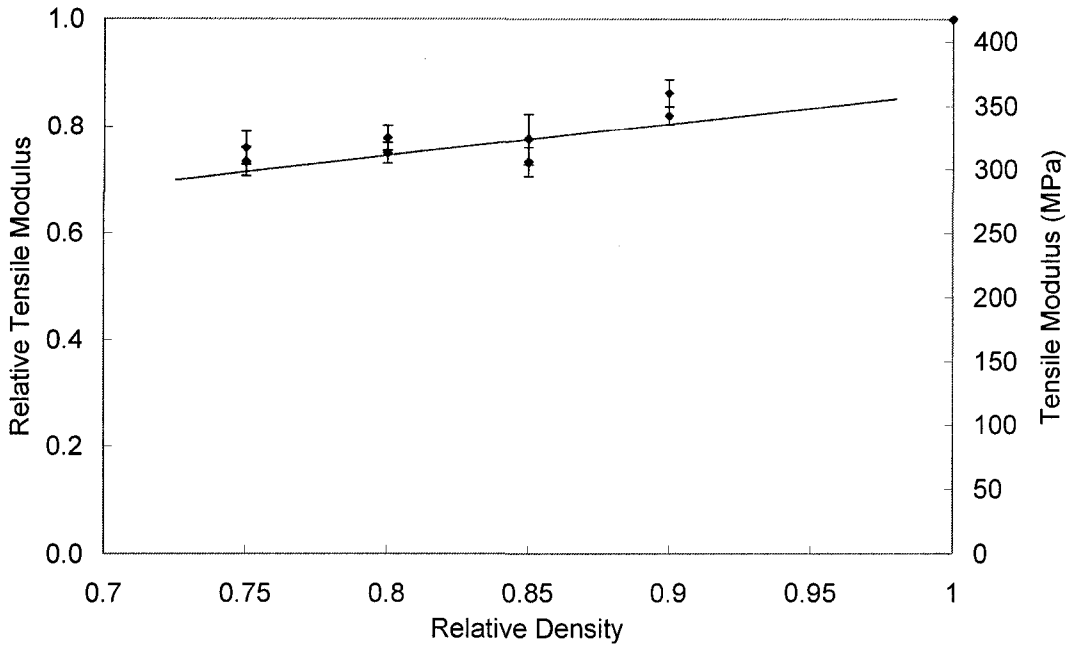


Figure 5-10: The effect of relative density on tensile modulus of injection molded TPO foams.

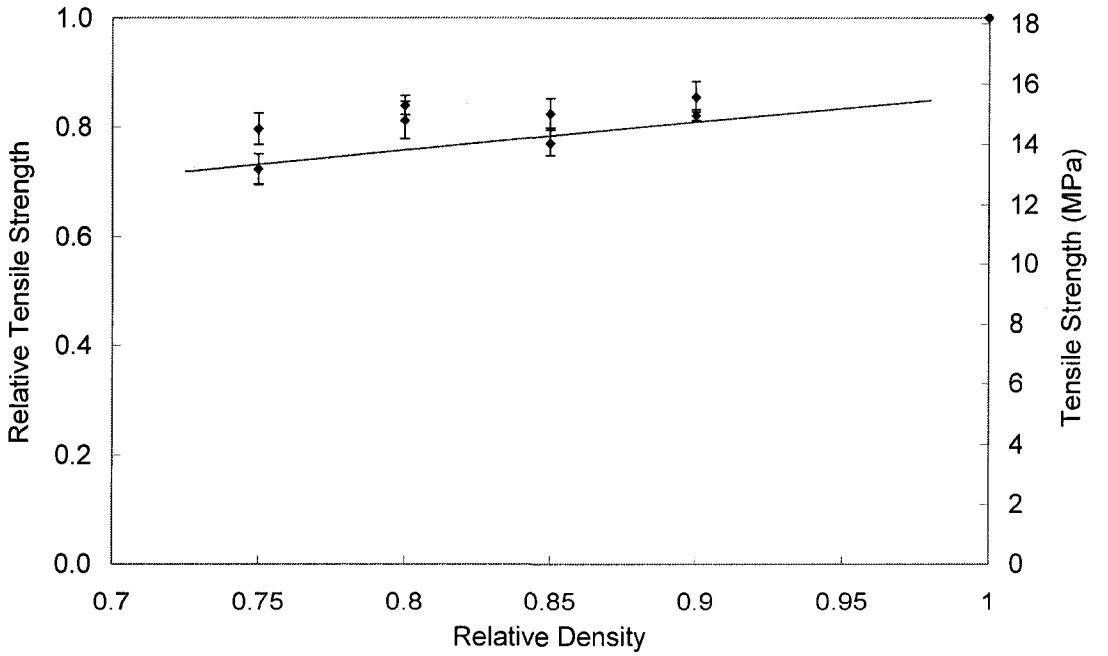


Figure 5-11: The effect of relative density on tensile strength of injection molded TPO foams.

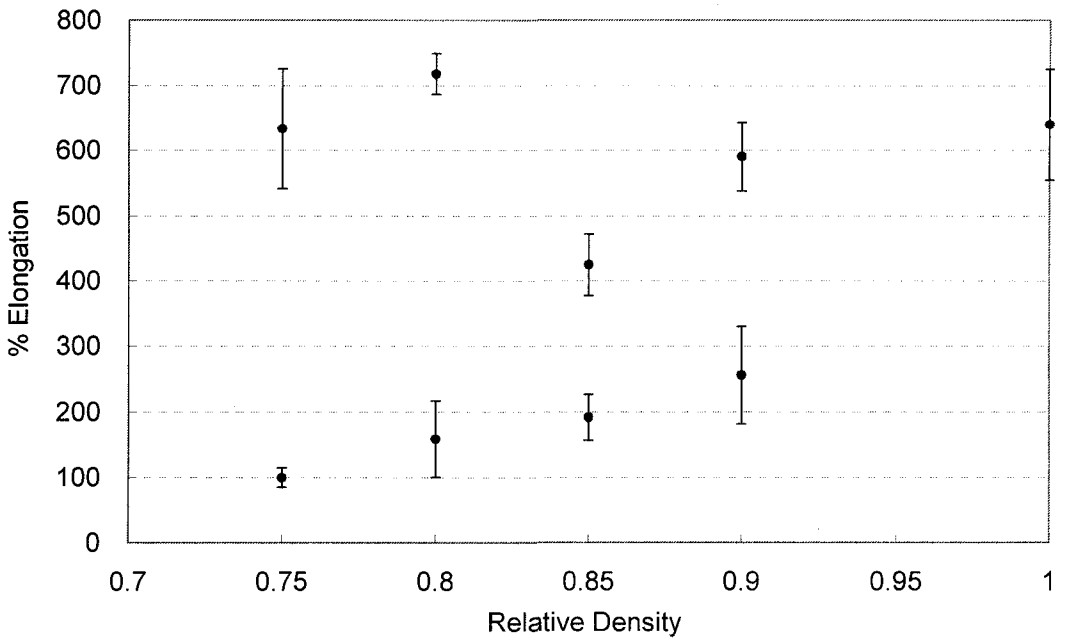


Figure 5-12: The effect of relative density on % elongation of injection molded TPO foams.

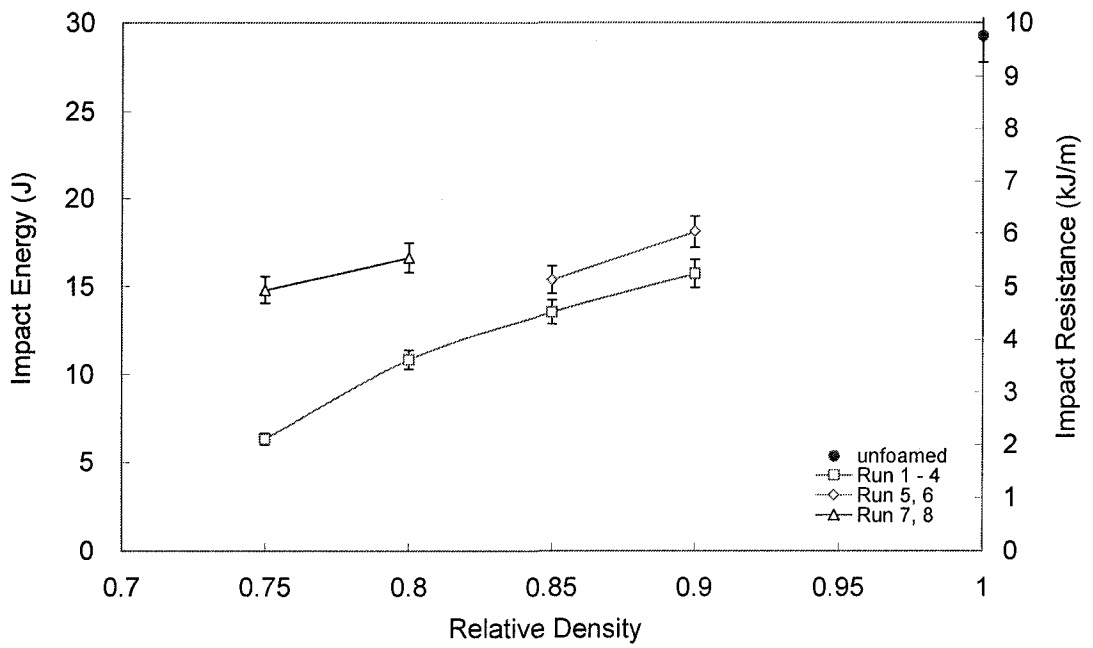


Figure 5-13: The effect of relative density on impact resistance of injection molded TPO foams. (Run 1-4: without using gas counter pressure; Run 5-8: with using gas counter pressure)

# Chapter 6
# Conclusions

The objective of this research is to investigate the correlations of the processing, structure and mechanical properties for cellular TPO foams. Closed-cell TPO foams were processed using the aforementioned two-stage batch approach and injection molding method. The microcellular and fine-celled TPO foams were prepared with different processing parameters in order to examine their effects on the mechanical properties of the foam structure. Elastic modulus, tensile strength, elongation at break, elastic recovery and impact resistance of various foamed TPO samples was characterized as a function of cell morphologies.

The experimental work presented in this research leads to the following conclusions:

1. The microcellular TPO foams were successfully processed by using two-stage batch foaming method. The cell morphology of the TPO foams can be effectively controlled by carefully altering the foaming parameters: saturation pressure, foaming temperature and foaming time.

2. For microcellular TPO90, TPO70, TPO50 and DTPO foams, the average cell size

increased very slightly with foaming time and foaming temperature. The change on cell density at various processing conditions is not significant. The relative foam density of the microcellular TPO foams was inversely proportional to saturation pressure, foaming temperature and foaming time.

3. A minimum relative foam density of 0.75 was obtained under a saturation pressure of 27.6MPa for TPO70. Higher saturation pressures are necessary to further decrease the relative foam density of the microcellular TPO foams.

4. The PP to Elastomer ratio of 7:3 is the optimal composition for both foamability and mechanical properties.

5. The mechanical properties of the microcellular TPO foams are directly related to the processing parameters which vary the cell morphologies. The results show that the tensile strength of TPO70 decreased only approximately 13% as the relative foam density decreased 22%. Similar results were observed in the other three TPO composites. Therefore, the weight reduction of TPO materials can be achieved without sacrificing much on the mechanical properties by introducing cellular structure in TPO materials.

6. Under the same processing parameters, the cell morphologies and mechanical properties of TPO foams vary with the TPO composition. However, the results show that the effects of processing parameters on the cell morphologies and mechanical

properties of the different TPO composites share a similar trend.

7. The constitutive models based on Gibson and Ashby were proposed to correlate to the structure-property relationship of various microcellular TPO foams. The proposed constitutive models for various TPO foams fit well to the experimental data.

8. The elastic recovery curves of microcellular TPO foams were successfully obtained. The results show that the first stage of elastic recovery curve dominated the full recovery process and the second stage contribute only approximately 10% of the full recovery process and this recovery appears to be associated with the recovery of the cellular structure of the foamed specimens.

9. The results also show that the elastic recovery is very sensitive to the relative density of the microcellular TPO foams. Up to 31% improvement in elastic recovery was achieved at 20% weight reduction by introducing microcellular structure in the TPO materials.

10. The compression set increased with the original compressive strain. In other words, less elastic recovery was observed as the original compressive strain increases.

11. At 25% weight reduction of the TPO material, the tensile strength only decreased 16.7% for the injection molded TPO foams. Therefore, the mechanical strength of

the injection molded TPO foams was successfully enhanced by introducing cellular structure in the TPO materials.

12. For the foamed TPO materials which is rubber toughened, the impact resistance is significantly decreased by the cellular structure due to the relatively week interface between the PP and the rubber phase in the TPO material.

13. The impact resistance and surface roughness of the injection molded TPO foams could be improved by using the gas counter pressure.

# Chapter 7
# Recommendations

1. The effect of cell morphology on mechanical properties of cellular TPO foams should be further investigated. The mechanical properties such as biaxial tensile property, flexural property and compression property of cellular TPO foams need to be examined in order to completely study the effect of cellular structure on mechanical properties of various TPO materials. .

2. The mechanical properties of cellular TPO foams at a very high relative foam density (>0.95) region should be further investigated. For each composition of microcellular TPO foam, a decrease in both tensile modulus and tensile strength at very high relative density was observed. More research needs to be done in order to understand and minimize the effect on the tensile properties at high relative density of the cellular TPO foams.

3. The structure-properties relationships of cellular TPO foams should be further investigated. The constitutive models proposed in this thesis only relate the mechanical properties as a function of the relative foam density. In addition, the

models are not able to relate the non-linear structure-properties relationship at the relative density above 0.95 of the foams. As a result, an alternative analytical model such as finite element analysis may be able to accurately study the non-linear structure-property relationship of the cellular TPO foams.

4. The impact resistance of cellular foams should be further investigated. The impact resistance reduced dramatically even at a very high relative foam density. Further research is necessary in order to minimize the effect on impact strength by introducing cellular structure in the TPO materials.

# References

[1] Kumar, V.; VanderWel, M. and Weller, J. 1994, Experimental Characterization of the Tensile Behavior of Microcellular Polycarbonate Foams, Journal of Engineering Materials and Technology, Transactions of the ASME, 116, 4, 439.

[2] Fu, J. and Naguib, H. E. 2005, Effect of Processing Parameters on Cellular Structures and Mechanical Properties of PMMA Microcellular Foams, Cellular Polymers, 24, 4, 177.

[3] Matuana, L. M.; Park, C. B. and Balatinecz, J. J. 1998, Structures and Mechanical Properties of Microcellular Foamed Polyvinyl Chloride, Cellular Polymers, 17, 1, 1.

[4] Martini, J. E.; Suh, N. P., and Waldman, F. A., 1984, Microcellular Closed Cell Foams and their Method of Manufacture, U.S. Patent, 06/403,831 (4,473,665).

[5] Xu, X.; Park, C.B.; Xu, D. and Pop-Iliev, R. 2003, Effects of Die Geometry on Cell Nucleation of PS Foams Blown with $CO_2$, Polymer Engineering Science, 43, 1378.

[6] Baldwin, D.F.; Park, C.B. and Suh, N.P. 1996, An Extrusion System for the Processing of Microcellular Polymer Sheets: Shaping and Cell Growth Control, Polymer Engineering and Science, 36, 10, 1425.

[7] Gendron R.; Daigneault L.E. 2003, Continuous Extrusion of Microcellular Polycarbonate, Polymer Engineering Science, 43, 1361.

[8] Park, C.B.; Baldwin D.F. and Suh, N.P. 1995, Effect of Pressure Drop Rate on Cell Nucleation in Continuous Processing of Microcellular Polymers Polymer Engineering and Science, 35, 432.

[9] Park, C.B. and Suh, N.P. 1996, Filamentary Extrusion of Microcellular Polymers Using a Rapid Decompressive Element, Polymer Engineering and Science, 36, 1, 34.

[10] Park, C.B.; Behravesh, A.H. and Venter, R.D. 1998, Low Density Microcellular Foam Processing in Extrusion Using $CO_2$, Polymer Engineering and Science, 38, 1812.

[11] Xu, J. Method for Manufacturing Foam Material Including Systems with Pressure Restriction Element. U.S. Patent 6,322,347,2001.

[12] Baldwin, D. F. and Suh, N. P. 1992, Microcellular Poly (Ethylene Terephthalate) and Crystallizable Poly (Ethelene Terephthalate) Characterization of Process Variables, SPE-ANTEC Technical Paper, 38, 1503.

[13] Colton, J. S and Suh, N. P. 1987, Nucleation of Microcellular Thermoplastic foam

with Additives: Part i: Theoretical Considerations, Polymer Engineering and Science, 27, 485.

[14] Colton, J. S and Suh, N. P. 1987, Nucleation of Microcellular Thermoplastic foam with Additives: Part ii: Experimental Results and Discussion, Polymer Engineering and Science, 27, 493.

[15] Kumar, V. and Suh, N. P. 1990, A Process for Making Microcellular Thermoplastic Parts, Polymer Engineering and Science, 30, 1323.

[16] Amon, M. and Denson, C. D. 1984, A Study of the Dynamics of Foam Growth, Analysis of the Growth of Closely Spaced Spherical Bubbles, Polymer Engineering and Science, 26, 255.

[17] Griffith, A. A. 1924, Theory of Rupture, First International Congress of Applied Mechanics, 1, 55.

[18] Waldman, F. A. 1982, Thesis, Department of Mechanical Engineering, Massachusetts Institute of Technology (MIT), Cambridge, MA.

[19] Martini, J.; Waldman, F. A. and Suh, N. P. 1982, The Production and Analysis of Microcellular Thermoplastic Foams, SPE-Technical Papers, 28, 674

[20] Kumar, V.; Weller, J. E., and Montecillo, R. 1992, Microcellular PVC, SPE-ANTEC Technical Papers, 1452-1456.

[21] Seo, W. J.; Jung, H. C.; Hyun, J. C.; Kim, W. N.; Lee, Y. B.; Choe, K. H. and Kim, S. B. 2003, Mechanical, Morphological and Thermal Properties of Rigid Polyurethane Foams Blown by Distilled Water, Journal of Applied Polymer Science, 90, 12-21.

[22] Collias, D. I. and Baird, D. G. 1994, Impact Toughening of Polycarbonate by Microcellular Foaming, Polymer, 35, 18, 3978-3983.

[23] Seeler, K. A. and Kumar, V. 1993, Tension-Tension Fatigue of Microcellular Polycarbonate: Initial Results, Journal of Reinforced Plastics and Composites, 12, 3, 359-376.

[24] Shimbo, M.; Baldwin, D. F. and Suh, N. P. 1995, Viscoelastic Behavior of Microcellular Plastics with Varying Cell Size, Polymer Engineering and Science, 35, 17, 1387.

[25] Fu, J., 2005, MASc Thesis, Development of Polymeric Foam Materials with Improved Mechanical and Acoustic Properties, Ottawa-Carleton Institute for Mechanical and Aerospace Engineering, University of Ottawa, Ottawa, Canada.

[26] Mishra, J. K.; Hwang, K. and Ha, C. 2005, Preparation, Mechanical and Rheological

Properties of a Thermoplastic Polyolefin (TPO)/organoclay Nanocomposite with Reference to the Effect of Maleic Anhydride Modified Polypropylene as a Compatibilizer, Polymer, 46, 6, 1995.

[27] Mehta, S.; Mirabella, F. M. and Rufener, K. 2004, Thermoplastic Olefin/Clay Nanocomposites: Morphology and Mechanical Properties," Journal of Applied Polymer Science, 92, 2, 928.

[28] Shah, S. and Kakarala, N. 2000, Requirements for Rapid Growth of All Olefinic Automotive Interiors, SPE-ANTEC Technical Papers, 1095.

[29] Gorski, R. A.; Ramsey, R. B. and Dishart, K. T. 1986, Physical Properties of Blowing Agent Polymer System-I. Solubility of Fluorocarbon Blowing Agents in Thermoplastic resins, Journal of Cellular Plastic, 22, 1, 21.

[30] Papadopoulou, C. P. and Kalfoglou, N. K. 2000, Comparison of Compatibilizer Effectiveness for PET/PP Blends: Their Mechanical, Thermal and Morphology Characterization, Polymer, 41, 7, 2543.

[31] Fan, X. S. 2006, Mechanical Properties of PP/Ethylene Acrylate Copolymer/$TiO_2$ Blends, SPE-ANTEC Technical Papers, 1771.

[32] Lu, J.; Wei, G. and Sue, H. 2000, Toughening Mechanisms in Commercial Thermoplastic Polyolefin Blends, Journal of Applied Polymer Science, 76, 3, 311.

[33] Liu, Y. and Kontopoulou, M. 2006, SPE-ANTEC Technical Papers, 248.

[34] Guo, G. 2001, Manufacture of Fine-Celled Plastic/Wood-Fiber Composite Foams Using CO2 as a Blowing Agent, Thesis, Department of Mechanical & Industrial Engineering, University of Toronto.

[35] Frich, K. C. and Saunders, J. H. 1972, Plastic Foams, Part I, Marcel Dekker Inc., N.Y.

[36] Marom, G. 1985, Polymer Permeability, Elsvier Applied Science Publishers, London

[37] Park, C. B. and Cheung, L. K. 1997, Study of Cell Nucleation in the Extrusion of Polypropylene Foams, Polymer Engineering Science, 37, 1.

[38] Hong, D.; Yoon, K. J. and Lee, K. Y. 2002, Structural Changes of Homopolymer Polypropylene Foam with Molecular Weights and Rheological Properties: (1) in Batch Process, Polymer, 26, 1, 61.

[39] Varma-Nair, M.; Handa, P. Y.; Mehta, A. K. and Agarwal, P. 2003, Effect of Compressed $CO_2$ on Crystallization and Melting Behaviour of Isotactic Polypropylene. Thermochimica Acta, 396, 57.

[40] Arora, K. A.; Lesser, A. J. and McCarthy, T. J. 1998, Compressive Behavior of Microcellular Polystyrene Foams Processed in Supercritical Carbon Dioxide, Polymer Engineering Science, 38, 2055.

[41] Arora, K. A.; Lesser, A. J. and McCarthy, T. J. 1998, Preparation and Characterization of Microcellular Polystyrene Foams Processed in Supercritical Carbon Dioxide, Macromolecules, 31, 4614.

[42] Stafford, C. M.; Russell, T. P. and McCarthy, T. J. 1999, Expansion of Polystyrene using Supercritical Carbon Dioxide: Effects of Molecular Weight, Polydispersity, and low Molecular Weight Components, Macromolecules, 32, 22, 7610.

[43] Wu, X. D. and Peng, Y. C. 2006, Foaming of Polystyrene/Supercritical $CO_2$ in Rapid Decompression and Cooling Process, Advanced Materials Research, 11-12, 761.

[44] Leung, S. N. and Park, C. B. 2006, Effects of Gas Content and Pressure Drop Rate on Foaming, SPE-ANTEC 2006, Technical Paper, 2775.

[45] Shen, J.; Han, X. and Lee, L. J. 2006, Nanoscaled Reinforcement of Polystyrene Foams Using Carbon Nanofibers, Journal of Cellular Plastics, 42(2), 105.

[46] Rodeheaver, B. A. and Colton, J. S. 2001, Open-celled Microcellular Thermoplastic Foam, Polymer Engineering and Science, 41, 3, 380.

[47] Wang, J.; Cheng, X.; Yuan, M. and He, J. 2001, An Investigation of the Microcellular Structure of Polystyrene/LCP Blens Prepared by using Supercritical Carbon Dioxide, Polymer, 42, 19, 8265.

[48] Mizumoto, T.; Sugimura, N.; Moritani, M.; Sato, Y. and Masuoka, H. 2000, CO2-Induced Stereocomplex formation of Stereoregular Poly(Methyl Methacrylate) and Microcellular Foams, Macromolecules, 33, 18, 6757.

[49] Goel, S. K.; Beckman, E. 1994, Generation of Microcellular Polymeric Foams using Supercritical Carbon Dioxide I: Effect of Pressure and Temperature on Nucleation, Journal of Polymer Engineering and Science, 34, 14, 1137.

[50] Nawaby, V.; Yamamoto, Y. and Honda, P. 2002, Kinetic Study on PMMA-$CO_2$ System by Raman Spectroscopy, SPE-ANTEC Technical Paper.

[51] Fu, J.; Jo, C. and Naguib, H. 2005, The Effect of the Processing Parameters on the Mechanical Properties of PMMA Microcellular Foams, SPE-ANTEC Technical Paper 2005, 2616.

[52] Leung, L.; Chan, C.; Song, J.; Tam, J. B.and Naguib, H. 2007, A Parametric Study on the Processing and Characterization of PLGA 50/50 Bioscaffolds, SPE-ANTEC

Technical Paper.

[53] Leung, L.; Perron J. and Naguib, H. 2006, Constitutive Modeling for Porous PLGA 85/15 Scaffold in Compression, ASME Congress 2006.

[54] Ito, Y.; Yamashita, M. and Okamoto, M. 2006, Foam Processing and Cellular Structure of Polycarbonate-based Nanocomposites, Macromolecular Materials and Engineering, 291, 773.

[55] Doroudiana, S.; Park, C. B. and Kortschot, M. T. 1998, Processing and Characterization of Microcellular Foamed High-Density Polyethylene/Isotactic Polypropylene Blends Polymer Engineering and Science, 38, 7, 1205.

[56] Doroudiani, S.; Park, C. B. and Kortschot, M. T. 1996, Effect of Crystallinity and Morphology on the Microcellular Foam Structure of Semicrystalline Polymers, Polymer Engineering and Science, 36, 21, 2645.

[57] Doroudiani, S.; Park, C. B. and Kortschot, M. T. 1996, Characterization of Microcellular foamed HDPE/PP blends, APE-ANTEC Technical Paper, 1914.

[58] Rachtanapun, P.; Selke, S. E. M.; Matuana, L. M. 2003, Microcellular Foam of Polymer Blends of HDPE/PP and their Composites with Wood Fiber, Journal of Applied Polymer Science, 88, 12, 2842.

[59] Baldwin, D. F.; Park, C. B. and Suh, N. P. 1996, Microcellular Processing Study of Poly(ethylene terephthalate) in the Amorphous and Semicrystalline States. Part I: Microcell nucleation, Polymer Engineering Science, 36, 1437.

[60] Baldwin, D. F.; Park, C. B. and Suh, N. P. 1996, A microcellular processing study of poly(ethylene terephthalate) in the amorphous and semicrystalline states Part II Cell growth and process design, Polymer Engineering and Science, 36, 11, 1446.

[61] Handa, P.; Wong, B.; Zhang, Z.; Kumar, V.; Eddy, S. and Khemani, K. 1998, Some Thermodynamic and Kinetic Properties of the System PETG-$CO_2$ and Morphological Characteristics of the $CO_2$-blown PETG Foams, Polymer Engineering Science, 39, 1, 55.

[62] ASTM International, D792, Standard Test Methods for Density and Specific Gravity (Relative Density) of Plastics by Displacement, 100 Barr Harbor Drive, PO Box C700, West Conshohocken, PA 19428-2959, United States.

[63] Sun, H. and Mark, J. E. 2002, Preparation, Characterization, and Mechanical Properties of some Microcellular Polysulfone Foams, Journal of Applied Polymer Science, 86, 7, 1692.

[64] Archer, E.; Harkin-Jones, E. and Kearns, M. P. 2004, Processing Characteristics and Mechanical Properties of Metallocene Catalyzed Linear Low-Density Polyethylene

Foams for Rotational Molding, Polymer Engineering and Science, 44, 4, 638.

[65] Stokes, V. K. 1991, Local Stiffness-Density Correlations for Polycarbonate Structural Foams, SPE-ANTEC Technical Paper, 1312.

[66] Collias, D. and Baird, D. G. 1995, Impact Behavior of Microcellular Foams of Polystyrene and Styrene-Acrylonitrile Copolymer, and Single-Edge-Notched Tensile Toughness of Microcellular Foams of Polystyrene, Styrene-Acrylonitrile Copolymer, and Polycarbonate, Polymer Engineering and Science, 35, 14, 1178.

[67] Hornberger, L.; Malloy, Robert. and Kadkol, P. 1991, Evaluating Mechanical Properties of Reinforced PC structural foam, Plastics Engineering, 47, 6, 25.

[68] Ozkul, M. H. and Mark, J. E. 1994, Effect of Preloading on the Mechanical Properties of Polymeric Foams, Polymer Engineering and Science, 34, 10, 794.

[69] Nimmer, R. P.; Stokes, V. K. and Ysseldyke, D. A. 1988, Mechanical Properties of Rigid Thermoplastic Foams - Part II Stiffness and strength data for modified polyphenylene oxide foams, Polymer Engineering and Science, 28, 22, 1501.

[70] Terauds, A. E.; Gailite, M. P.; Tolks, A. M. and Kregers, A. F. 1989, Evaluation of the elastic properties of reinforced foams plastics, Mechanics of Composite Materials, 25, 3, 292.

[71] Nishikawa Y.; .Yang, X.; Kisaka, S; Nakai, Asami and Hamada, Hiroyuki 2006, "Mechanical Properties of Foamed PP Sheet", SPE-ANTEC 2003 Technical Paper, 2765.

[72] Kumar, V. and Weller, J. E. 1991, Microcellular polycarbonate. Part I. Experiments on bubble nucleation and growth, SPE-ANTEC 91, May 5-9 1991, Society of Plastics Engineers, Brookfield, CT, USA, Montreal, Que, Can, 37, 1401.

[73] Gibson, L. J. and Ashby, M. F. 1999, Cellular Solid: Structure and Properties. Second Edition, Cambridge University Press, Cambridge.

[74] Wimberly, D.T. J. 1991, Evaluation of a Linear Finite Element Analysis Model for Extruded Low Density Foam, SPE-ANTEC Technical Paper, 1308.

[75] Lee, H.; Fasulo, P. D. and Rodgers, W. R. 2005, TPO Based Nanocomposites Part 1 Morphology and Mechanical Properties, Polymer, 46, 25, 11673.

[76] Liu, Y. and Kontopouloua, M. 2006, Mechanical Properties and Morphology of PP and TPO/Nanosilica Nanocomposites, SPE-ANTEC Technical Paper, 248.

[77] ASTM International, D395-01, Standard Test Methods for Rubber Property-Compression Set, 100 Barr Harbor Drive, PO Box C700, West Conshohocken, PA 19428-2959, United States.

[78] Zitzumbo, R.; Ornelas-Rodriguez, F.J.; Lopez, M.; Alonso, S.; Yanez, J.; Avalos, F.; Ortiz, J.C.; Zizumbo, A. 2005, Laser Technology Application: Deformation and Elastic Recovery of Semi-Crystalline Polymers, European Polymer Journal, 42, 1298.

[79] Talal, S. and Miller Tate, P. C. 1999, Comparison of the Recovery Mechanisms of Rigid Polymer Foams Following Long Term Compression, School of Applied Chemistry, Kingston University, UK.

[80] Doroudiani, S.; Kortschot, M. T. 2003, Polystyrene Foams: II. Structure-Impact Properties Relationships, Polymer Science, 90, 5, 1421.

[81] Barlow, C.; Kumar, V.; Flinn, B.; Bordia, R.K.; Weller, J. 2001, Impact strength of high density solid-state microcellular polycarbonate foams Journal of Engineering Materials and Technology, 123, 2, 229.

[82] Bledzki, Andrzej K.; Kuhn, Joanna; Kirschling, Hendrik and Pitscheneder, Walther 2007, Microcellular Injection Molding or PP and PC/ABS with Precision Mold Opening and Gas Counterpressure, SPE-ANTEC 2007 Technical Paper, 2084.

[83] Tovar-Cisneros, Carlos; Gonzalez-Nunez, Ruben and Rodrigue, Denis, The Effect of Mold Temperature on Morphology and Mechanical Properties of Injection Molded HDPE Structural Foam, SPE-ANTEC 2007 Technical Paper, 2120.

[84] Stupak, P. R. and Donovan, J. A. 1991, Effect of Bead Fusion on the Energy Absorption of Polystyrene Foam. Part I. Fracture Toughness, Journal of Cellular Plastics, 27, 5, 484.

[85] Stupak, P. R. and Donovan, J. A. 1991, Effect of Bead Fusion on the Energy Absorption of Polystyrene Foam. Part II. Energy Absorption, Journal of Cellular Plastics, 27, 5, 506.

[86] Loveridge, P. and Mills, N. J. 1991, Mechanism of the Recovery of Impacted High Density Polyethylene Foam, Cellular Polymers, 10, 5, 393.

[87] Bureau, M. N.; Champaqne, M. F. and Gendron, R. 2004, Impact-Compression-Morphology Relationship in Polyolefin Foams, SPE-ANTEC Technical Paper, 3135.

[88] Bureau, M. N.; Champaqne, M. F. and Gendron, R. 2005, Impact-Compression-Morphology Relationship in Polyolefin Foams, Journal of Cellular Plastics, 41, 1, 73.

[89] Duan, Y.; Saigal, A. and Greif, R. 2003, Impact Behaviour and Modeling of Engineering Polymers, Polymer Engineering and Science, 43, 1, 112.

[90] Stokes, V.K. (GE); Nimmer, R.P.; Ysseldyke, D. A. 1988, Mechanical properties of rigid thermoplastic foams - Part I: Experimental considerations, Polymer Engineering and Science, 28, 22.

[91] Kumar, V.; Nadella, K. and Li, W. 2003, Production of Thick Microcellular Thermoplastic Sheets, SPE-ANTEC Technical Paper.

[92] ASTM D638-03, 2005, Standard Test Method for Tensile Properties of Plastics, ASTM International, United States.

[93] Deshmane, C.; Yuan, Q. and Misra, R. D. K. 2007, High Strength-Toughness Combination of Melt Intercalated Nanoclay-Reinforced Thermoplastic Olefins, Materials Science and Engineering A, 460-461, 277.

[94] Wunderlich, B. 1980, Macromolecular Physics, 3, Crystal Melting Academic Press, New York.

[95] Kirshenbaum, I.; Wilchinsky, Z. W. and Groten, B. 1964, Heat and Entropy of Fusion of Polypropylene, Journal of Applied Polymer Science, 8, 2723.

[96] Goel, S. K. and Beckman, E. J. 1993, Generation of Microcellular Polymers using Supercritical $CO_2$, Cellular Polymers, 12, 4, 251.

[97] Wang, J.; Cheng, X. and Zheng, X. 2003, Preparation and Characterization of Microcellular polystyrene/polystyrene Ionomer Blends with Supercritical Carbon Dioxide, Journal of Polymer Science, Part B: Polymer Physics, 41, 4, 368.

[98] Han, X.; Shen, J. and Wingert, M. 2006, $CO_2$ Foaming Based on Polystyrene/Poly (Methyl Methacrylate) Blend and Nanoclay, SPE-ANTEC Technical Paper, 2695.

[99] ASTM International, D5420, Standard Test Method for Impact Resistance of Flat, Rigid Plastic Specimen by Means of a Striker Impacted by a Falling Weight (Gardner Impact), 100 Barr Harbor Drive, PO Box C700, West Conshohocken, PA 19428-2959, United States.